DALHOUSIE UNIVERSITY

2021

Sustainable TDA Backfilling Alternatives and Applications

Hany El Naggar, Ph.D., P.Eng.

Professor, Department of Civil and Resource Engineering
Centre for Innovation in Infrastructure

Table of Contents

Executive Summary

The number of disposed of tires every year in Nova Scotia is more than the number of residents with 1.4 million passenger tire equivalents collected in 2020. Finding sustainable ways to dispose of these tires continues to be a problem throughout the world, not only in Nova Scotia. Disposal issues, along with a continuing increase in tire production, have resulted in an increase in tire stockpiles. Stockpiling scrap tires is not a viable option since stockpiles can be a fire hazard and a breeding ground for mosquitos and vermin, which can transfer dangerous diseases like encephalitis to humans. In Canada, about 40 % of these tires on average cannot be further processed, as it is not generally economical and ends up as waste occupying valuable landfill space. Consequently, there is a huge demand and opportunity for the development of valuable products that may be derived from waste tires. Over the last ten years, Dr. El Naggar and his research team are engaged in several research projects aiming to explore innovative applications of Tire Derived Aggregates (TDA) in several geotechnical engineering areas considering their life cycle costing benefits. The team studied the feasibility of using TDA and mixtures of TDA and sand or gravel as an alternative backfilling material. Over the course of the research, direct shear tests, simple shear tests, consolidated drained triaxial tests, and cyclic triaxial tests were performed on different samples of TDA and TDA mixtures to explore their static and dynamic characteristics.

Divert NS is a great partner and supporter of our research group. The previous two research grants helped in the training of three master's students and one current doctorate student. This collaboration results in developing a number of sustainable TDA backfilling alternatives and applications. The findings of this research were disseminated in several national and international conferences and published in top-tier international journal articles.

Ground-borne vibrations originating from machine foundations are steady-state periodic vibrations characterized by their low-amplitude excitations and low to high-frequency. Most of these vibrations propagate in the soil in the form of surface waves and can travel for long distances. In principle, machine foundations should be designed such that the dynamic forces of machines are transmitted to the soil through the foundation in such a way that all kinds of harmful effects, including ground-borne vibrations, are eliminated. Vibration isolation techniques have been used successfully over the last few decades to reduce machine vibrations. Since TDA is a rubber-based material and carries its characteristics, it has an excellent damping ability recommending it to be used as a vibrations barrier when vibrations control is required. Hence, the main focus of the recent research conducted by our team in the first phase of this project was focused on characterizing the dynamic properties of TDA and investigating its merit to be used as a damping material substituting other expensive options like geofoam (Moussa and El Naggar, 2020; Moussa and El Naggar, 2021; and Moussa et al., 2021).

In the second phase, the focus will be shifted to conduct a large-scale experimental evaluation of the proposed innovative use of TDA to control ground-borne vibrations. This experimental proof of concept is curial to showcase the innovative aspects of the proposed solution and provide practicing engineers with the data they need for design.

1. Introduction

1.1. Background

The number of scrap tires generated in Nova Scotia each year approximates the number of residents in the province. Moreover, in Alberta around five million tires are discarded annually (Moussa and El Naggar 2019). It is anticipated that as the population of Canada grows, the number of scrap tires will also increase (Meles 2016). Due to associated environmental and health hazards, the disposal of scrap tires in landfill is no longer permitted in Nova Scotia; thus, the stockpiling of scrap tires is not a viable option (Edinçliler et al. 2010).

The disposal of scrap tires in landfill has resulted in serious environmental impacts in terms of contamination of the land, air, and soil. Furthermore, the accumulation of discarded tires in landfill has negative affects on human health, due to the leaching of heavy metals and harmful chemicals into the soil. When these toxins enter the groundwater, contact of humans and animals with the contaminated water poses significant health risks. Hence, the development of environmentally friendly alternatives for the use or disposal of scrap tires is an urgent matter, (Moussa and El Naggar 2019).

The use of material made from shredded scrap tires in geotechnical engineering applications is becoming a more widespread alternative approach, to permit the recycling of discarded tires. Due to their versatile properties, shredded scrap tires serve as a useful geotechnical material in civil engineering applications (Humphrey et al. 1993 and Lee et al. 1999). Scrap tires can be shredded into particles of various sizes. The ASTM D6270 classification specifies seven categories of shredded scrap tire products, according to the size ranges of the particles. Tire derived aggregate (TDA) is produced by shredding scrap tires to form particles ranging in size from around 75 to 450 mm. The ASTM D6270 distinguishes two types of TDA. Type A TDA, with a maximum

dimension of 200 mm in any direction, is most suitable for insulation, drainage, and vibration dampening applications. In contrast, type B TDA, with a maximum dimension of 450 mm in any direction, is suitable for use as a lightweight backfill material for embankments or behind retaining walls (ASTM D6270). Table 1.1 summarizes the ASTM D6270 classification of shredded scrap tire products. Shredded scrap tire products that are often used in rubber-soil mixtures include tire shreds, tire chips and granulated rubber, as illustrated in Figure 1.1.

Table 1.1 ASTM D6270 classification of shredded scrap tire products

Category	Subcategory	Size Ranges
Powdered Rubber	-	< 0.425 mm
Ground Rubber		0.425 to 2 mm
Granulated Rubber		0.425 to 12 mm
Tire Chips		12 to 50 mm
Tire Shreds		50 to 305 mm
Tire Derived Aggregate (TDA)	Type A TDA	Around 75 to 100 mm, with a maximum dimension of 200 mm in any direction
	Type B TDA	Around 150 to 305 mm, with a maximum dimension of 450 mm in any direction
Rough Shreds	-	From 50 x 50 x 50 mm to 762 x 50 x 100 mm

Due to the expanding widespread application of these products, research has recently been increasingly focused on investigating various aspects of their geotechnical behavior (El Naggar et al. 2016, Sparkes et al. 2019, Meles et al. 2016, McCartney et al. 2017 and Moussa and El Naggar 2021). For example, Mahgoub and El Naggar (2019) have illustrated the benefits of using a layer of TDA above pre-existing pipes and under shallow foundations. In addition, El Naggar et al. (2013) used TDA inclusions around a box culvert and showed their effectiveness in reducing static and seismic demands on the culvert.

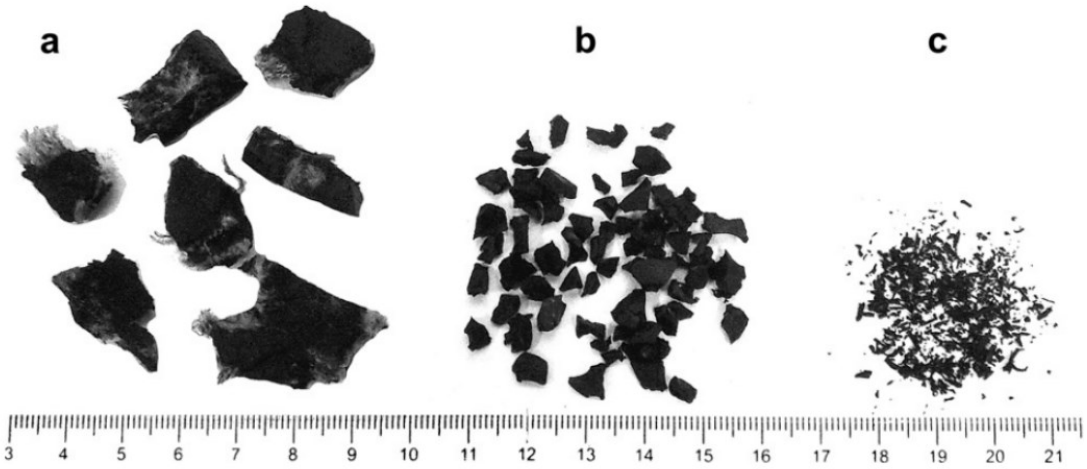

Figure 1.1: Three shredded scrap tire products found in the ASTM D6270 classification: a) tire shreds, b) tire chips, and c) granulated rubber

Furthermore, several researchers have shown that adding shredded scrap tires to granular soils such as sand or gravel is beneficial for vibration screening and the mitigation of liquefaction caused by earthquakes and other sources of vibration (Tsang 2008, Pitilakis et al. 2015 and Hazarika et al. 2010). Studies have also shown that adding rubber materials to granular soils can improve the soil shear strength (Ahmed 1993, Edil and Bosscher 1994, Zornberg et al. 2004, Attom 2006 and Chenari et al. 2017).

1.2. Objectives

The use of TDA in civil engineering applications is getting more and more important due to its outstanding geotechnical properties. Hence, this report study aims to highlight the shear strength parameters and behavior of such relatively new recycled material. Also, the dynamic behavior and properties of TDA is investigated to utilize this material in various dynamic applications related to civil engineering projects.

2. Mechanical Properties of TDA

2.1. Development of an empirical hyperbolic material model for TDA utilizing large-scale triaxial testing

Introduction

Available TDA triaxial data obtained with large-scale machines is limited and is not comprehensive. Also, most triaxial tests performed on TDA have used mixtures of soil and TDA. In the present research, a series of consolidated drained triaxial tests have been performed on TDA in accordance with ASTM D7181-11. The TDA tested is almost the same size as that used in many civil engineering projects (i.e., tire chips TDA). The tests were performed by using a large-scale triaxial machine with a sample diameter of 152 mm (6 in) and a height of approximately 2.1 times the diameter. The tests were performed on TDA containing steel wire, and only the protruding part of the steel was removed to protect the membrane. In order to replicate a variety of real-world conditions, the tests were performed for a wide range of confining pressures. The results of deviatoric stress versus strain, corrected for volume change as per ASTM D7181-11, are presented and discussed, and empirical equations for a number of strength and stiffness parameters are proposed. The empirical equations are then used to develop a hyperbolic material model for TDA.

Material

The TDA material used in this research was manufactured from passenger car scrap tires by Halifax C&D Recycling Ltd. The TDA complies with the ASTM D6270-17 standard. The only alteration made by the researchers was the removal of protruding parts of the steel wires to protect the triaxial membrane. Removal of the protruding steel also prevents the TDA particles from locking together via the steel. The effect of removing the protruding steel on the mechanical properties of the specimens is unknown. Sieve analysis was performed in accordance with ASTM C136/C136M- 14, with the exception of the minimum sample size of 6 to 12 kg, permitted as per

ASTM C136/C136M-14, as the unit weight of TDA is much lighter than conventional soils. Figure 1(a) illustrates the TDA particle size distribution used for this experiment. As indicated in the figure, the TDA particles used ranged in size from 13 mm to 31 mm, with D50 = 22 mm. It should be noted that as mentioned in ASTM D6270-17, Type A TDA shall have a maximum dimension of 200 mm, measured in any direction, and 100% of the material should pass through the 100-mm square mesh sieve. Besides, a minimum of 95% of TDA passing the 75- mm square mesh sieve, with a maximum of 50% passing the 38- mm square mesh sieve and a maximum of 5% passing the 4.75- mm sieve. Therefore, based on the gradation, despite the material is very close to Type A TDA, it is classified as tire chips as more than 50% of the particles pass through the 38-mm square mesh sieve. The average aspect ratio of the used TDA particles, defined as the ratio between the length to the width of the particle, was about approximately 2.1. Figure 1(b) shows an example of the particles used in the experiment.

Triaxial Test Apparatus

Figure 2.1(c) shows the large-scale triaxial test apparatus that was used in the research. The shaft of the test apparatus was extended to accommodate the excessive amount of consolidation and the higher amount of strain needed for the test. The sample diameter was 152 mm (6 inches), and the

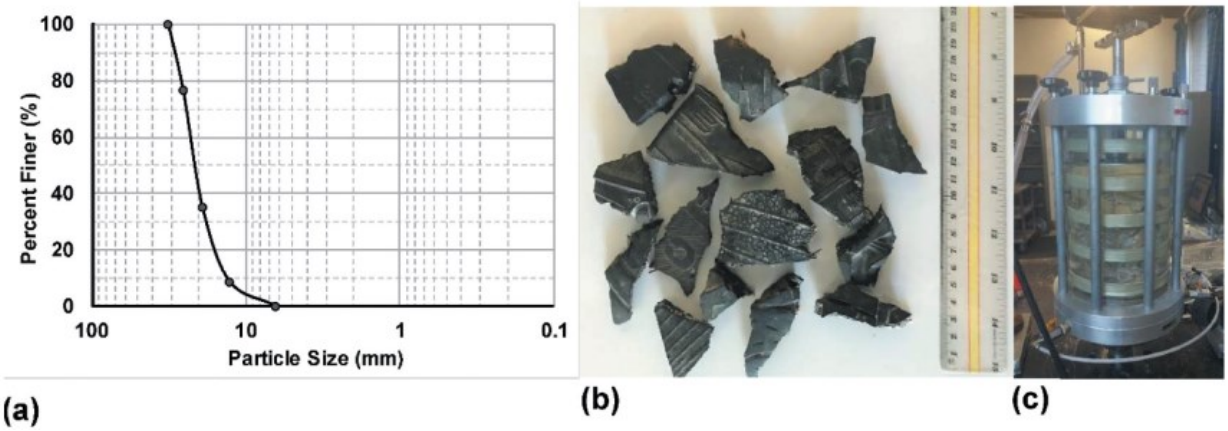

Figure 2.1: (a) Used TDA gradation, (b) Example of particles used, and (c) The used large scale triaxial test apparatus.

height of the sample was approximately 320 mm (12.6 inches), which is around 2.1 times the sample diameter and is in the range permitted by ASTM D7181-11. An Instron 8501 hydraulic load frame was used for the axial loading. The load and the displacement were recorded at a frequency of 20 Hz. The displacement was set at a constant rate calculated according to ASTM D7181-11. To control the pressure and record the volume change of the sample and the cell during the test, two GDS advanced pressure-volume controllers (ADVDPCs) were used. Both ADVDPCs were kept at the same height and were calibrated before the start of each test. The cell pressure was controlled to account for the volume change caused by the shaft movement and changes in the volume of the sample.

Sample preparation

Before preparation of the specimens, all TDA particles were checked for protruding steel wires. If these were present, only the protruding parts of the wires were clipped to preserve the integrity of the membrane around the specimens. The specimens were compacted in five layers by using a steel rod. As shown by Humphrey and Manion (1992) and Kowalska (2016), introducing water has an insignificant influence on the dry density of TDA; thus, the specimens were kept dry during compaction. Although it is permissible to perform compaction on air-dried or oven-dried TDA as per ASTM D6270-08, the researchers noticed a slight change in the physical properties of oven dried TDA and used only air drying. The dry density of all the compacted specimens was 710 ± 5% kg/m^3. During compaction, special care was taken to protect the membrane. The membrane used was a relatively thick Humboldt membrane, with a thickness of 0.635 mm (0.025 inches). ASTM standard D7181-11 specifies a correction to be applied if the error in the deviatoric stress introduced by the membrane thickness is more than 5% of the deviatoric stress. The most critical cases in the experiments in this study were those with low confining pressure at high strains. Even

for these cases, the error never reached 4%; for this reason, the correction was not applied. Although the measures described were taken to protect the membrane, more than half the tests performed had to be repeated due to the puncturing of the membrane. Puncturing occurred more frequently as the confining pressure increased. It should be noted that the samples in different tests were freshly built every test, where the specimens were built by emptying the container and then compacting TDA for each confining pressure case. The only deviation from ASTM standard D7181-11, which occurred during sample preparation, was that the maximum TDA particle size was not smaller than 1/6 of the specimen diameter. However, it should be noted that this ASTM standard was developed for soil and natural aggregates and that no standards exist for testing TDA with triaxial machines. Furthermore, even for conventional aggregates, the maximum particle size ratio is not broadly agreed upon. For example, the British Standard BS 1377–8:1990 specifies a larger allowed maximum particle size than that specified by the ASTM (maximum particle size of 1/5 of the specimen diameter, BS 1377–8:1990), which is satisfied in this research. Large particle sizes lead to increased voids at the sample perimeter, which in turn can result in indentation errors or perforation of the membrane and lower sample density. The results presented in this paper are for TDA samples that did not have any membrane indentation errors or perforations. The density of the tested samples was about the same as those obtained from the compaction test. The tested samples also consisted of well-graded TDA, as can be seen from the particle size distribution curve shown in Figure 1. Hence, in the opinion of the authors, the boundary effect of TDA has less influence than that of conventional aggregates because the individual TDA particles are more flexible and conform more to the applied pressure.

Testing procedure

A total of 9 successful consolidated drained (CD) triaxial compression tests were performed as part of this research. The dimensions of each specimen were measured prior to the beginning of the saturation stage. Because of the large particle size and high void ratio, saturation was relatively fast and straightforward. The B value was measured for every test, and it was always greater than 0.95. As with the saturation stage and for the same reasons, consolidation was relatively quick. To calculate the rate of axial loading, the volume change and deformation of the specimens undergoing consolidation were recorded and plotted against the logarithm of the elapsed time. Due to the high permeability of the specimens, the rate calculated was greater than the maximum rate that could be controlled by the ADVDPC, so the rate of 1 mm/min was chosen as the rate of axial loading. During consolidation, the samples underwent a considerable change in volume, and the shaft had to be adjusted to keep contact with the shrinking sample. The volume change of the sample had a direct relationship to the confining pressure applied. Below is the equation for the curve best fitted to the volume change of the sample:

$$VP = 3.12\sigma_3^{0.39} \quad (1)$$

where VP is the percentage of volume change, and σ_3 is the confining pressure of the sample (kPa). Figure 2.2 shows the volume change of different samples during the consolidation stage plotted against the confining pressure, together with the fitted curve.

During the axial loading, the amount of load, the displacement and the volume change inside the cell and the sample were recorded. These values were later used to adjust the dimensions of the sample and to calculate the amount of deviatoric stress and strain. During the tests, at higher strains, the specimens started to bulge visibly, and the assumption that the specimen deforms as a right circular cylinder was no longer valid. It was also not possible to determine accurate values

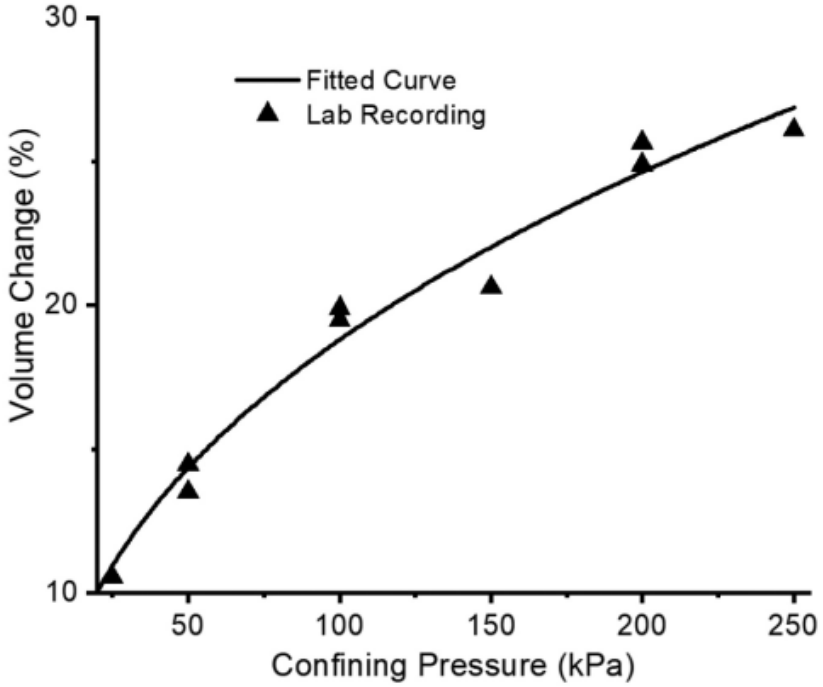

Figure 2.2: Volume change of the different samples during consolidation.

for the bulging, which occurred because of the elastic nature of the specimen. Following unloading, the specimens reverted almost to their initial form. For these reasons, the researchers did not continue the tests at strains greater than 20%.

Results and discussion

The triaxial compression test was performed at six different confining pressures. The confining pressures used were 25, 50, 100, 150, 200, and 250 kPa. These confining pressures were chosen to resemble the stress levels expected in embankments, retaining walls, and shallow and deep backfills. Because of the random nature of the TDA particles and to prove repeatability, for confining pressures of 50, 100, and 200 kPa, the test was repeated two times. Figure 2.3 (a) shows the volumetric strain versus the axial strain for different confining pressures. The changes in volumetric strain during axial loading had no meaningful relationship to the confining pressure applied and essentially exhibited similar trends.

While both the steel and rubber present in the TDA are elastic to a high degree, the combination of steel and rubber forms a more complex material, particularly since the particle reorientation that occurs during axial loading can change the orientation of the steel. The presence of voids that can be filled during axial loading adds another layer of complexity to the behavior of the specimens.

Deformation which occurs in saturated soils is attributed primarily to the reorientation and rearrangement of soil particles and the expulsion of water from the void spaces, while the deformation of soil particles is considered insignificant (Yi et al. 2015). In contrast, TDA particles are made mainly of rubber, which exhibits near perfect elastic behavior with a Poisson's ratio of 0.5. This means that the deformation of each TDA particle under load is reversible without any change in volume. Nevertheless, as in the deformation of soil, TDA particles as a group can undergo reorientation and rearrangement under load to fill the void spaces available. Figure 2.3(b) compares the average amount of volumetric strain recorded in this study with the amount observed by Lee et al. (1999) and Youwai and Bergado (2003). The two studies used for comparison used TDA with smaller particles, with a maximum effective size of only 15 mm. The figure shows that changes in volumetric strain in the present study occurred more rapidly than in the other studies.

Figure 2.3 (a) Volumetric strain versus axial strain, and (b) Comparison of the volumetric strain with that observed by Lee et al. (1999) and Youwai and Bergado (2003) The random nature of the TDA particles raises a question concerning the repeatability of the tests performed. To address this question, the triaxial test was performed two times each for the confining pressures 50, 100, and 200 kPa. Figure 2.4 plots the deviatoric stress against the axial strain for each of these tests. It is evident from the figure that the results are in strong agreement with one another. This demonstrates the consistency of the results.

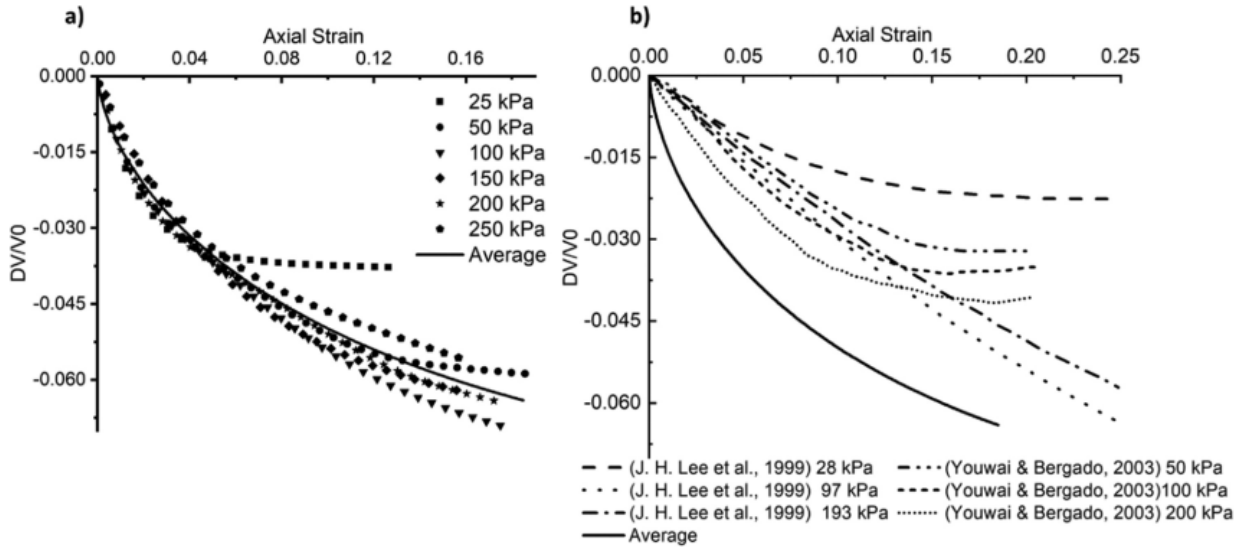

Figure 2.3: (a) Volumetric strain versus axial strain, and (b) Comparison of the volumetric strain with that observed by Lee et al. (1999) and Youwai and Bergado (2003)

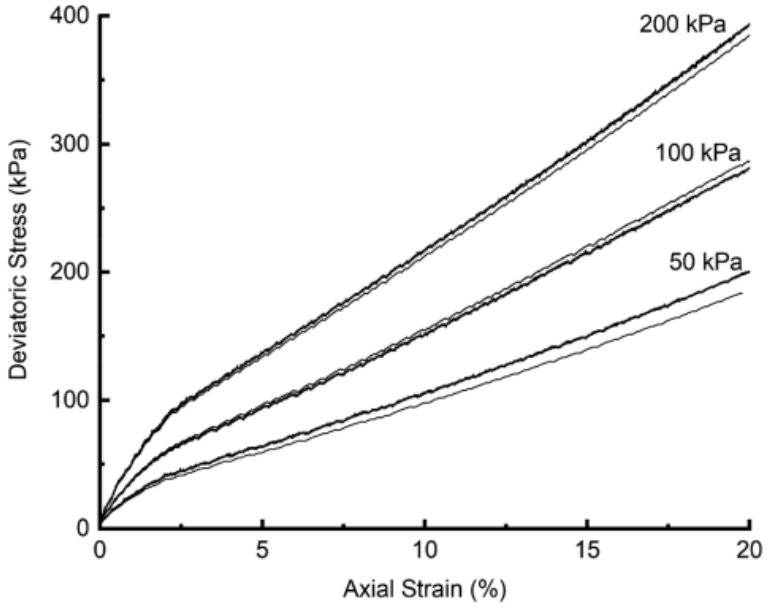

Figure 2.4: Repeatability of the triaxial tests.

Stress-strain relationships

In order to fit the best curve to the laboratory results, various regression methods were used for the results associated with each confining pressure, with axial strain as the variable. The equations

with two exponential terms had the highest R^2 while maintaining simplicity. To find a reasonably simple equation that accepts both axial strain and confining pressure as input variables, the coefficients of the exponential terms were replaced with a linear line, with confining pressure as the variable. With the aid of the least-squares method, the coefficients of the linear line were determined such that R^2 for the final σ equation is 0.985. This procedure was repeated to fit the best equation to the value of E50 calculated from the laboratory results. The equations below use the amount of strain and confining pressure as input variables and calculate the amount of deviatoric strain and secant modulus (E50):

$$\sigma = a\varepsilon^{0.73} \tag{2}$$

$$a = -249 + 31\sigma_3 - 0.366\sigma_3^2 + 0.002\sigma_3^3 - 3.3 \times 10^{-6}\sigma_3^4 \tag{3}$$

$$E_{50} = 11.36\sigma_3 + 448.73 \tag{4}$$

where σ is the deviatoric stress (kPa), σ_3 is the confining pressure (kPa), ε is the amount of axial strain, and E50 is the secant modulus (kPa) at the maximum strain allowed (ε_{ult} = 0.15 in most applications as per ASTM D7181-11).

Figure 2.5(a) plots deviatoric stress against axial strain for different confining pressures and compares the results with the fitted curves. As shown in the figure, the fitted curves are in very good agreement with the laboratory results. The results indicate that the behavior of the samples started nonlinearly and then behaves linearly, starting near the 5% strain vicinity, approximately, till the end of the test. This behavior may be explained as follows: at the beginning of the test, the voids between the particles are large and hence stimulate the nonlinear behavior of the TDA-voids matrix. After sufficient compression occurs (i.e., around 5% strain), the voids volume reduces substantially, and the behavior is governed by the linear elasticity of the rubber material itself.

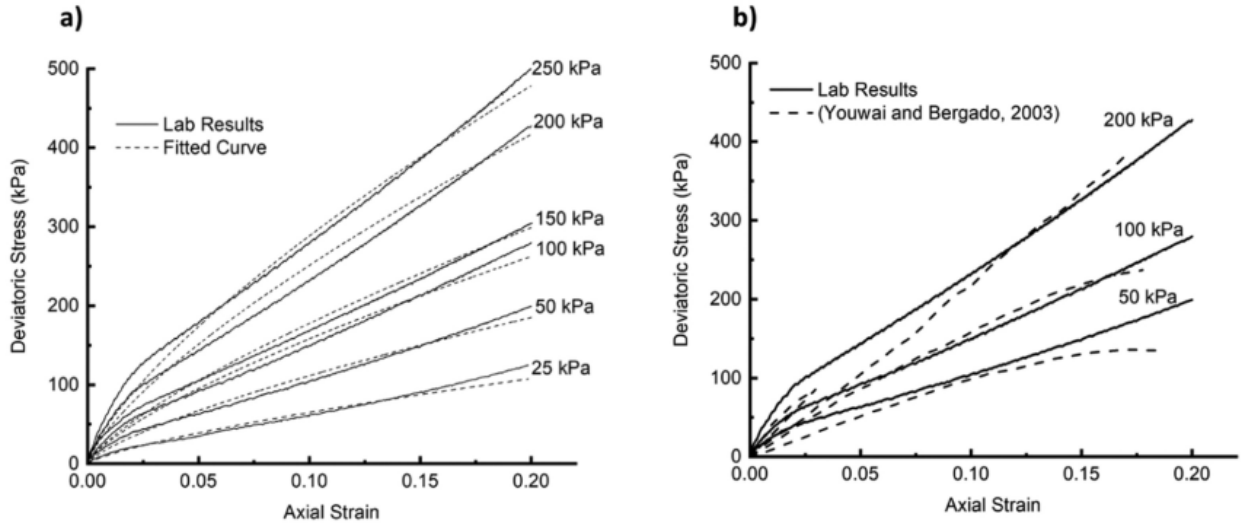

Figure 2.5: (a) Comparison between the laboratory results and the empirical equations, and (b) Comparison of the laboratory results with those of Youwai and Bergado (2003)

Figure 5(b) compares the results of this study with those of Youwai and Bergado (2003). It can be seen from Figure 5(b) that a similar trend between the results of Youwai and Bergado (2003) and the findings of this study were found.

The nature TDA as a composite material (i.e., rubber and steel) and the presence of voids that can be filled during axial loading adds another layer of complexity to the behavior of the specimens. These factors may be the cause of the starting nonlinear behavior observed in this investigation as explained in detail above.

Hyperbolic Model for TDA

Duncan and Chang (1970) proposed a simple, practical nonlinear stress-strain relationship that is easy to implement in a finite element analysis of soil. The advantages of their model are its simplicity and the fact that the values required in the model can be determined from the results of triaxial tests. The disadvantages of their model are: (1) the assumption of hyperbolic behavior for stress-strain curves of soil, which means that the model cannot predict the residual strength of soil after the peak stress; (2) the fact that the model can predict only the elastic behavior of soil and

fails to predict the plastic behavior; and (3) the fact that the model assumes that the volumetric strain of the soil is only compressive, and cannot represent the dilatant behavior of soils (1999). Although these disadvantages limit the applicability of the model for soil, since the triaxial test results presented in this paper show no residual strength or dilatant behavior for TDA, this model can provide a good representation of the TDA behavior.

According to the hyperbolic model:

$$\sigma = \frac{\varepsilon}{\frac{1}{E_i} + \frac{\varepsilon R_f}{\sigma_f}} \tag{5}$$

where E_i is the initial tangent of Young's modulus, σ_f is the deviatoric stress at failure, and R_f is the failure ratio. The value of E_i can be calculated from equation 4.

Assuming that the failure occurs at $\varepsilon = 0.15$, the value of σ_f can be calculated as:

$$\sigma_f = 1.2384\sigma_3 + 73.476 \tag{6}$$

By substituting Equations (4) and (6) in Equation (5) and tweaking the value of R_f to obtain the best fit for the laboratory results, the value of R_f can be calculated to be ranging from 0.1 to 0.2. This yields the equation:

$$\sigma = \frac{\varepsilon}{\frac{1}{11.36\sigma_3 + 448.73} + \frac{\varepsilon R_f}{1.2384\sigma_3 + 73.476}} \tag{7}$$

Figure 7 compares the values calculated by Equation (7) with the laboratory results. The values calculated by Equation (7) are also very close to the values of the empirical Equation (2). As shown in Figure 6, there is very good agreement between the results, which is an indicator that the proposed empirical hyperbolic model is capable of simulating the behavior of TDA under different

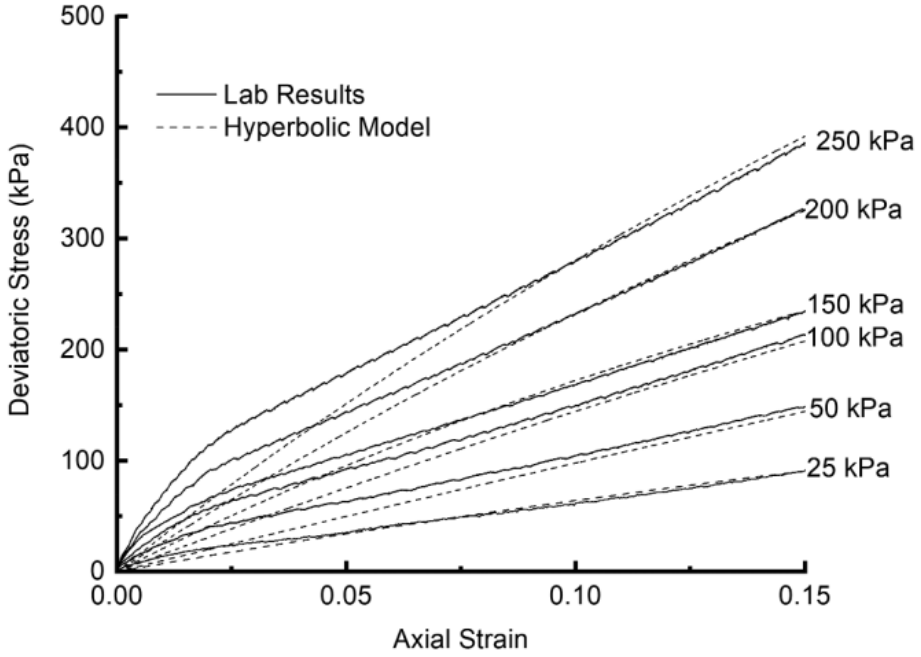

Figure 2.6: Comparison between the hyperbolic model and the laboratory results.

confining pressures. However, the agreement is less for confining pressures of 200 kPa and larger at strain levels below 2.5%; however, it is on the conservative side.

TDA strength parameters

As is evident, the deviatoric stress never reached its peak maximum during the tests. ASTM D7181-11 suggests that in cases where the maximum principal stress cannot be obtained, the deviatoric stress at 15% axial strain should be considered as the maximum stress. Some researchers have used the stress at 10% axial strain as the maximum stress. Depending on the strain considered and its corresponding stress, the results of the internal angle of friction and cohesion calculated by using the Mohr-Coulomb failure criterion will be different. The empirical equations below represent the best-fit curve for our laboratory results to calculate the angle of internal friction and cohesion. To give the reader the option to decide which criterion to use (i.e., at $\varepsilon = 10\%$ or 15%), the equations below provide the strength parameters at the assumed ultimate axial strain, ε.

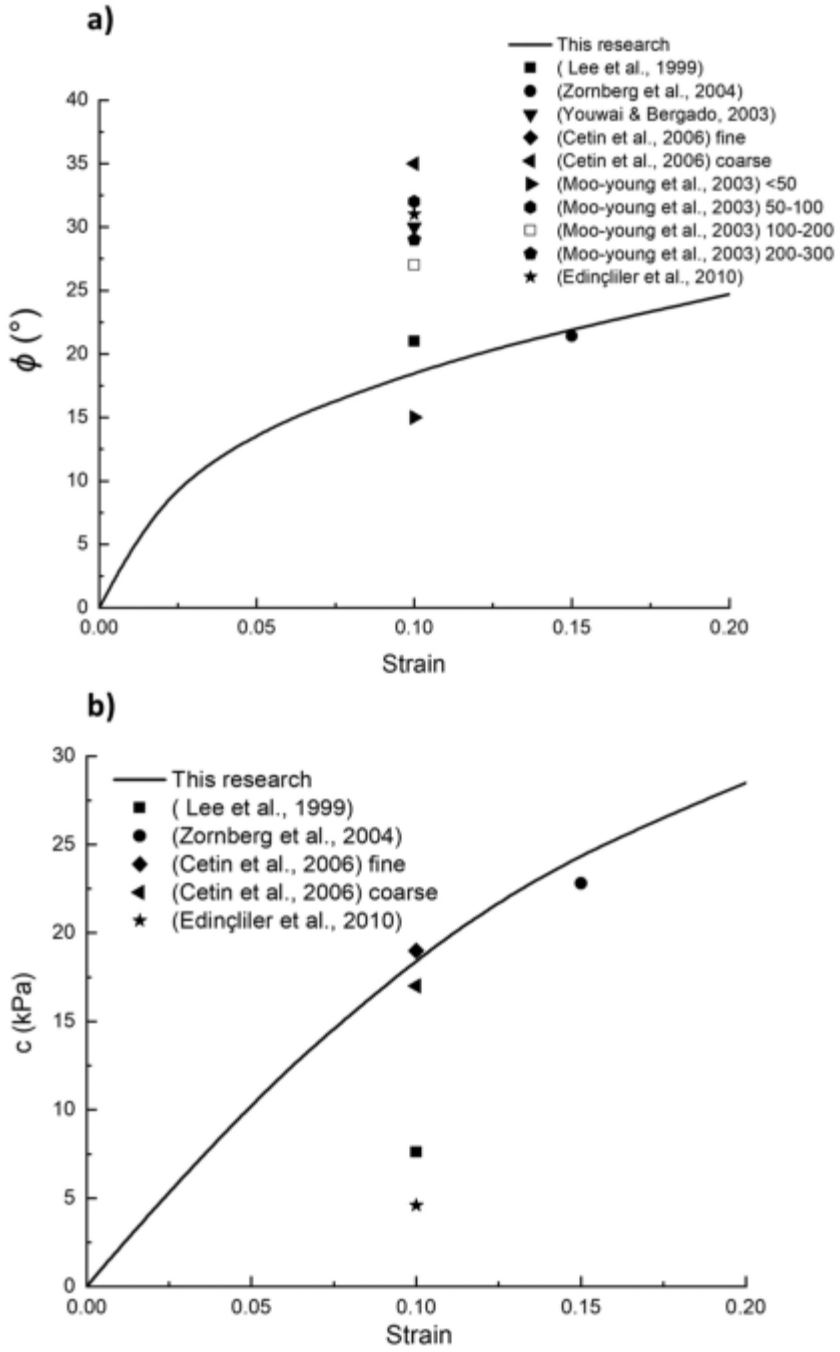

Figure 7: Comparison of (a) internal friction angles, and (b) cohesion values, obtained by different researchers.

$$c = -424.58\varepsilon^2 + 227.4\varepsilon \quad (8)$$

$$\varphi = 0.96\varepsilon^{0.457} \quad (9)$$

where ϕ is the angle of internal friction (°), and c represents the amount of cohesion (kPa). Substituting $\varepsilon = 0.15$ in the equations above yields $\phi = 23.1°$ and c = 25 kPa.

Figure 2.7(a) and 7(b) compare the results for ϕ and c with the results obtained by other researchers. Moo-Young et al. (2003), Cetin, Fener, and Gunaydin (2006) and Edinçliler, Baykal, and Saygılı (2010) calculated the values of ϕ and c based on the results of direct shear tests. Moo-Young et al. (2003) tested four different TDA particle sizes: smaller than 50 mm, between 50 and 100 mm, between 100 and 200 mm, and between 200 and 300 mm. Cetin, Fener, and Gunaydin (2006) tested two different particle sizes: fine, with particles smaller than 0.4 mm; and coarse, with particles between 2 and 5 mm. Edinçliler, Baykal, and Saygılı (2010) tested very small particles, measuring approximately 0.6 mm. It should be noted that shear strength parameters obtained from direct shear tests are always different than those obtained from triaxial testing due to the limitations of the direct shear test, which is summarized above, however the results are compared here to show the range of variation.

As in this study, Lee et al. (1999), Zornberg, Cabral, and Viratjandr (2004) and Youwai and Bergado (2003) based the values of ϕ and c on the results of triaxial tests. The size of the TDA particles used by Lee et al. (1999) was between 5 to 40 mm. Zornberg, Cabral, and Viratjandr (2004) used TDA particles with a width of 12.7 mm and four different aspect ratios. Youwai and Bergado (2003) used TDA particles ranging from 4 to 13 mm.

As shown in Figure 2.7(a) and 7(b), there is no general agreement among the results obtained by the different researchers, except the study by Zornberg, Cabral, and Viratjandr (2004). It can be seen from the figures that the values of the shear strength parameters reported by Zornberg, Cabral, and Viratjandr (2004) are compatible with the estimated values by the current study at 15% strain. The particle size and shape, the presence or absence of steel, and the type of test conducted are

some of the parameters that can influence the calculated values of ϕ and c. The size and shape of the TDA particles can influence the void ratio of the samples, which in turn affect the stiffness and strength parameters. Also, the presence of steel can increase the stiffness of the sample, and at the same time, if the protruding steel wires are long enough, they can cause TDA particles to become entangled with one another, which can increase the amount of cohesion. Finally, the predefined failure surface and restrictions regarding the confining pressure applied can influence the results achieved by direct shear tests.

Summary and conclusions

Consolidated drained triaxial tests were conducted on tire derived aggregate particles the same size as those used in civil engineering projects. An advanced large-scale triaxial testing system was employed in accordance with the ASTM D7181-11standard. The triaxial tests were performed at various testing conditions. Based on the test results, an empirical hyperbolic material model has been proposed to simulate the behavior of tire derived aggregates. The following are the conclusions drawn from the present study:

- Peak deviatoric stress was not observed in the stress-strain response of tire derived aggregates. Hence, the termination strain was fixed as 20%.
- The samples tested at higher confining pressures tended towards losing more water during the consolidation stage than the samples tested to lower confining pressures.
- The stress-strain response of the tire derived aggregates is found to be nonlinear at the start and then behaves almost linearly afterwards. The particle rearrangement during axial loading could be the reason for the observed initial non-linear stress-strain behavior.

- No correlation could be found between the applied confining pressure and the observed volumetric strains. During axial loading, the samples showed no significant difference in changes in volumetric strains recorded. The possible reason could be the size of the tire derived aggregates adopted for testing in the present study.
- The parameters such as particle size and shape, the presence or absence of steel, and the type of test conducted can influence the shear strength parameters of tire derived aggregates.
- The proposed empirical hyperbolic material model is capable of simulating the behavior of tire derived aggregates under different confining pressures.

2.2. Effect of Sample Size on TDA Shear Strength Parameters in Direct Shear Tests

Direct Shear Test

Direct shear tests were performed on three types of apparatus: large-, medium-, and small-scale direct shear machines. With the large-scale apparatus, tests were performed by using square shear boxes measuring 305 x 305 mm and 225 x 225 mm. While in the medium-scale apparatus, tests were performed using a 150 x 150 mm square shear box. Whereas, with the small-scale apparatus, tests were performed by using shear boxes measuring 100 3 100 mm and 60 3 60 mm. The height of the mold of the 305 mm shear box was modified to be 210 mm instead of 160 mm by installing a 50 mm extension on the shear box as shown in Figure 2.8, to accommodate the high compressibility of TDA, making the aspect ratio W/H = 1.45, where W is the width of the box and H is the total sample height. The shear boxes measuring 225 3 225 mm and 150 3 150 mm were also designed and constructed with a height of 210 mm, resulting in aspect ratios W/H of 1.07 and 0.71, respectively. Moreover, the height of the small-scale shear boxes was only 43 mm, resulting in aspect ratios W/H of 2.33 and 1.40, respectively. This information is summarized in Table 3 and illustrated in Figure 2.8. ASTM D3080 recommends that the minimum specimen width should be greater than ten times the maximum particle size. Furthermore, the minimum initial specimen thickness should not be less than six times the maximum particle diameter. However, it should be noted that these recommendations are mainly for conventional soils as ASTM D3080 was developed for testing of soils under consolidated drained conditions, not for TDA.

The shear boxes used in this study were divided into lower and upper parts, as shown in Figure 2.8; the height of each part is shown in Table 2.3. The lower part of the shear boxes was the movable part which moved in a horizontal direction away from the machine via an electric motor

Figure 2.8: Shear boxes and tire-derived aggregate (TDA) sample used in the research.

Table 2.1: Shear Box Characteristics

Shear box dimensions						
		1	2	3	4	5
Length (L) (mm)	na	305	225	150	100	60
Width (W) (mm)	na	305	225	150	100	60
Height (H) (mm)	Lower part	80	80	80	18	18
	Upper part	130	130	130	25	25
Aspect ratio (W/H)	na	1.45	1.07	0.71	2.33	1.40
Aspect ratio (W/D_{max})	na	8	6	4	2.6	1.6

Note: na = not applicable.

and had a height of 80 mm in the large- and medium-scale direct shear boxes and 18 mm in the two small-scale direct shear boxes.

Each of the direct shear apparatuses used had three linear variable displacement transducers (LVDT). One was connected to the load cell to measure the shear force (kN). The second barely touched the shear yoke and measured the vertical displacement (mm), while the third barely

touched the lower part of the shear box and measured the horizontal displacement (mm). The LVDTs were connected to a data acquisition system to record the data received from the LVDTs. The normal stresses, applied to the samples in the direct shear tests by means of a deadweight system, ranged from a minimum of 50.1 kPa up to a maximum of 196.4 kPa.

TDA Sample Characteristics

The TDA sample used was obtained from Halifax C&D Recycling Ltd. The sample was referred to as 1.5-in. TDA, in accordance with the maximum particle size (D_{max}) in the sample. Sieve analysis was conducted on the sample in accordance with ASTM D6913-04. The graduation curve obtained is shown in Figure 2.9. The unit weight of the tested TDA ranged between 6.3 and 8.3 kN/ m^3, depending on the applied normal stress.

As summarized in Table 4, the effective particle size (D10) of the TDA sample was found to be 12 mm (0.47 in.), the average particle size (D50) was 24.5 mm (0.96 in.), the coefficient of uniformity was 0.74, and the coefficient of curvature was 2.25. The tested sample had

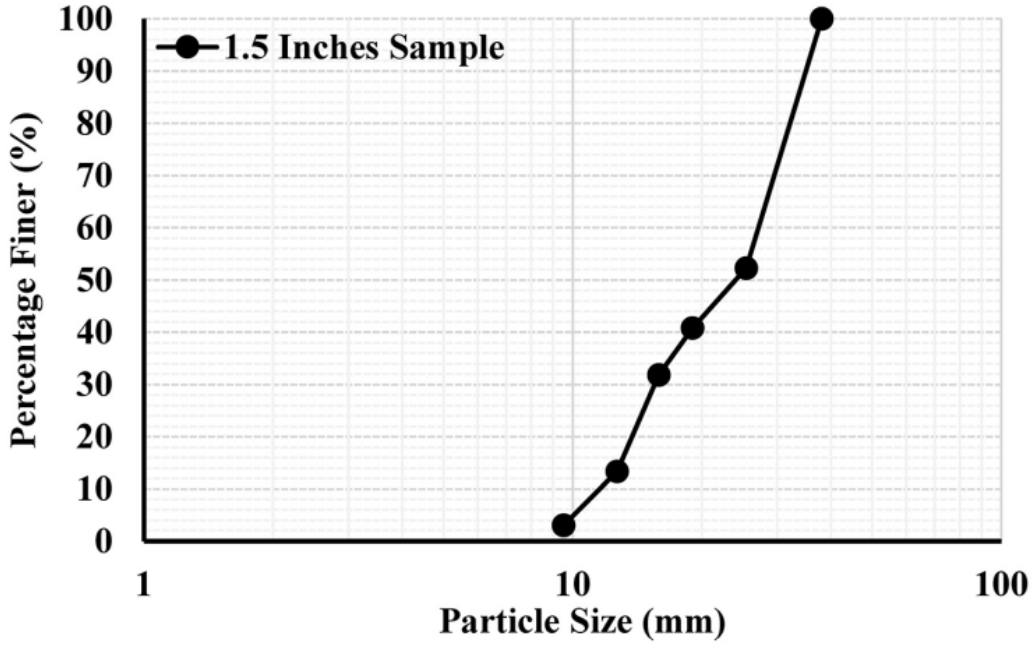

Figure 2.9: Graduation curve for the 1.5-in. tire-derived aggregate sample

Table 2.2: Properties of the Tire-Derived Aggregate Sample Used

	D10	D30	D50	D60	Coefficient of curvature (C_c)	Coefficient of uniformity (C_u)
(mm)	12	15.5	24.5	27	2.25	0.74
(in.)	0.47	0.61	0.96	1.06	2.25	0.74

approximately 61% flat particles and 39% elongated particles. The average length of the tested sample was 32 mm, while the average width and thickness were 21 and 7 mm, respectively, and the length to width ratio was found to be approximately 1.52.

Testing Procedures

The 1.5-in. TDA sample was tested in accordance with ASTM D3080 Standard test method for direct shear tests of soils under consolidated drained conditions. First, the sample was prepared in accordance with ASTM D6913-04, and the graduation curve was obtained, as shown in Figure 2.9. The sample was then mixed well to prevent particle segregation. After that, the sample was divided into five parts, to form five layers. These were poured into the shear box layer by layer, with the proper compaction for each layer, for a total compaction energy of 38,000 (Joules). Thus, the minimum required compaction energy was reached, which is 60% of the modified proctor energy, according to ASTM D6270-08.

For the 305 mm shear box, 75 blows with the modified proctor hammer were used to compact each layer, with a total of 375 blows for the whole sample. For the 225 mm shear box, 45 blows were used to compact each layer, with a total of 225 blows for the entire sample. Likewise, for the sample in the 150 mm shear box, 20 blows were used to compact each layer, with a total of 100 blows for the entire sample. In contrast, the samples in the 100 and 60 mm shear boxes were oriented by hand to ensure proper void filling and to prevent the sample from overflowing the shear box, since at 43 mm the height of the shear box was somewhat low relative to the sample size.

The TDA samples in the shear boxes measuring 305, 100, and 60 mm were sheared under three applied normal stresses of 50.1, 98.8, and 196.4 kPa. However, for the 225 mm shear box, the normal stresses applied were 87.9, 98.8, and 196.4 kPa, because the hydraulic arm for this shear box could not apply normal stress less than 87.9 kPa. Moreover, the normal stresses applied to the150 mm shear box were 151, 175, and 196.4 kPa. For all tests, actual in-the-box unit weight ranging between 6.3–8.3 kN/m3 was maintained (the actual unit weight is that of the sample in the shear box after applying the respective normal stress).

The shearing rate was 0.5 mm/min for the large- and medium-scale direct shear tests and 1 mm/min for the small-scale direct shear tests. Low shearing rates were chosen to prevent any overestimation of the calculated shear stresses, and the samples were in a dry condition, so no accumulation of pore water pressure occurred. To the best of the authors' knowledge, the shearing rate used was lower than shearing rates used in the testing of TDA recorded in the literature (Engstrom et al. 1994, Humphrey et al. 1993, Moo-Young et al. 2003, Xiao et al. 2013, Bernal et al. 1997 and Sparkes et al. 2019). Moreover, researchers have shown that the effect of the shearing rate on the shear strength parameters of cohesionless soils in drained conditions is not significant (Yamamuro and Lade 1993, Tika et al. 1996 and Anim and Fakhi,I 2012).

Results Comparison and Discussion

Stress-Strain Curves

A total of 25 tests were performed to study the effect of the specimen size on the TDA shear strength results. Some of these tests were duplicated to verify the results. Since, the stress-strain curves did not show a clear peak for the considered shear strain range (i.e., around the 14% strain), the shear strength parameters were calculated at 10% of the horizontal strain percentage as recommended by ASTM D3080-11 and by Strenk et al. (2007) among several other researchers.

Figure 2.10 plots the shear stress (kPa) against the horizontal strain (%) for shear boxes having the same applied normal stress. It was observed that the shear stress at 10% horizontal strain was almost identical for the shear boxes measuring 300 and 100 mm (within 5%) and slightly higher in the 60 mm shear box (6% higher). The results obtained for the shear boxes measuring 225 and 150 mm are shown separately, in Figure 2.11, because the normal stresses applied to these shear boxes differed from those applied to the shear boxes previously discussed. Since the normal stresses of 88 and 98.8 kPa were very close, the stress-strain curves shown in Figure 2.11a for these normal stresses are also very close. The same occurred in Figure 2.11b for the normal stresses of 175 and 196.4 kPa. Moreover, the graphs illustrate clearly that as the normal stress applied to the sample increased, the attained shear stress increased for all of the shear boxes.

The shear stresses at 10% horizontal strain for the different normal stresses applied are summarized in Table 2.3 for ease of reference. These shear stresses were used to calculate the shear strength parameters of the TDA sample. Figure 2.12 shows the relationship between shear stress and normal

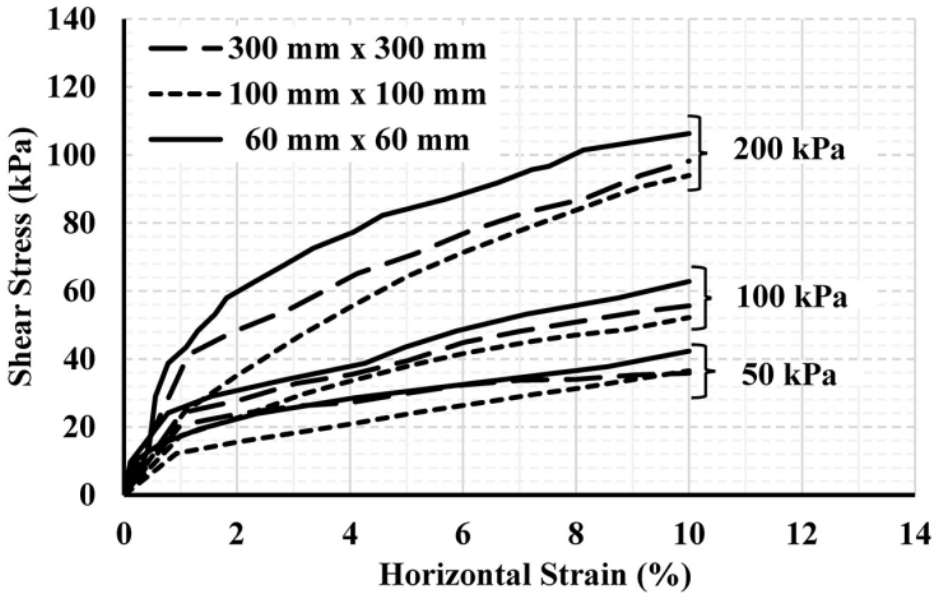

Figure 2.10: Shear stress (kPa) versus (horizontal displacement/box width) percent for the 300, 100, and 60 mm shear boxes.

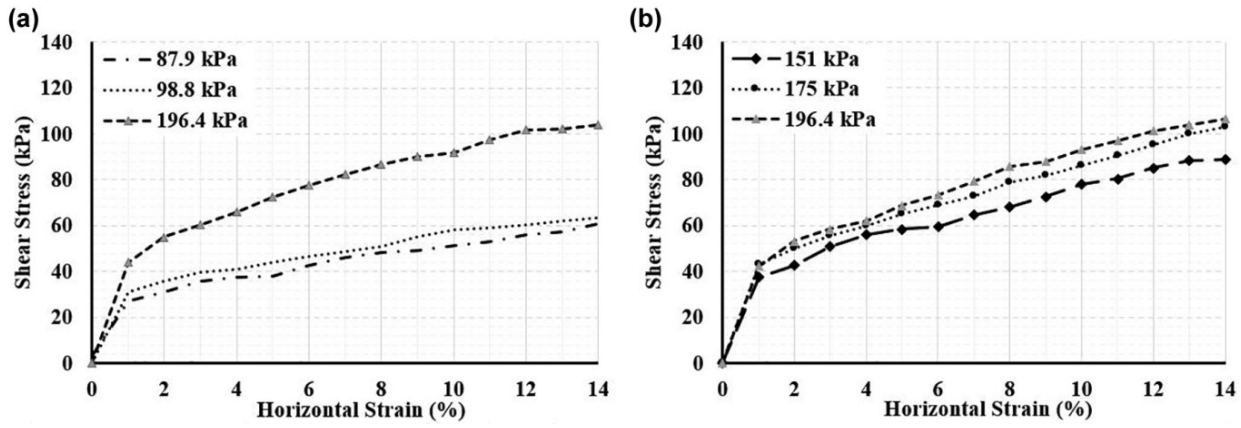

Figure 2.11: Shear stress (kPa) versus (horizontal displacement/box width) percent for: (a) the 225 mm shear box; and (b) the 150 mm

Table 2.3: Shear Stresses (kPa), Angle of Internal Friction and Cohesion for the Shear Boxes

Shear box	Normal stress (kPa)	Shear stress at 10% horizontal strain (kPa)	Angle of internal friction (°)	Cohesion (kPa)
305 × 305 mm	50.1	36.6	22.0	16.4
	98.8	56.2		
	196.4	95.8		
225 × 225 mm	87.9	51.4	22.0	16.6
	98.8	57.5		
	196.4	96		
150 × 150 mm	151	75	22.1	14.0
	175	86		
	196.4	93.4		
100 × 100 mm	50.1	36.5	22.4	14.0
	98.8	51.8		
	196.4	95.8		
60 × 60 mm	50.1	38.4	23.9	16.1
	98.8	59.5		
	196.4	103		

stress for all the tests. Describing the mileage points based on linear equations made it possible to determine the shear strength parameters as shown in Table 2.3.

Angle of Internal Friction and Cohesion

It was observed that the angle of internal friction exhibits a slight increase as the shear box size decreases, as shown in Figure 13. However, for the 60 mm shear box, the angle of internal friction showed a significant increase as shown in the figure. There was no increase in the angle of internal friction with the decrease in shear box size from 305 to 225 mm (i.e., for specimen width to maximum particle size, W/D_{max}, of 8 and 5.9 respectively). A negligible increase in the angle of

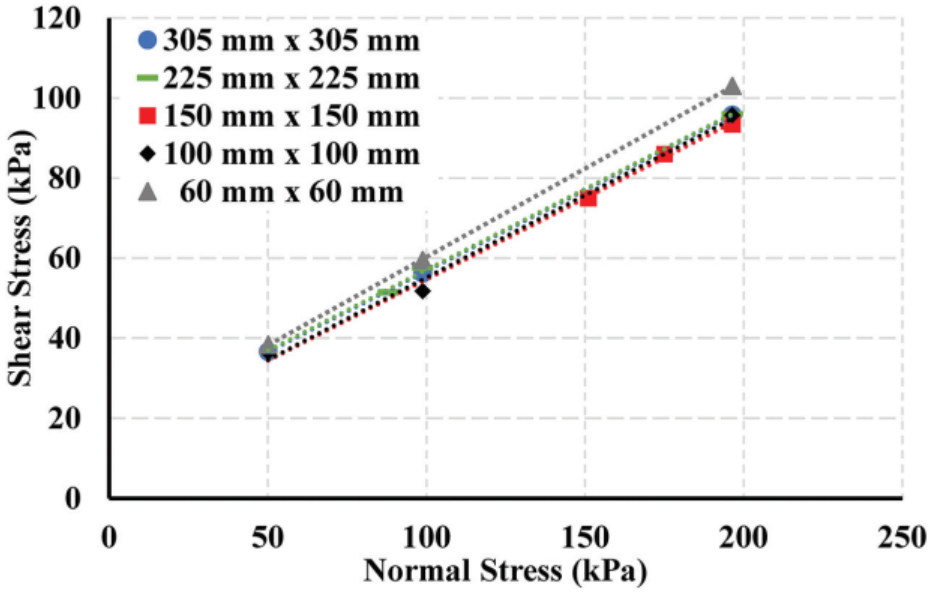

Figure 2.12: Shear stress versus normal stress for all the tests.

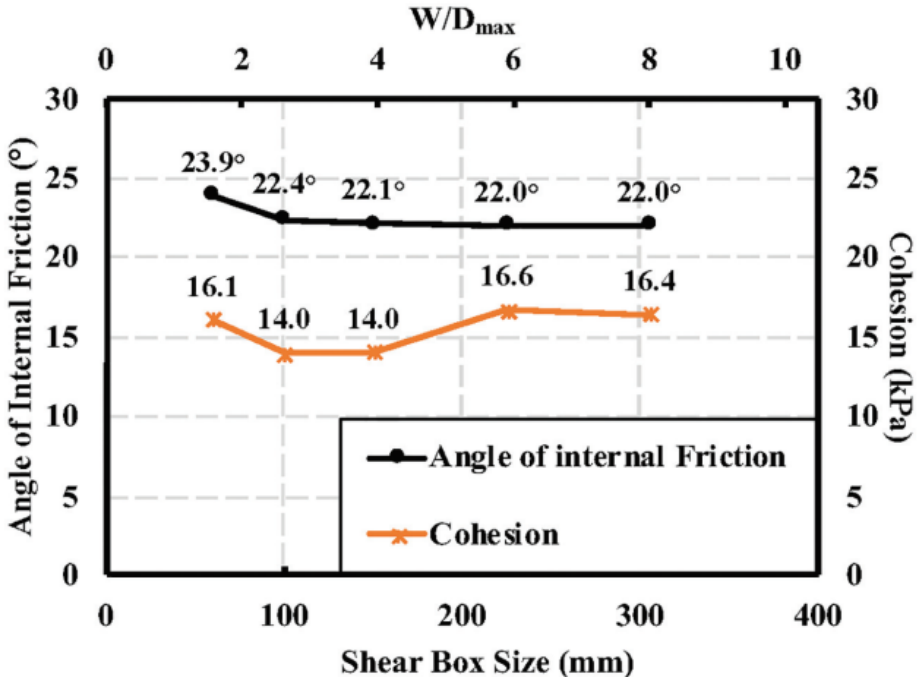

Figure 2.13: Angle of internal friction (°) versus shear box size

internal friction of almost 0.1° occurred with the decrease in shear box size from 225 to 150 mm (i.e., for the W/D_{max}= 4 test). The angle of internal friction increased by only 0.3° with the decrease in shear box size from 150 to 100 mm (W/D_{max}= 2.6). Finally, there was a sizable increase of 1.5°

in the angle of internal friction with the decrease in shear box size from 100 to 60 mm. On the other hand, the cohesion resulting from interlocking among the TDA particles was almost identical for the shear boxes measuring 305, 225, and 60 mm. While it was less by only 2 kPa in the 150 and 100 mm shear boxes, respectively, which is marginal. The average cohesion for all the mentioned shear boxes was around 16 kPa, which is practically small. So, the shear strength of TDA is primarily controlled by its angle of internal friction. It can be seen in Figure 6 that the difference in the angle of internal friction between $W/D_{max}= 4$ and $W/D_{max}= 6$ is only 0.1°. Therefore, based on the obtained results, it is recommended that a shear box with an aspect ratio (W/D_{max}) greater than or equal to 4 should be used when evaluating the shear strength parameters of TDA. If a smaller box is to be used, the differences in the strength parameters should be taken into consideration when TDA shear test results are used in the design.

One of the previous studies conducted on a TDA sample having a maximum particle size of 1.5 in., similar to the sample used in this study, was done by Humphrey et al. (1993) using a 286 mm square shear box in which the angle of the internal friction was reported to be 25. The difference between Humphery's finding and the angle of internal friction reported in this research for the 305 mm shear box could be a result of the difference in the dimensions of the two used shear boxes and that the TDA used in Humphrey was tested in its original state without removing the protruding wires so the interlocking between the particles as well as the extra friction between the protruding wires and the shear box walls resulted in a higher shear resistance.

Vertical Strain Behavior

Moreover, as shown below in Table 4, for the shear boxes measuring 305, 225, and 150 mm, the strain behavior was contractive under all normal stresses applied to the sample. However, for the shear boxes measuring 100 and 60 mm, the strain behavior was contractive-dilative. As a result of

Table 4: Strain Behavior under the Normal Stresses Applied to the Different Shear Boxes

Shear box	Normal stress (kPa)	Unit weight after normal stress is applied (kN/m^3)	Strain behavior
305 × 305 mm	50.1	6.3	Contractive
	98.8	7.25	
	196.4	8.3	
225 × 225 mm	87.91	6.34	Contractive
	98.8	7.3	
	196.4	8.1	
150 × 150 mm	151	6.33	Contractive
	175	7.28	
	196.4	8.22	
100 × 100 mm	50.1	6.4	Contractive-dilative
	98.8	7.34	
	196.4	8.25	
60 × 60 mm	50.1	6.3	Contractive-dilative
	98.8	7.3	
	196.4	8.1	

the compressibility of the TDA particles and the presence of voids within the TDA sample, the TDA particles tended to fill these voids by being compressed and sliding on each other leading to a contractive strain behavior in the first three shear boxes. However, the TDA particles in the smaller shear boxes are relatively large compared with the shear box size. So, the particles tend to slide on each other during shearing till not enough space exists within the sample, so the particles start to push against the shear box top plate leading to a contractive-dilative behavior.

Conclusion

To study the effect of sample size on the shear strength parameters of TDA, a nominal 1.5-in. TDA sample was tested by using five different shear boxes, in a total of 25 tests. In addition, some tests were duplicated to validate the results. From the test results, the following conclusions can be drawn:

- The angle of internal friction of TDA increases as the size of the shear box decreases while the cohesion did not show a definite trend.
- The increase in the TDA angle of internal friction observed for the small shear box (60 3 60 mm) could affect the design; thus, such results must be used with caution. Therefore, for evaluations of TDA shear strength, the use of a direct shear box with an aspect ratio of shear box width to maximum particle size (W/D_{max}) of 4 or larger is recommended.
- The difference in cohesion among the different used shear box sizes was negligible, with a maximum variation of 2.4 kPa, which would not affect the design. The contractive-dilative strain behavior observed in the two smaller shear boxes probably occurred as a result of the presence of large TDA particles that did not have enough space to be compressed. Because this behavior contrasts with TDA behavior in real site conditions, the contractive strain behavior observed in the shear boxes measuring 305, 225, and 150 mm could be a more reliable indicator to use when considering the settlement behavior of TDA layers in engineering projects such as road subgrades and road embankments.
- ASTM D3080-11 recommends a W/D_{max} ratio greater than 10. This ratio should not be imposed for TDA since the results of the TDA tests showed that the same shear strength was obtained when using shear boxes with a W/D_{max} ratio as low as 4.

2.3. Effect of the Particle Size on TDA Shear Strength Parameters in Triaxial Tests

Materials and Methods

The TDA samples tested in this research were shredded at Halifax C&D Recycling Ltd., Halifax, Nova Scotia, Canada, using the conventional tires shredding method by passing scrap tires through shredders in successive shredding cycles until reaching the targeted particle size range. In this study, five TDA samples with different maximum particle sizes, D_{max}, of 19.05, 25.4, 38.1, 50.8 and 76.2 mm, were tested. The used TDA samples are classified as Type A—TDA as per ASTM D6270-08 with an average aspect ratio of approximately 2, defined as the ratio between the length to the width of the particle.

Any protruding steel wires from the TDA particles were removed entirely to protect the triaxial membrane from puncturing. So, the shear strength parameters, especially the cohesion resulting from these samples, are expected to be slightly conservative compared to the actual TDA used in civil engineering applications. The samples were sieved following the ASTM C136/C136M—14 procedures. In this study, the TDA samples were having a particle size range between 9.5 mm up to the maximum particle size (D_{max}) existing in each sample, as shown in the gradation curves in Figure 2. Besides, the samples were named according to their maximum particle sizes (D_{max}). The compacted unit weight of the tested samples was 6.6 ± 0.3 kN/m^3.

The properties of the five samples are summarized in Table 2.5. The coefficient of uniformity increases as the maximum particle size increases, which means that the sample with larger particle sizes covers more particle size range than the samples with smaller particle sizes.

Large-Scale Triaxial Apparatus

In total, 18 consolidated drained large-scale triaxial tests were performed to assess the effect of the particle size on the shear strength and stiffness parameters of TDA. The samples were tested using

Table 2.5: Characteristics of the TDA used in the research.

Characteristics	Sample#1	Sample #2	Sample #3	Sample #4	Sample #5
D_{10} (mm)	9.8	10	12	13.1	13.2
D_{30} (mm)	12.4	13.2	16	19	25
D_{50} (mm)	14	16	25	29.5	33
D_{60} (mm)	15.5	17	27.5	33	39
D_{max} (mm)	19.05	25.4	38.1	50.8	76.2
Size Range (mm)	9.5–19.05	9.5–25.4	9.5–38.1	9.5–50.8	9.5–76.2
C_u	1.58	1.70	2.29	2.52	2.95
C_c	1.01	1.02	0.78	0.84	1.21
USCS Classification	Poorly graded	Poorly graded	Poorly graded	Poorly graded	Poorly graded

a large-scale triaxial cell 152 mm (6 inches) in diameter by 320 mm in height, which is around 2.1 times the sample diameter and is in the range suggested by ASTM D7181-11. The axial loading was applied using the Instron 8501 hydraulic load frame (Norwood, MA, USA). A 1 mm/min shearing rate was used in this study calculated in compliance with ASTM D7181-11 to allow the dissipation of any excess pore water pressure. An external load cell was used to record the axial load. Moreover, a linear variable displacement transducer (LVDT) was used to record the axial displacement. Two GDS Advanced Pressure-Volume Controllers (ADVDPC) were used to record the volume change of the sample and control the pressure during the shearing phase. The two pressure-volume controllers were kept at the same height and calibrated before each test to minimize the errors. Figure 3 shows the triaxial apparatus used in this research.

The height of the shaft used in the triaxial apparatus was increased to accommodate the excessive consolidation that occurs to the TDA samples due to the presence of large voids between the TDA particles and also to allow reaching the targeted 20% strain level. The connection between the piston and specimen cap was a rigid connection so that the titling in the specimen cap will be minimal, as recommended by ASTM D7181-11. Choosing a rigid connection between the shaft

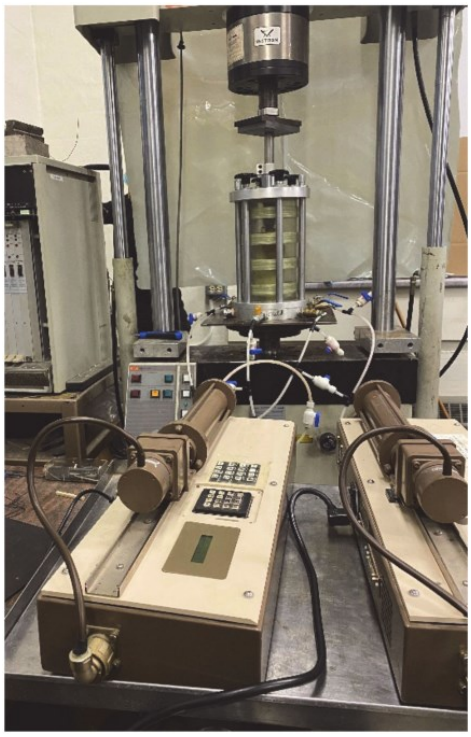

Figure 2.14: The Triaxial testing setup.

and the specimen cap is recommended when testing a highly elastic material as TDA because TDA particles have very random shapes that will be too tough to level the surface of the sample without cap tilting. This kind of connection was modified after Baldi et al. (1988) by permission from ASTM International, and it was verified by some researchers as Lade (2016).

Testing Scheme

The TDA samples were checked for any protruding steel wires to avoid the puncture of the triaxial membrane. The specimens were compacted using a modified proctor hammer. Extensive care was given to the membrane during compaction to avoid membrane puncturing, and the compaction was done on five layers. According to ASTM D6270-08, compaction energy higher than 60% of the standard proctor will not affect the compacted unit weight of TDA significantly. So, compaction energy equal to, or slightly higher than, 60% of the standard proctor was applied to each sample. Researchers found that oven-dried TDA has different physical properties, and adding

water to the sample will not affect the compacted unit weight. So, compaction was done on air dried samples (Ahmed and Lovell 1993, Humphrey and Eaton 1995, Moussa and El Naggar 2020 and 2021 and Moo-Young et al. 2003).

The sample preparation was done in the following steps. First, the split mold was secured around the bottom and the top using hose clamps and a relatively thick Humboldt membrane was stretched around the split mold. Then, a vacuum was applied between the membrane and the compaction mold so the membrane will be stretched. After that, the sample was divided into five portions and each portion was weighed and added to the mold so that the compaction will be applied on five layers till reaching the targeted compacted unit weight. Next, the surface was levelled, and a porous stone was added to the top of the sample and the sample was inverted and centered over the base of the triaxial covering the two water inlets. The specimen cap and a porous stone were added to the top surface of the sample after levelling it as possible. In order to ensure the isolation between the cell pressure and the backpressure, two hose clamps were tightly secured around the specimen cap and the triaxial bottom plate. After that, the sample height and diameter were measured three times to calculate the initial volume of the specimen. Then, the shaft was connected to the specimen cap with grease on it to minimize the friction, and the cylindrical triaxial cell was assembled and placed in the center of the load frame. Finally, the loading frame was lowered to be barely touching the sample so that the uplift force, during saturation, will not push the shaft upward.

The triaxial was filled up with water at a low pressure of 10 kPa, to circulate the water through the entire triaxial cell and the two pressure-volume controllers while the drainage was kept open so large air bubbles will stream out of the system. This flushing procedure minimized the errors that may occur due to the compression of the air bubbles. At that point, back pressure is applied to the sample, so the air voids inside the sample are loaded up with water and entrapped air will be

removed from the entire system. The saturation process is a function of time and pressure. However, due to the high permeability and drainage coefficient of TDA, the saturation phase is relatively simple and fast compared to natural soils. The Skempton's pore water pressure parameter (B) was used to measure the degree of the sample saturation, and all the samples were saturated until reaching a minimum (B) value of 0.98.

The consolidation stage is achieved by increasing the confining pressure while keeping the pore pressure of the sample constant, and it is also considered to be relatively fast. Three confining pressures were used in the research: 50, 100 and 200 kPa. The volume of water driven out of the sample during the consolidation stage was measured using a plastic graduated measuring cylinder, and it was observed that a significant contraction occurred to the samples during the consolidation stage, so the height of the shaft had to be increased to reach the desirable strain level.

To measure the shearing rate, the volumetric change was plotted against the logarithm of the time elapsed. However, the high permeability of TDA resulted in a shearing rate higher than the rate that could be controlled by our volume pressure controllers. So, a lower rate of 1 mm/min was used for all the samples. In the initial tests, a 30% strain level was achieved. However, the samples were subjected to a severe potential of membrane puncturing, so a 20% strain level was chosen for the tests, which is sufficient since the TDA is an elastic material with no peak in its stress-strain curve, and according to ASTM D7181-11, in the absence of maximum stress, the deviatoric stress at 15% should be considered as the maximum stress. Usually, TDA experiences a linear bulging after 10% strain due to the tilting of the specimen cap. However, using a fixed connection between the specimen cap and the shaft resulted in a right circular cylinder deformation as shown in Figure 2.15.

Figure 2.15: The sample deformation at 20% Strain. (mm).

Triaxial tests have several sources of errors that need to be corrected for in order to have more accurate results. Correction for the cross-sectional area during the consolidation and shearing phases is considered the primary source of errors in triaxial tests. Several researchers studied the cross-sectional area correction factor, were they recommended different correction equations to get the effective cross-sectional area.

However, in this research, an advanced MATLAB 2020b model was done to get an exponential equation for the volumetric change from which the effective cross-sectional area and the volumetric strain were calculated. These correction factors were applied to the results before evaluating the shear strength parameters.

Results

A total of 18 triaxial tests were conducted under consolidated drained conditions using three confining pressures; 50, 100, 200 kPa to resemble the stress levels expected in backfills, embankments and behind retaining walls. A total of five samples were tested, having an increasing maximum particle size (D_{max}) ranging between 19.05–76.2 mm. All the samples had a diameter of 150 mm and a height of 320 mm.

Consistency and Repeatability of the Tests

The random nature of TDA raises some doubts regarding the repeatability and accuracy of the driven tests. So, the 25.4 mm sample was duplicated under the three confining pressures to validate the repeatability and accuracy of the results. Figure 16 shows that the deviatoric stress-strain curves of the duplicated tests are in strong agreement, which proves the consistency and the accuracy of the results. The volumetric strain for the duplicated tests also showed an agreement between the results, as shown in Figure 17. The difference between the curves is minimal, which could be neglected and will not significantly affect the shear strength parameters.

Stress-Strain Curves

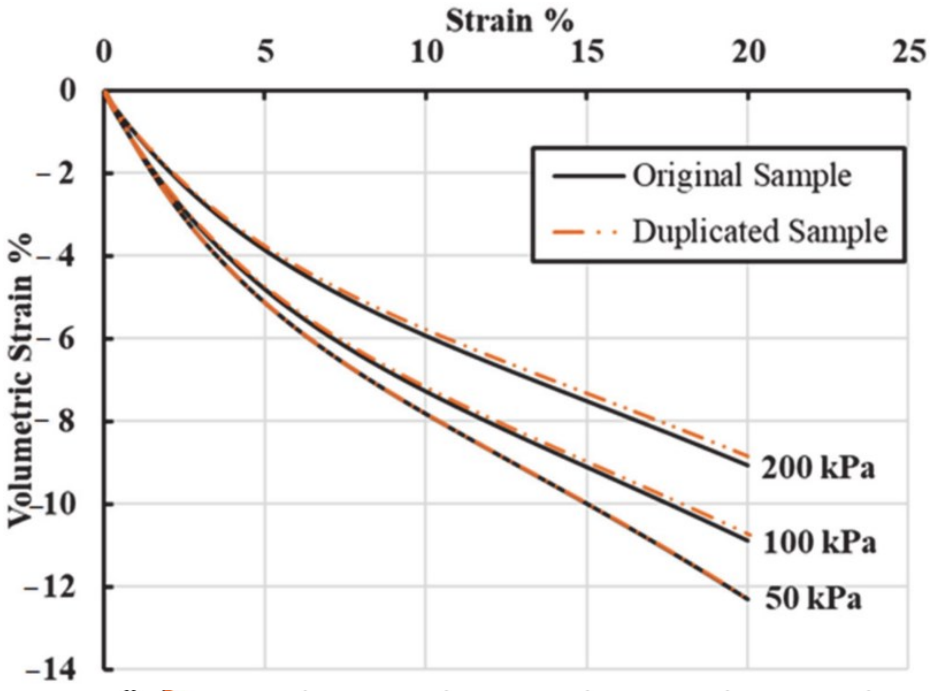

Figure 2.17: Volumetric strain vs. strain % curves for the duplicated tests for the 25.4 mm

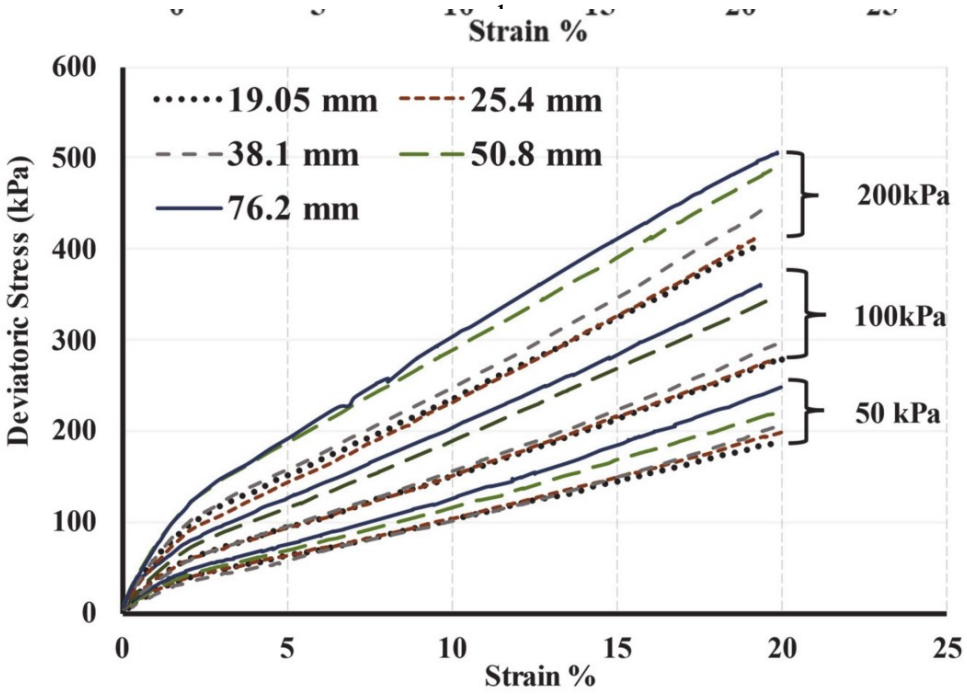

Figure 2.18: Deviatoric stress-strain curves for the five samples.

Figure 2.18 shows that all the samples exhibited a bilinear stress-strain behavior with a close initial stiffness for the 19.05, 25.4 and 38.1 mm samples and a higher stiffness for the 50.8 and 76.2 mm samples. The samples undergo an initial steep increase in the deviatoric stress up to 2% strain,

followed by a linearly increasing deviatoric stress up to 20% strain level. The deviatoric stress-strain curves of this study are in agreement with the previous studies conducted by Chaney et al. 1996, Lee et al. 1999, Youwai and Bergado 2003, and Zornberg et al. 2004. These researchers reported fairly linear deviatoric stress-strain curves. The slight difference in the results between this study and the previous studies may be attributed to: (1) The different maximum particle size used. (2) Different samples with different gradation curves. (3) Different TDA composition depending on the TDA source (4) Most importantly, the random nature of TDA.

TDA samples do not reach a peak in their deviatoric stress-strain curves, and this phenomenon is clearly observed in Figure 2.18. However, ASTM D7181-11 recommended considering the deviatoric stress at 15% to be the maximum stress when no peak is observed in the stress-strain curve. Several practitioners used the deviatoric stress at 10% strain as the maximum stress for TDA to evaluate the shear strength parameters. In this study, shear strength parameters were calculated at both 10% and 15% strain levels. Mohr-Coulomb failure criterion was used in evaluating the shear strength parameters for the five tested samples. The angle of internal friction and cohesion were evaluated as using the following equation from Holtz and Kovacs (1981).

$$\tau = c' + \sigma' \tan\varphi' \tag{10}$$

where t is the deviatoric stress at 10% and 15% strain levels, c' is the effective cohesion, which is the y-intercept, and φ' is the effective angle of internal friction.

Table 2.6 shows that the angle of internal friction increased by increasing the maximum particle size, D_{max}. However, cohesion was almost constant within a range of 3.3 kPa or less. Moreover, considering the deviatoric stress at 10% strain as the maximum stress results in more conservative shear strength parameters.

Table 2.6: The shear strength parameters for the five samples.

Sample (D_{max})	Strain 10%		Strain 15%	
	Angle of Internal Friction, φ' (°)	Cohesion, c' (kPa)	Angle of Internal Friction, φ' (°)	Cohesion, c' (kPa)
19.05 mm	17.8	21.6	21.3	30.5
25.4 mm	18.3	21.6	21.5	29.5
38.1 mm	18.6	19.4	22.3	28.7
50.8 mm	21.4	20.5	23.8	30.6
76.2 mm	21.8	23.4	25.6	32

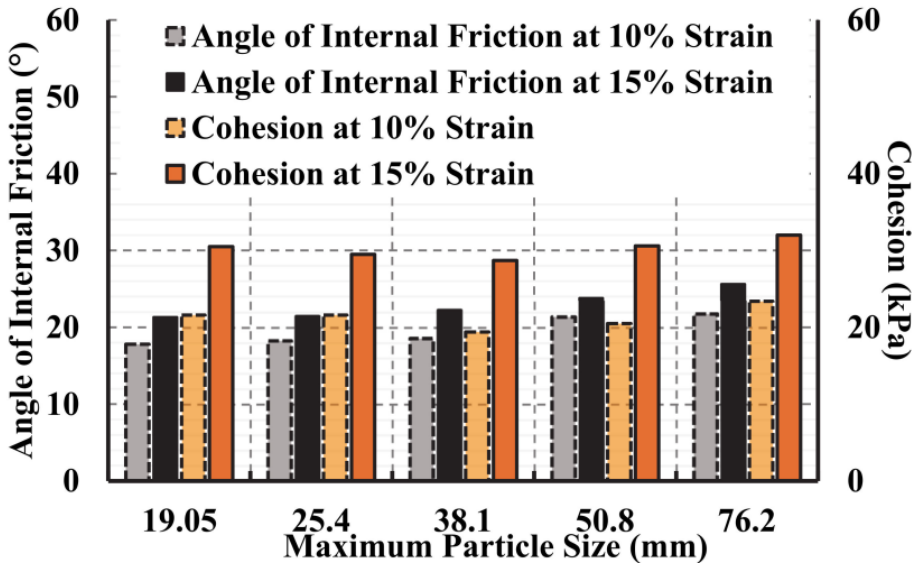

Figure 2.19: Angle of internal friction and cohesion for the five samples.

To simplify the understanding of the results, the results were plotted in columns, as shown below in Figure 2.19. The maximum difference in the angle of internal friction and cohesion between the samples is 4◦ and 4 kPa, respectively, when considering the maximum stress to be at 10% strain. While the maximum difference becomes 4.3◦ and 3.3 kPa, respectively, when considering the maximum stress to be at 15% strain. It can be noted that up to a maximum D50 of 38.1 mm, the strength parameters were very close.

Figures 2.20 and 2.21 present the relations between the angle of internal friction and the cohesion, at 10% strain, with the uniformity coefficient, C_u, of the tested TDA samples and their maximum

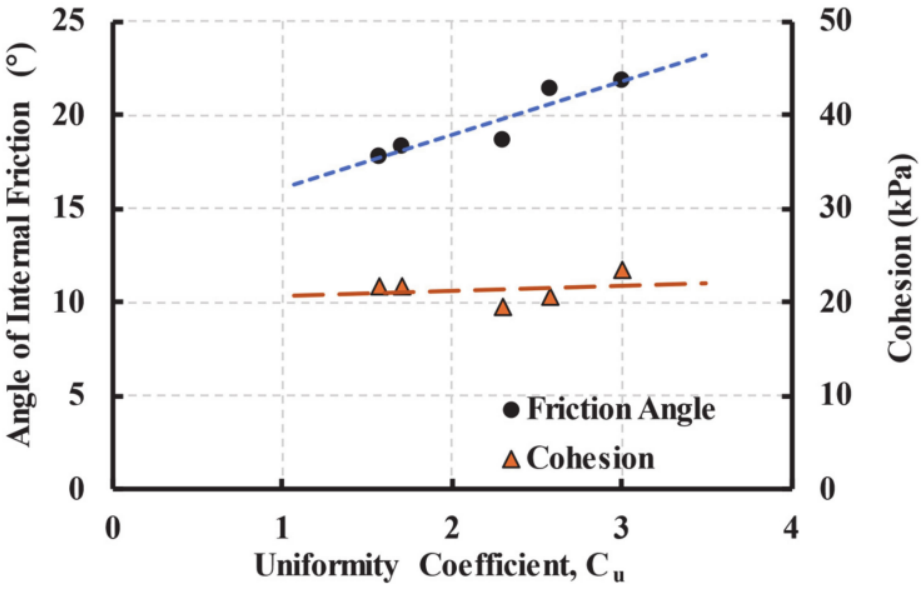

Figure 2.20: Angle of internal friction and cohesion for the five samples vs. their uniformity coefficient.

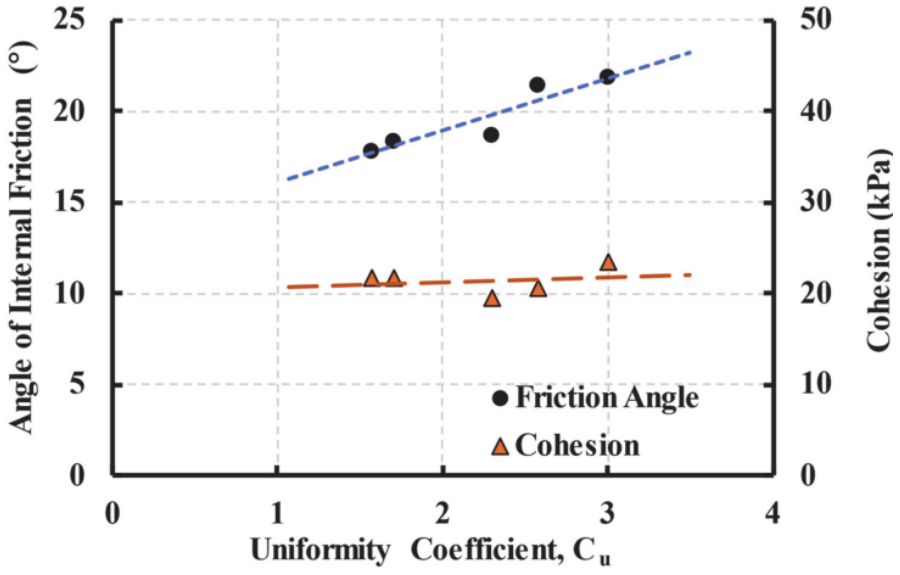

Figure 2.21: Angle of internal friction and cohesion for the five samples vs. their maximum particle sizes.

particle size, D_{max}, respectively. It can be seen from the figures that the relationships between those parameters and friction angle are linear and increase as the C_u and D_{max} increase. However, those parameters were found to have an insignificant effect on the cohesion.

Volumetric Strain

The deformation that happens for saturated nature soils is mainly due to the expulsion of water from the samples voids, the reorientation of the soil particles and the deformation of the soil particles, which is almost negligible (Yi et al. 2015). However, highly elastic material as TDA deforms for the following reasons: (1) Reorientation of the TDA particles, which is generally irrecoverable when unloaded; (2) Compression of the TDA particles, unlike conventional soils, and this is generally recoverable when unloaded. (3) Unlike conventional soils, bending of TDA particles contributes to the majority of the compression that happens to the TDA when loaded (Meles et al. 2013).

Figure 2.22a–c show the volumetric strain that occurred to the five samples under the three confining pressures. The samples showed a steep volumetric contraction followed by a steady decrease in the rate of volumetric change as the strain increases. The maximum particle size (D_{max}) did not show a correlation with the volumetric strain % as under the 50 kPa confining pressure, the volumetric strain % decreased by increasing the maximum particle size. However, under the 100 and 200 kPa confining pressures, there was no correlation between the maximum particle size and the confining pressures, as shown in the following figures. Overall trends in volumetric responses are very similar under the three confining pressures with a little decrease in the magnitude as the confining pressure increase. The confining pressure showed an inversely proportional correlation with the volumetric strain as the volumetric strain decreased when the confining pressure increased. The samples showed a volumetric strain % between 10–12.5% under the 50 kPa confining pressure. However, this range decreased to be 9–10.8% under 100 kPa confining pressure, and the range decreased more under the 200 kPa to be 7.5–9.25%. This

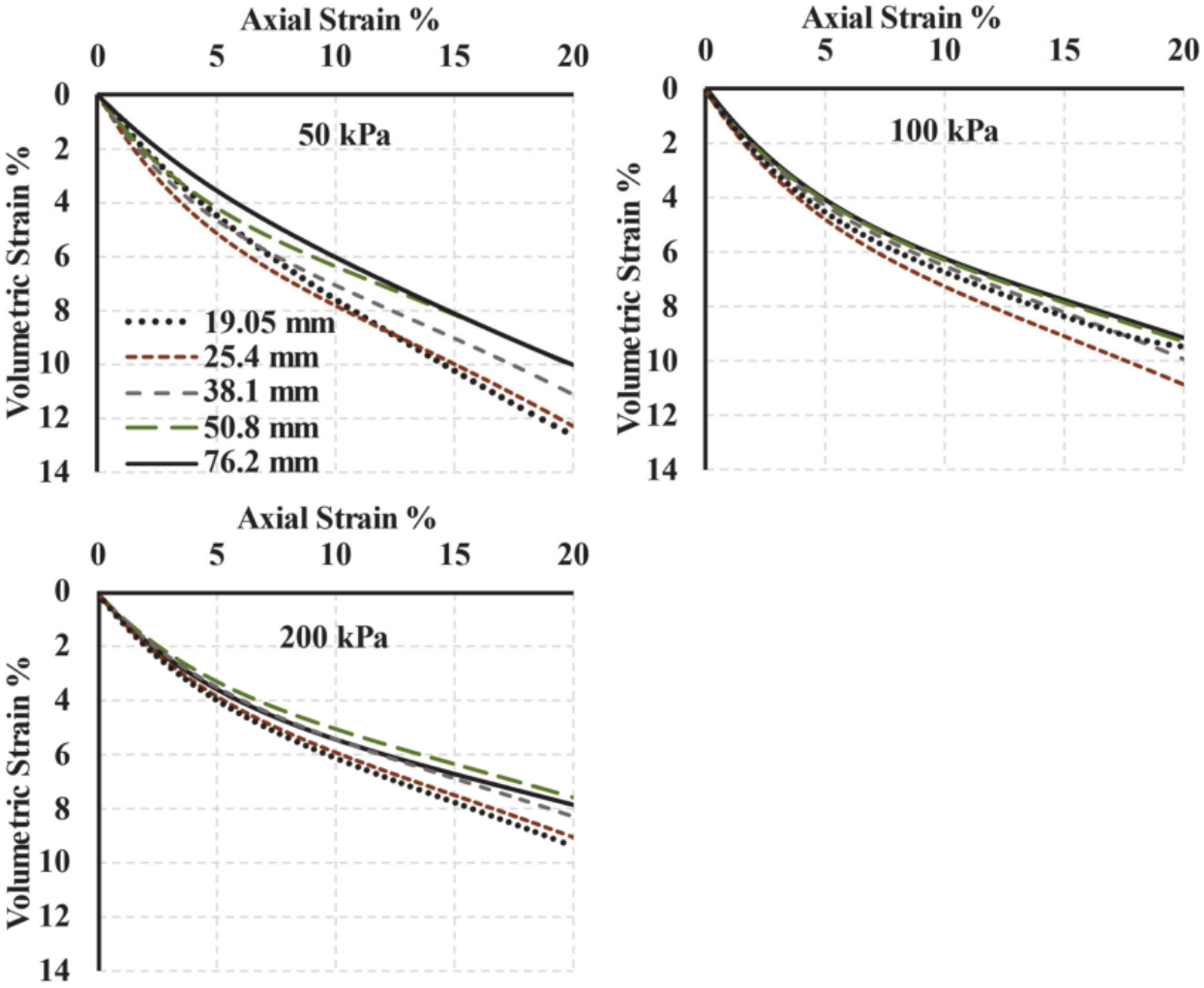

Figure 2.22: Volumetric strain % for the samples under 50 kPa, 100 kPa, and 200 kPa confining pressures, respectively.

behavior could be attributed due to the presence of fewer voids within the samples when the confining pressure increases.

Stiffness

The particle size effect on the stiffness of the five samples was evaluated by calculating the secant elastic modulus, E50, as reported in Figure 2.23. Generally, the elastic modulus reported in this study is in agreement with the elastic modulus of tire rubber reported by [6] that ranged between

730–2400 kPa. The secant elastic modulus was calculated using the following equation from Holtz and Kovacs (1981):

$$E_{50} = \frac{\tau_{50}}{\varepsilon} \tag{11}$$

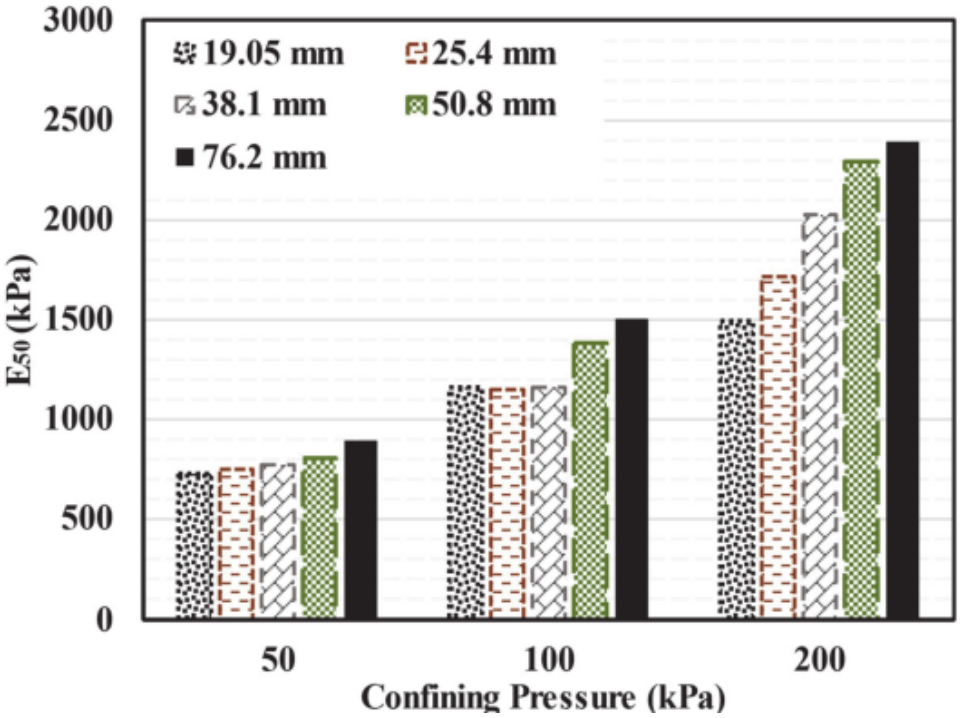

Figure 2.23: The secant elastic modulus at 10% strain.

where τ_{50} is half of the deviatoric stress at 10% and ε is the corresponding axial strain.

Figure 2.23 shows that the secant elastic modulus increases when the particle size increases. In addition, the fact that the elastic modulus increases when the maximum particle size increases is attributed to the less freedom the particles with larger size have to reorient within the sample as the maximum particle size (D_{max}) is increasing while the triaxial cell diameter was kept constant. It could also be attributed to the presence of less steel wires in the smaller particles, unlike the large particles, which usually contain much higher steel wires content.

Stiffness Degradation of TDA

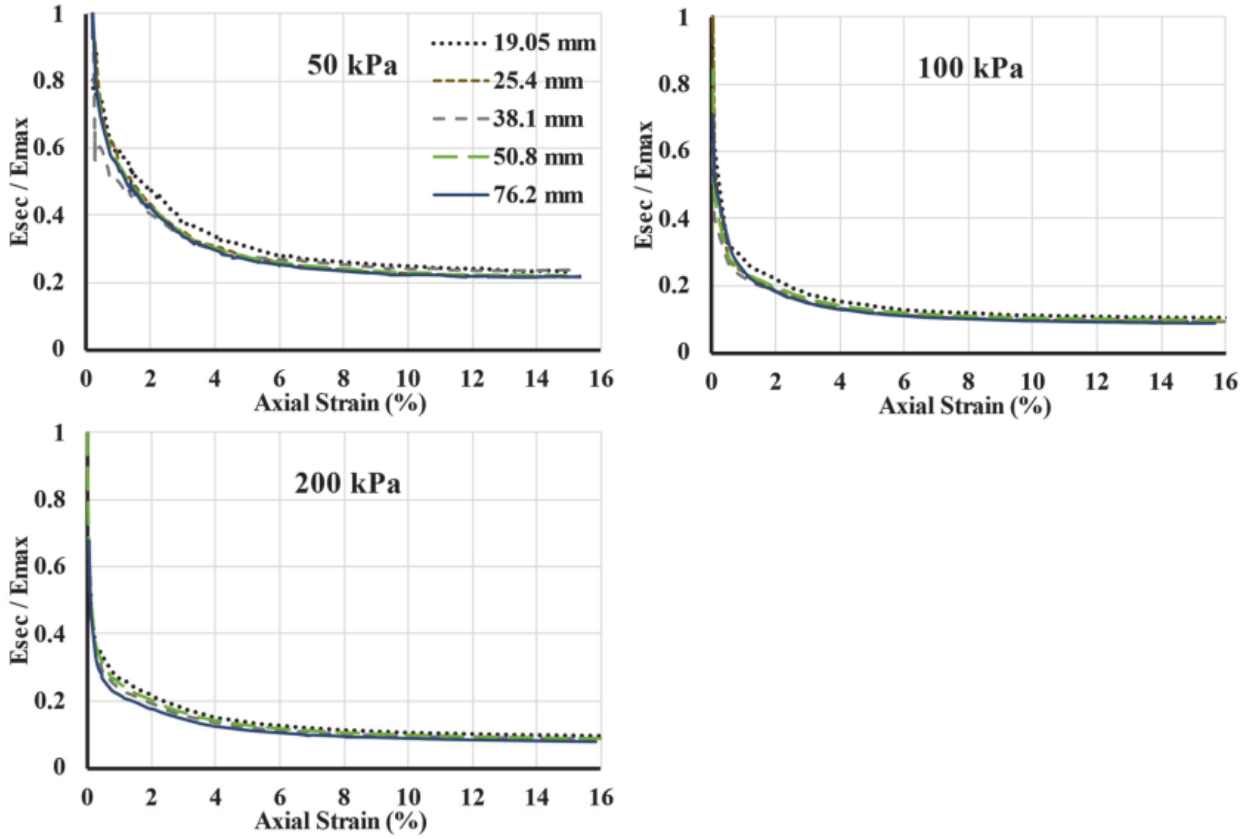

Figure 2.24: Stiffness degradation curves for TDA based on the strain levels.

The stiffness behavior of geomaterials under static loading could be classified according to strain levels (Atkinson and Sallfors 1991) As shown in Figure 2.24, at all strains, the overall stiffness of all specimens under the confining pressure of 200 kPa is higher than those under 100 kPa. Likewise, the stiffness of all specimens under confining pressure of 100 kPa is higher than those under 50 kPa. Figure 13 shows the stiffness degradation behavior of TDA based on the strain levels under the three considered confining pressures. Atkinson and Sallfors (1991) divided strain levels into three distinct groups, (i) very small strains, (ii) small strains, and (iii) large strains. Very small strains could only be induced by geophysical means, and the stress-strain relationships cannot be reliably measured in the lab using mechanical means at this strain level. Hence, it is assumed that the stress-strain behavior is linear elastic in the very small strain range (Atkinson and Sallfors 1991). For TDA, it can be seen from Figures 2.23 and 2.24 that upon reaching a strain level near

0.02%, the stress-strain behavior becomes noticeably nonlinear, and the secant modulus, E_{sec}, begins to degrade nonlinearly with the increasing strain. This strain zone is defined as the small strain zone and ends at a strain level of about 0.3%. The onset of the large strain behavior zone occurs at a strain level of about 0.3%. Also, it can be noticed from Figure 13 that at a strain level of about 1%, the secant modulus of TDA becomes relatively small and loses 50 to 80% of its threshold. Under confining pressures of 100 and 200 kPa, the TDA loses approximately 90% of its stiffness at a 5% strain.

Conclusions

To study the particle size effect on the TDA's shear strength and stiffness parameters, a series of large-scale triaxial tests were conducted on five different TDA samples with maximum particle size (D_{max}) ranging between 19.05–76.2 mm. Based on the results of this study, it could be concluded that:

- The effective angle of internal friction of TDA increases by increasing the maximum particle size.
- The effective angle of internal friction was also found to increase as the coefficient of uniformity increases.
- The cohesion of TDA did not show a defined correlation with the particle size as the cohesion exhibited a slight decrease followed by an increase by increasing the particle size. i.e., the interlocking cohesion of TDA is not significantly affected by the particle size (the difference was less than 3.3 kPa at most). The same conclusion was reported by El Naggar et al. [6] from direct shear tests on TDA.
- The secant elastic modulus of TDA increases by increasing the maximum particle size (D_{max}) or the confining pressure.

- At all strains, the overall stiffness of all specimens increases as the confining pressure increase.
- Upon reaching a strain level near 0.02%, in the small strain zone, the stress-strain behavior becomes noticeably nonlinear, and the secant modulus, E_{sec}, begins to degrade nonlinearly with the increasing strain up to a strain level of about 0.3%.
- The onset of the large strain behavior zone occurs at a strain level of about 0.3%. At a strain level of about 1%, in the large strain zone, the secant modulus of TDA becomes relatively small and loses 50 to 80% of its threshold.
- At higher strain levels, 5% and more, under confining pressures of 100 and 200 kPa, the TDA loses approximately 90% of its stiffness.

3. TDA Soil Mixtures

3.1. Sustainable Mixtures of TDA and Class A Gravel

Material

The gravel and TDA used in this experiment were graded according to the ASTM standard. The gravel used in the experiment was type 1 gravel per Nova Scotia Transportation and Public Works Standard Specification which is equivalent to the commonly known Class A gravel. The particle size distribution of the gravel is shown in Figure 3.1a The TDA used was shredded and manufactured by Halifax C&D Recycling Ltd from discarded passenger tires. The TDA was tested for size gradation and metal fragments, and it complied with Type A TDA per ASTM D6270-08 standard. Figure 3.1b depicts the TDA particle size distribution used in this experiment. As evident from the figure, the size of the TDA particles was in the range of 13-63 mm. To protect the triaxial membrane, the protruding part of the steel wires were removed from the TDA particles. Removing the protruding steel can diminish the ability of TDA particles to interlock during the test which

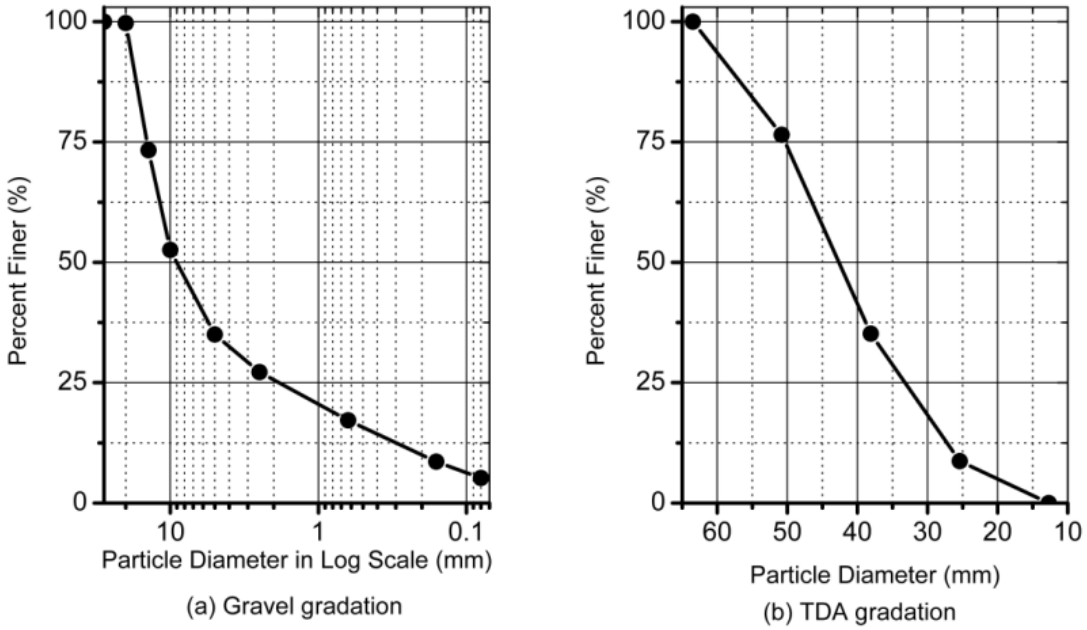

Figure 3.1: Particle size distributions of gravel and TDA.

can decrease the cohesion of the samples. Figure 3.2 represents the results of the optimum water content test for the gravel in accordance with ASTM D698-12.

Triaxial Test Apparatus and Sample Preparation

All triaxial tests in this research were conducted using a large-scale triaxial apparatus capable of testing samples of 152 mm in diameter. In order to apply the axial loading an Instron 8501 hydraulic load frame, capable of recording the load and displacement at a frequency of 20 Hz, was used. Two GDS Advanced Pressure Volume Controllers were utilized to record the volume change of the sample and cell while keeping the pressure constant.

Five sets of samples with different compositions were prepared. Each set included three samples to be tested under three different confining pressures. The sample sets consisted of one set of pure gravel as the reference case and four different compositions of gravel and TDA as shown in Table 3.1. Before compaction, water was added to the gravel to reach optimum moisture content. All samples were compacted with the compaction energy of 600 kilojoules per cubic meter using a standard Proctor.

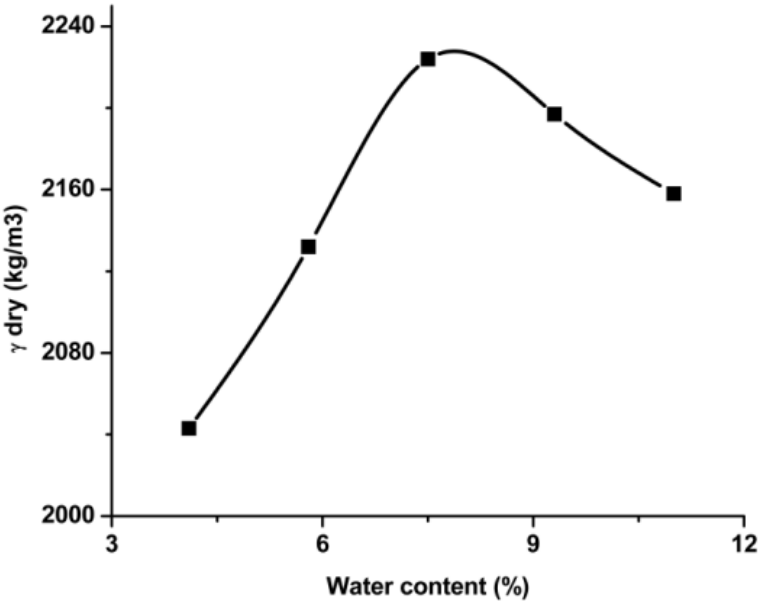

Figure 3.2: Optimum water content of Gravel.

Table 3.1: Mixture properties.

Composition	TDA (%) by weight	Gravel (%) by weight	Dry density (kg/m^3)
Gravel	0	100	2108
M5	5	95	1815
M10	10	90	1749
M20	20	80	1593
M30	30	70	1483

Results and Discussions

As mentioned, for each sample during the axial loading, the volume changes inside the sample were recorded. Using these changes in volume, the amount of volumetric strain of the sample was calculated and plotted against the axial strain. Figure 3.3 compares the amount of volumetric strain of the samples under confining pressure of 100kPa. As shown in the figure, the volumetric strain in the samples with a lower amount of TDA resembles the gravel which is to be expected. On the other hand, as the percentage of TDA increases, this resemblance diminishes. Additionally, it was observed in the experiment, in samples with a lower amount of TDA, confining pressure influences volumetric strain. However, this influence reduces as the percentage of TDA increases. This can be seen more prominently in M30 samples which behave similar to pure TDA sample.

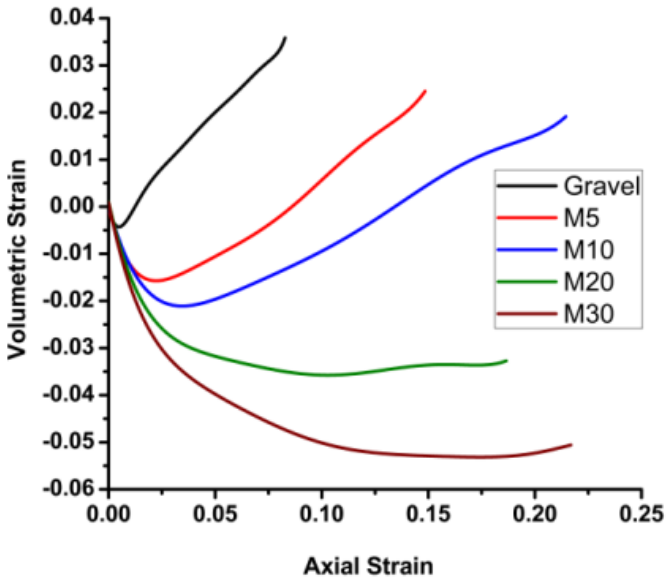

Figure 3.3: Volumetric strain of the samples under 100 kPa confining pressure.

The results of deviatoric stress versus strain for all the sample sets at confining pressures of 50kPa, 100kPa and 200kPa are compared in Figure 3.4. The ASTM correction for changes in length and volume were applied when plotting the graphs. It can be seen that for all samples except M30 after the deviatoric stress reaches a peak amount, it starts decreasing gradually. In other words, as the percentage of TDA increases, the sample behavior shifts from pure gravel behavior towards pure TDA behavior which is to be expected. It is possible that if the test were continued beyond the strain of 20%, the deviatoric stress would have reached a peak maximum but continuing the test was beyond the capabilities of the triaxial apparatus. Even reaching these high amounts of strain

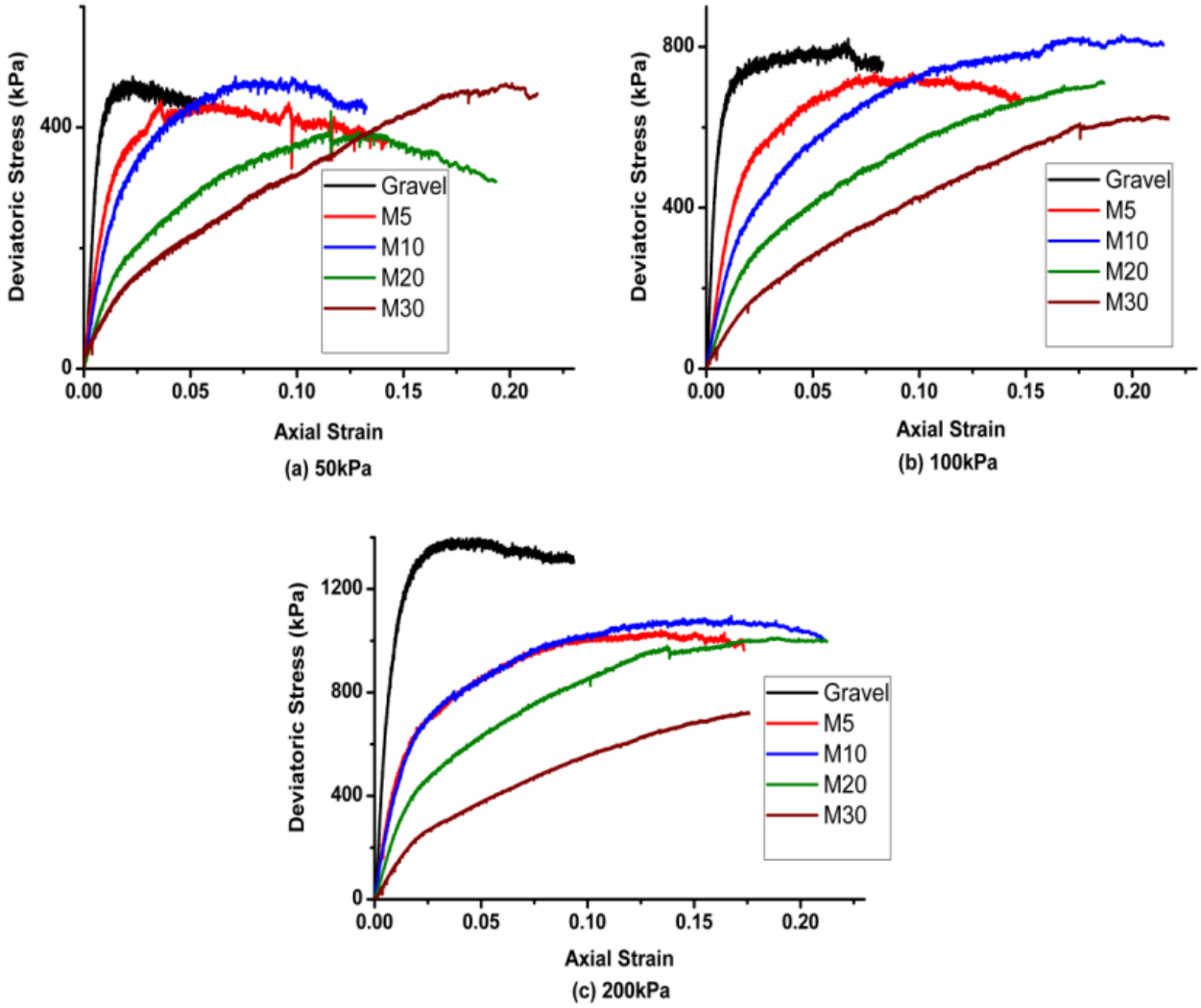

Figure 3.4: Comparison of deviatoric stress vs. strain in each confining pressure.

required tweaking the triaxial machine and extending the axial loading shaft. It is evident that as the percentage of TDA increases, the curves become less steep. That is to say, increase in the percentage of TDA reduces the stiffness of the samples. In addition, the increase in the percentage of TDA increases the strain that the peak maximum deviatoric stress occurs in. Compared to the results of other TDA mixtures, it seems that the M10 has a higher amount of peak maximum deviatoric stress in all three confining pressures.

Table 3.2 provides the values for cohesion and the angle of internal friction for different mixtures based on Mohr-Coulomb failure criterion. These values were calculated using the ultimate limit state. The table suggests that by adding TDA to gravel, the angle of internal friction decreases while the cohesion increases.

Table 3.2: Values of cohesion and the angle of internal friction.

Composition	Cohesion (kPa)	The angle of internal friction (φ)
Gravel	-	49
M5	62	41
M10	68	42
M20	51	42
M30	109	36

Conclusions

In this study, a series of triaxial tests were performed on different mixture compositions of TDA and gravel. The gravel used in this study was Class A gravel. The TDA used in the study was TDA type A per ASTM D6270-08 which is the size used in most civil engineering projects. Sample sets were prepared with varying percentages of TDA. Each sample set was tested in three different confining pressures, and the results of deviatoric stress and volumetric strain versus axial strain were depicted. Finally, the values of cohesion and the angle of internal friction for each mixture

composition were presented. Based on the results of the conducted testing program, the following conclusions can be drawn:

- As the percentage of TDA in compositions increases, the volumetric strain of the samples changes its behavior;
- Increase in the percentage of TDA leads to increases in the strain that the maximum stress occurs in;
- The sample with 10% TDA exhibits higher amounts of maximum deviatoric stress compared to the other TDA mixtures;
- Sample with lower amounts of TDA have higher strength compared to samples with higher amounts of TDA;
- Adding TDA to gravel increases the cohesion while decreases the angle of internal friction.

3.2. Evaluation of the Shear Strength Behavior of TDA Mixed with Fine and Coarse Aggregates for Backfilling around Buried Structures

Methodology

To address the evaluation of the behavior of soil – TDA mixtures, three types of soil were selected and mixed with various amounts of TDA, ranging from 0% to 100% by weight. The soil types selected were gravelly (coarse grain) soil, sandy (medium grain) soil, and clayey (fine grain) soil. Large-scale direct shear box (305 mm × 305 mm × 220 mm) tests were then performed at confining pressures of 50.1, 98.8, and 196.4 kPa.

Previous research has utilized different experimental approaches, including direct shear tests and the triaxial compression method, to evaluate the shear strength properties and compressibility behavior of TDA and soil-TDA mixtures. In a triaxial compression test, there is full control of the confining pressure and saturation, and the failure progresses in a natural plane. However, there is no control over the pore water pressure at the shear surface in direct shear tests, and the failure plane lies in a predetermined horizontal direction, which may not be the weakest plane. On the other hand, the greater simplicity of direct shear tests compared to the triaxial compression method has made direct shear testing a versatile, frequently used tool for geotechnical designers.

Laboratory Experiments

Materials

The TDA sample used in this study was type A TDA, which was shredded and processed by Halifax C&D Recycling Ltd., located in Enfield, Nova Scotia, Canada. Because most of the TDA particles were flat and elongated, a histogram analysis was performed to find the particle size distribution of the TDA sample, as recommended by Foose et al. (1996) and El Naggar et al.

(2016). To conduct the histogram analysis, a TDA sample weighing about 5 kg was randomly selected and a ruler was used to measure the particles in every direction.

According to ASTM D3080, the maximum particle size of aggregates should be at least 10 times smaller than the length of the shear box, to eliminate boundary effects. However, Humphrey and Sandford (1993) have suggested that for aggregates with larger particles, such as TDA, a direct shear test can be performed with particles that are four times smaller than the length of the shear box. The test results of these researchers showed that the boundary effect is minimized in this case, and the particles are sheared in the box with minimal external effects. This finding was confirmed by Zahran and El Naggar (2020), who likewise recommended the aspect ratio of particles four times smaller than the length of the shear box to eliminate the effect of the size of the shear box in the evaluation of TDA shear strength parameters.

In addition, according to Foose et al. (1996), the use of tire shreds with a maximum length that is less than half the diameter of a direct shear ring reduces the boundary effect during shearing. Since the length of the shear box used in this study was limited to 305 mm, TDA particles exceeding 75 mm in length were removed from the sample (amounting to only 3.9% of the sample). Thus, the maximum particle size was limited to one-fourth of the shear box length, to eliminate boundary and size effects (Humphrey and Thomas 1993 and Zahran and El Naggar 2020). Figure 3.5a presents the histogram of the initial TDA sample, and Figure 3.5b shows the histogram of the sample used in this study, following the removal of the particles exceeding 75 mm in length. As shown in Figure 3.5, TDA particle lengths were mainly in the ranges of 30–40 mm, 40–50 mm, 50–60 mm, 60–70 mm, and 70–75 mm.

The TDA particles had an average length/width aspect ratio of 2.8, and an average thickness of 8.9 mm. The dry unit weight (γ_d) of the TDA sample was determined in accordance with the standard

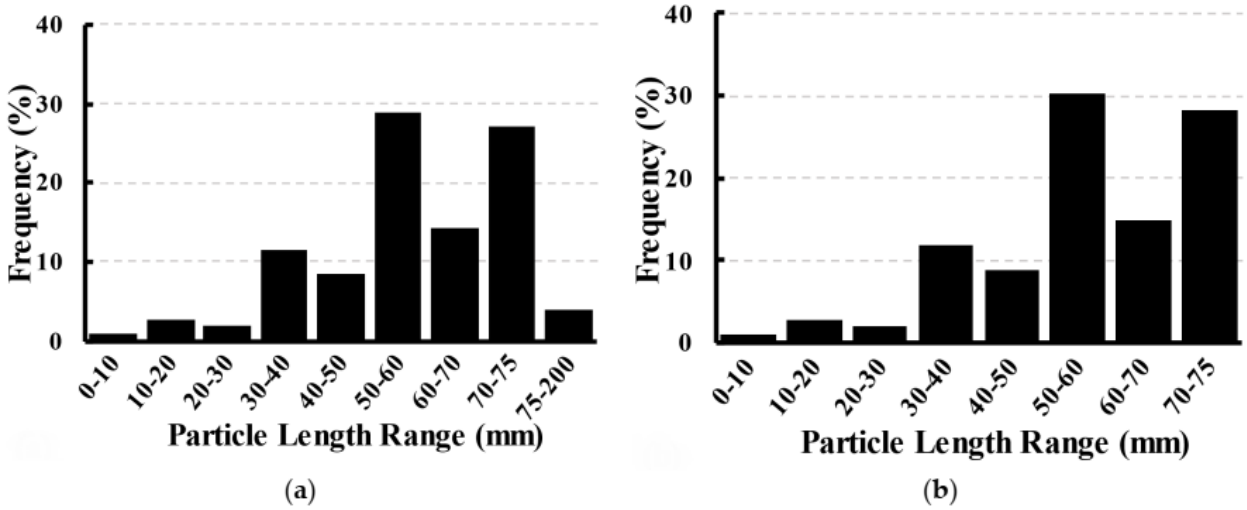

Figure 3.5: Histograms of (a) the initial TDA sample and (b) the TDA sample used in the shear box tests.

test method described in ASTM D698. It should be noted that due to the flexibility of the TDA particles, the compaction energy had a negligible effect on the dry unit weight. Therefore, in accordance with Humphrey and Sandford (1993), 60% of the standard Proctor energy was applied to the specimen. Similarly, because the addition of water to the TDA sample had no effect on the dry unit weight, the compaction test was performed on an air-dried sample (Cecich et al. 2016 and ASTM D6270). Table 3.3 shows the physical properties of the TDA sample used in the shear box tests.

Table 3.3: Characteristics of the TDA and soils used in this study.

Characteristics	TDA	Soil Type		
		Gravelly	Sandy	Clayey
D_{10} (mm) [1]	19	0.30	0.24	0.007
D_{30} (mm) [1]	28	2.40	0.42	0.021
D_{50} (mm) [1]	45	5.90	0.65	0.048
D_{60} (mm) [1]	49	7.00	0.80	0.075
Coefficient of uniformity, C_u [2]	2.58	23.33	3.33	10.71
Coefficient of curvature, C_c [2]	0.84	2.74	0.92	0.84
Optimum water content, ω (%)	-	7.50	13.0	14.0
Maximum dry density, γ_m (kN/m^3)	6.82	19.2	16.8	18.4
Plasticity index, *PI*	-	-	-	9.3

[1] D_{10}, D_{30}, D_{50} and D_{60} represent the particle diameters where the percentage of particles with diameters below these values are 10%, 30%, 50% and 60%, respectively. [2] $C_u = \frac{D_{60}}{D_{10}}$, $C_c = \frac{D_{30}^2}{D_{10}D_{60}}$.

According to ASTM D6270, to ensure the effective use of TDA particles, rubber-to-rubber contact should be maximized by reducing the amount of exposed steel. In this study, wire cutters were therefore used to remove exposed wires from the edges of the TDA particles.

Relatively uniform gravelly and sandy soils obtained from a local supplier were used in this study. In addition, a clayey soil was obtained from land in Enfield, Nova Scotia. In a natural condition, the clayey soil sample had a clayey till characteristic. Therefore, it was first dried at 110 ◦C for 24 h, and then broken down into fine grains before being used in the study. The particle size distribution of the soil samples was determined by using a sieve analysis in accordance with ASTM D422. It should be noted that for the clayey soil, first a sieve analysis was performed to find the distribution of particles larger than 75 μm (retained on the no. 200 sieve). Then, a hydrometer analysis was conducted to find the distribution of particles smaller than 75 μm (which passed through the no. 200 sieve). Figure 3.6 shows the particle size distribution of the TDA and soil samples used in this study.

To find the dry unit weight and optimum water content (ω) of the soil samples, standard Proctor compaction tests were performed in the laboratory in accordance with ASTM D698. An Atterberg

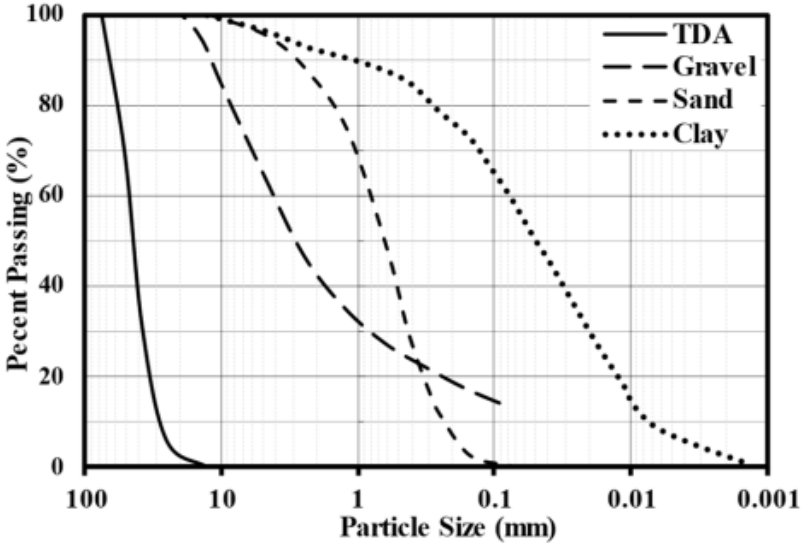

Figure 3.6: Particle size distribution of the TDA and soil samples used in this study.

limit test was also performed on the clayey soil, in accordance with the standard test method described by ASTM D4318, to determine the plasticity index. Table 3.3 presents the physical characteristics of the soil samples used in this study. In accordance with the unified soil classification system procedure (USCS and ASTM D2487), the gravelly soil was classified as well-graded gravel with sand, the sandy soil was classified as poorly graded sand, and the clayey soil was classified as sandy lean clay. Similarly, the TDA was classified as poorly graded, in accordance with the USCS.

Sample Preparation

As described above, in this study three, types of soil were selected to be mixed with TDA particles. Before being mixed with the TDA, the soil samples were dried in an oven for 24 h at 110 ºC and were then broken down into fine grains if required. The TDA sample was air dried at room temperature for 72 h. Following drying of the materials, the required percentages of the soil and TDA samples were measured carefully by weight, according to the planned mixing ratios. In addition, the optimum water content of each soil sample was determined, and a corresponding amount of water was added to each soil sample. The materials were transferred to a tray, where they were mixed carefully until a consistent mixture was obtained. As mentioned above, the optimum water content for compaction of the TDA particles was found to be zero; hence, no water was added to the TDA particles. The mixed materials were then poured gently into the shear box in five layers and compacted by using standard compaction efforts. At each step, the mixture on the tray was mixed thoroughly before being poured into the shear box. Special care was taken, and continuous observations were made, to prevent any inconsistency in the mixtures. This ensured that segregation of the soil and TDA particles did not occur as the sample was prepared and transferred into the shear box. It should be noted that segregation is likely to occur in mixtures

with high percentages of TDA. When segregation occurs, the soil settles beneath the TDA particles, and the mixture loses its consistency. Edil and Bosscher (1994) conducted a series of triaxial tests on mixtures of sand and tire chips. They found that with a tire chip content greater than 30% by volume, segregation increased between the sand and the tire chip particles. Bosscher et al. (1992) likewise conducted a field study, where they observed that segregation occurs in mixtures containing more than 50% TDA by volume.

Table 3.4 shows the percentage of TDA by weight for each mixture. TDA percentages of 0%, 10%, 25%, 50%, and 100% were used. The name of each mixture indicates the mixture contents, where G stands for gravel, S for sand, C for clay, and T for TDA. The digits at the end of each mixture name indicate the percentage of TDA by weight. For example, mixture GT25 contains gravel and TDA, with 25% TDA by weight. It should be noted that the percentage of TDA by weight is defined as the ratio of the weight of the TDA to the total weight of the soil-TDA mixture.

The particle size distributions of the gravel-TDA, sand-TDA, and clay-TDA mixtures are presented in Figure 3.7. Figure 3.7a shows that for a TDA content of up to 25% TDA by weight,

Table 3.4: Properties of the soil-TDA mixtures.

Mixtures	TDA % (by Weight)	Soil % (by Weight)	γ_{bulk} (kN/m^3)	Friction Angle (°)	Cohesion (kPa)
		Gravel-TDA			
GT0	0	100	19.84	44.0	24.8
GT10	10	90	18.38	45.4	17.0
GT25	25	75	14.77	43.9	14.7
GT50	50	50	10.21	42.2	15.4
GT100	100	0	6.81	23.9	18.2
		Sand-TDA			
ST0	0	100	18.73	37.1	4.8
ST10	10	90	17.72	38.4	13.4
ST25	25	75	15.73	38.3	14.3
ST50	50	50	12.06	31.8	16.2
ST100	100	0	6.81	23.9	18.2
		Clay-TDA			
CT0	0	100	20.40	18.8	21.8
CT10	10	90	18.93	32.3	29.2
CT25	25	75	15.33	25.6	29.0
CT50	50	50	11.00	25.0	19.6
CT100	100	0	6.81	23.9	18.2

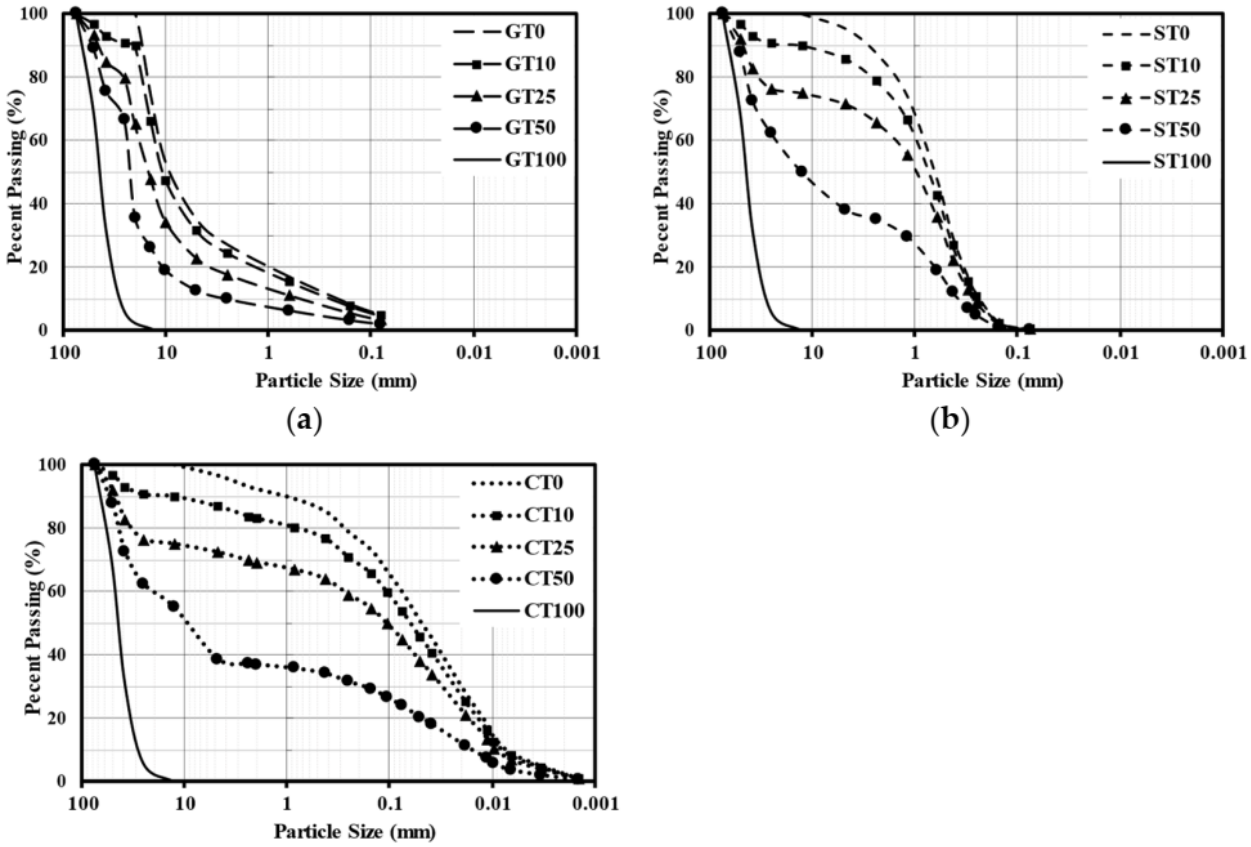

Figure 3.7: Particle size distributions of the (a) gravel-TDA, (b) sand-TDA, and (c) clay-TDA mixtures.

the gravel mixtures had fairly similar gradation characteristics, with D50 values ranging from 9 mm to 13 mm. The gradation characteristics of the gravel-TDA mixture with 50% TDA varied to a greater extent, as the D50 of this mixture was 21 mm, approximately double that of the mixtures GT0, GT10, and GT25. As can be seen in Figure 3.7b, the sand-TDA mixtures exhibited a similar trend, which was further accentuated in the clay-TDA mixtures, shown in Figure 3.7c.

Results and Discussion

Dry Unit Weight of the Mixtures

In Figure 3.8, bulk unit weight is plotted against TDA content for the gravel-TDA, sand-TDA, and clay-TDA mixtures used in the large-scale direct shear tests. For comparison purposes, the TDA content ranges from 0% (corresponding to pure soil) to 100% (corresponding to pure TDA). It can

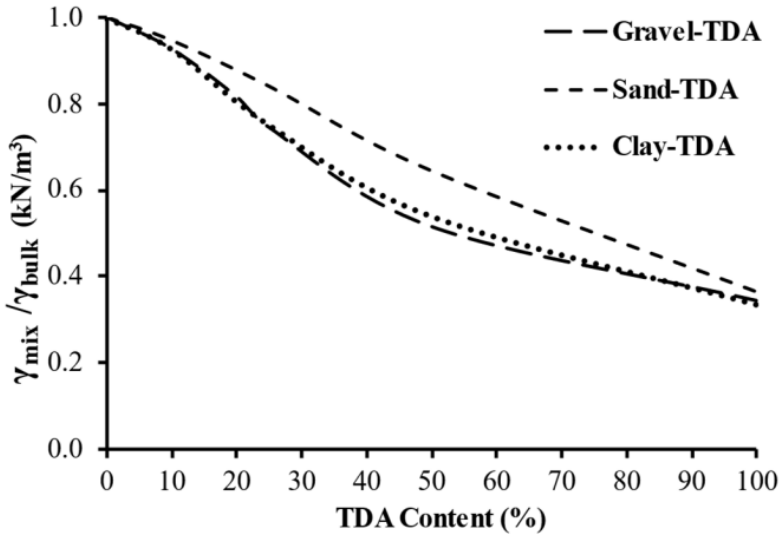

Figure 3.8: Bulk unit weight versus TDA content for the soil-TDA mixtures.

be seen that the dry unit weight of the mixtures decreased considerably as the percentage of TDA increased. It should be noted that this decrease in dry unit weight is due to the low dry unit weight of the TDA (6.82 kN/m3), which is less than half that of the conventional soils used in this study. A reduction in dry unit weight is beneficial for the design of a retaining wall or a box culvert, since in such applications, the lateral earth pressure needs to be minimized for an economic design. In addition, if the soil beneath a fill layer is weak, the use of a light soil mixture helps to overcome this problem. Hence, soil-TDA mixtures can be a useful lightweight alternative in geotechnical applications, especially for backfilling over or around buried pipes and culverts.

Shear Stress versus Shear Strain Behavior

For all of the considered soil-TDA mixtures (i.e., gravel-TDA, sand-TDA, and clay-TDA), direct shear tests were conducted at three confining pressures of 50.1, 98.8, and 196.4 kPa. Figure 3.9 shows the shear stress plotted against shear strain for all mixtures at the considered confining pressures. As shown in Figure 3.9, for 100% gravel (GT0), a peak shear stress was observed at all

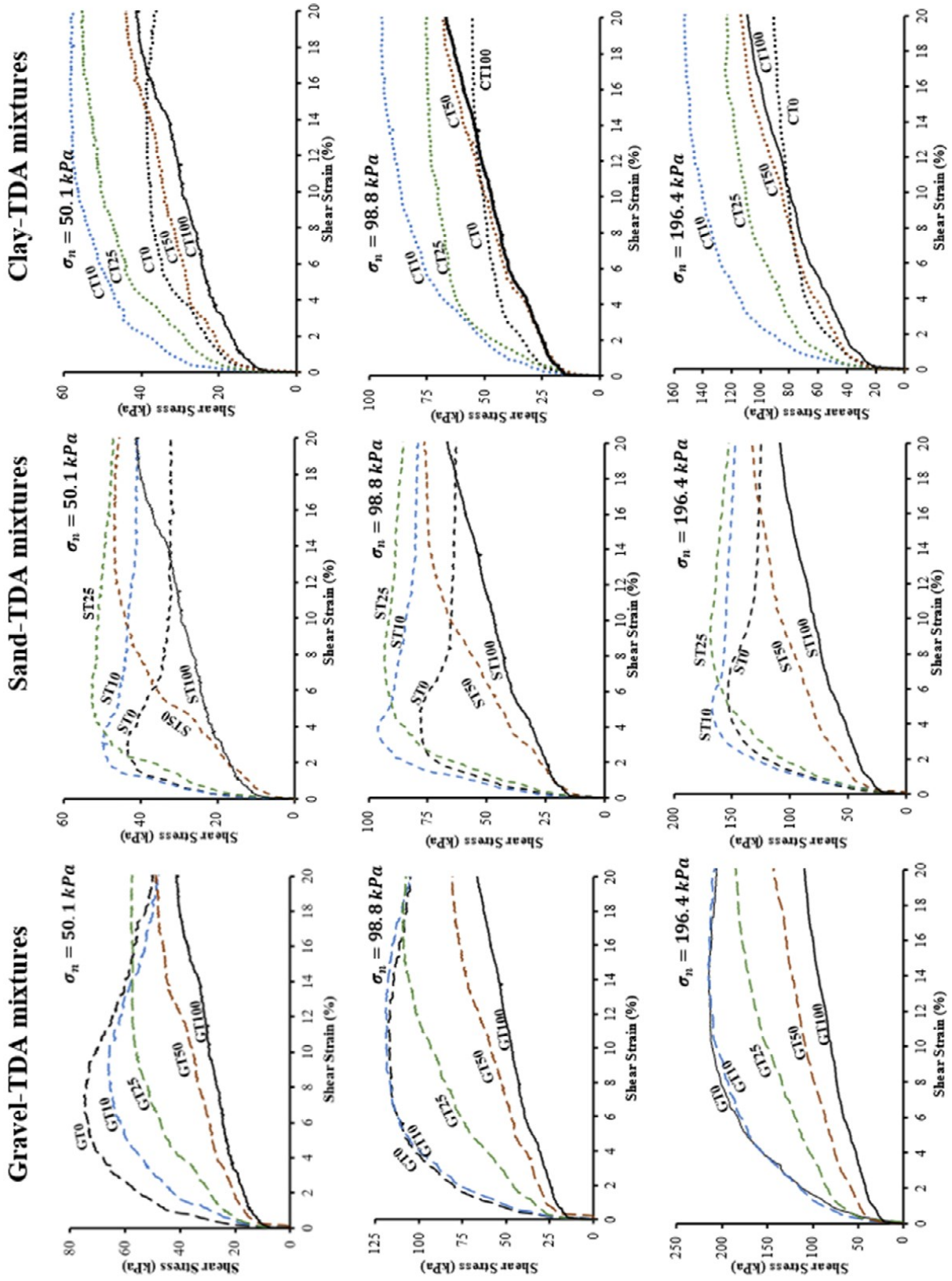

Figure 3.9: Shear stress versus shear strain for the gravel-TDA, sand-TDA, and clay TDA mixtures at confining pressures of 50.1, 98.8, and 196.4 kPa

confining pressures, indicating the shear strength of the samples. Likewise, for the 100% sand (ST0) sample, a clear peak shear stress was also observed at all the confining pressures, indicating the shear strength of the samples in a similar fashion. On the other hand, for the clay-TDA mixtures CT0 and CT10, a peak shear stress was observed at a confining pressure of 50.1 kPa, indicating the shear strength of the samples. However, up to a shear strain of 24%, no peak shear stress was exhibited by any of the samples at confining pressures of 98.8 and 196.4 kPa; in other words, the clay-TDA mixtures exhibited strain-hardening behavior.

It can be seen in Figure 3.9 that the addition of TDA to the gravel decreased the shear strength resistance of the mixtures upon shearing at all of the considered confining pressures. It should be noted that the addition of up to 10% TDA by weight to the gravel did not result in a significant reduction in shear resistance at the confining pressures of 98.8 and 196.4 kPa. It is evident from the figure that the addition of up to 25% TDA by weight to the gravel at confining pressures of 50.1 and 98.8 kPa and the addition of up to 10% TDA by weight at a confining pressure of 196.4 kPa decreased the peak shear resistance gradually at a higher shear strain. For mixtures containing more than 25% TDA by weight at confining pressures of 50.1 and 98.8 kPa, and more than 10% TDA by weight at 196.4 kPa, no peak shear stress was exhibited up to a shear strain of 24%. In other words, the addition of TDA to the gravel resulted in a strain-hardening behavior of the gravel-TDA mixtures, and they did not fail upon applied shearing.

It can also be seen from Figure 3.9 that the addition of up to 10% TDA by weight to the sand then increased the peak shear stress at a similar shear strain. At a confining pressure of 50.1 kPa, increasing the TDA content from 10% to 25% further increased the peak shear stress at a greater shear strain. However, at confining pressures of 98.8 and 196.4 kPa, increasing the TDA content from 10% to 25% by weight did not significantly change the peak shear resistance of the sand-

TDA mixtures. However, the peak shear resistance of the ST25 mixture occurred at a higher shear strain than was the case for the ST10 mixture. Increasing the TDA content to more than 25% then reduced the shear resistance of the mixtures at all the confining pressures considered. It should be noted that mixtures containing more than 50% TDA at a confining pressure of 50.1 kPa and more than 25% TDA at confining pressures of 98.8 and 196.4 kPa did not reach a peak shear stress upon shearing. In other words, the addition of TDA contributed to a strain-hardening behavior of the mixtures in a similar fashion to that observed in the gravel-TDA mixtures.

On the other hand, it is evident from Figure 3.9 that adding up to 10% TDA by weight to the clay increased the peak shear stress significantly at all the confining pressures considered. However, the further addition of TDA beyond 10% by weight then decreased the shear resistance of the mixtures, with no failure occurring up to a shear strain of 24%. It should be noted that although increasing the TDA content from 10% to 25% decreased the shear resistance of the mixtures, the shear resistance was still higher than the shear resistance of clay alone (CT0). It should likewise be noted that, if failure is considered to occur at 10% relative lateral displacement for mixtures that do not exhibit a peak shear stress, among all the mixtures, the highest shear resistance was observed for mixture CT10 and the lowest shear resistance was observed for clay alone (CT0) at all the confining pressures considered. Finally, a comparison of the shear stress versus shear strain results at the confining pressures considered showed that increasing the confining pressure from 50.1 to 196.4 kPa enhanced the shear resistance of mixtures containing the same amount of TDA.

Vertical Displacement versus Shear Strain Behavior

Figure 3.10 shows the vertical displacement plotted against shear strain for the gravel-TDA, sand-TDA, and clay TDA mixtures at the three considered confining pressures. It was observed that gravel-TDA mixtures containing up to 25% TDA by weight were initially compressed and then

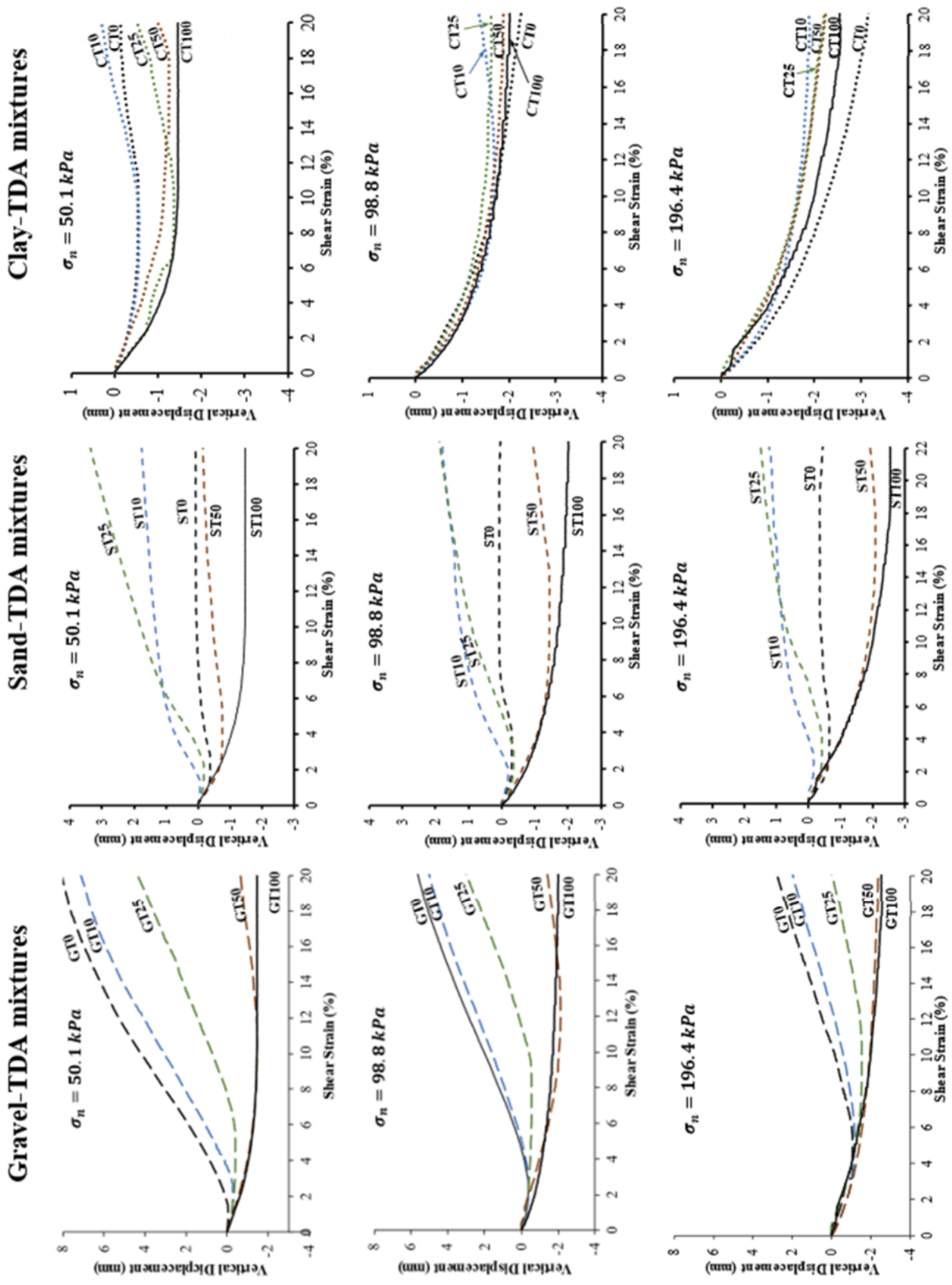

Figure 3.10: Vertical displacement versus shear strain for the gravel-TDA, sand-TDA, and clay TDA mixtures at confining pressures of 50.1, 98.8, and 196.4 kPa

dilated upon shearing. For 100% gravel (GT0), compression was negligible at a confining pressure of 50.1 kPa, and the specimen was mainly dilated upon shearing. However, gravel mixtures containing more than 25% TDA by weight were mainly compressed upon shearing at all the confining pressures considered. It should be noted that in gravel-TDA mixtures containing up to 25% TDA by weight, the dilation upon shearing was greater at a lower TDA content, with 100% gravel (GT0) exhibiting the greatest dilation. In mixtures containing more than 25% TDA by weight, compression increased at a higher TDA content, with pure TDA (GT100) exhibiting the greatest compression.

In general, adding TDA to gravel increased the compressibility behavior of the mixtures upon shearing. Figure 3.10 also indicates that the dilation behavior of the mixtures decreased at greater confining pressures. In mixtures containing more than 25% TDA by weight, increasing the confining pressure from 98.8 to 196.4 kPa caused only a slight change in the compressibility behavior of the mixtures upon shearing. For the sand-TDA mixtures, it was observed that mixtures containing up to 25% TDA by weight were initially compressed and then dilated upon shearing, at all the confining pressures considered similar to the same trend observed for gravel mixtures. For 100% sand (ST0), the dilation upon shearing was not significant at any of the confining pressures, and the sample returned to almost its initial height after compression. In contrast, mixtures containing more than 25% TDA by weight were mainly compressed upon shearing. It should be noted that sand-TDA mixtures containing 10% and 25% TDA by weight exhibited a similar dilation upon shearing at confining pressures of 98.8 and 196.4. However, mixtures containing 50% and 100% TDA by weight exhibited similar compression behavior upon shearing at all the confining pressures considered.

In general, adding TDA to sand increased the compressibility behavior of the mixtures upon shearing. Figure 3.10 also indicates that the dilation behavior of the sand mixtures decreased at greater confining pressures opposite to the behavior observed in the gravel mixtures. As shown in Figure 9, at a confining pressure of 50.1 kPa, pure TDA (CT100) was only compressed upon shearing, but all the other mixtures were initially compressed and then dilated upon shearing. For 100% clay (CT0), the amount of dilation upon shearing was insignificant at a confining pressure of 50.1 kPa, and the specimen returned to its initial height after compression. Thus, at a confining pressure of 50.1 kPa, the addition of TDA increased the compressibility behavior of the mixtures upon shearing, with pure TDA (CT100) exhibiting the greatest compression. It should be noted that clay mixtures containing up to 10% TDA by weight exhibited similar compression upon shearing at a confining pressure of 50.1 kPa. However, the dilation of the mixture containing 10% TDA (CT10) was greater than that of clay alone (CT0). At confining pressures of 98.8 and 196.4 kPa, all the clay mixtures were only compressed upon shearing. It should also be noted that adding up to 10% TDA to the clay decreased the compression behavior of the mixture upon shearing significantly at confining pressures of 98.8 and 196.4 kPa. The further addition of TDA, beyond 10% by weight, then increased the compressibility behavior of the mixtures, however the compression observed was still less than that of clay alone. At confining pressures of 98.8 and 196.4 kPa, the greatest compression upon shearing was exhibited by 100% clay (CT0). Figure 3.10 also indicates that the compression behavior of the mixtures increased at greater confining pressures.

Mohr–Coulomb Failure Criterion for the Mixtures

The Mohr–Coulomb failure criterion was used to find the cohesion and angle of internal friction for the soil-TDA mixtures used in this study. As explained above, each specimen was tested at the

three normal stresses: 50.1, 98.8, and 196.4 kPa. Failure was defined at a peak or, in the absence of a peak, at 10% relative lateral displacement. The Mohr–Coulomb failure envelope is defined as a linear relationship between the normal stress and the corresponding shear strength. The slope of the line represents the angle of internal friction and the interception of the line with y-axis shows the cohesion. The Mohr–Coulomb failure envelopes (Figure 3.11) for the mixtures were determined by referring to the shear stress versus relative lateral displacement behavior of the mixtures, as obtained from the direct shear tests. The shear strength parameters of the mixtures (the cohesion and the angle of internal friction) were then determined from the failure envelopes. The properties of the mixtures considered in this study are summarized in Table 3.4. A discussion

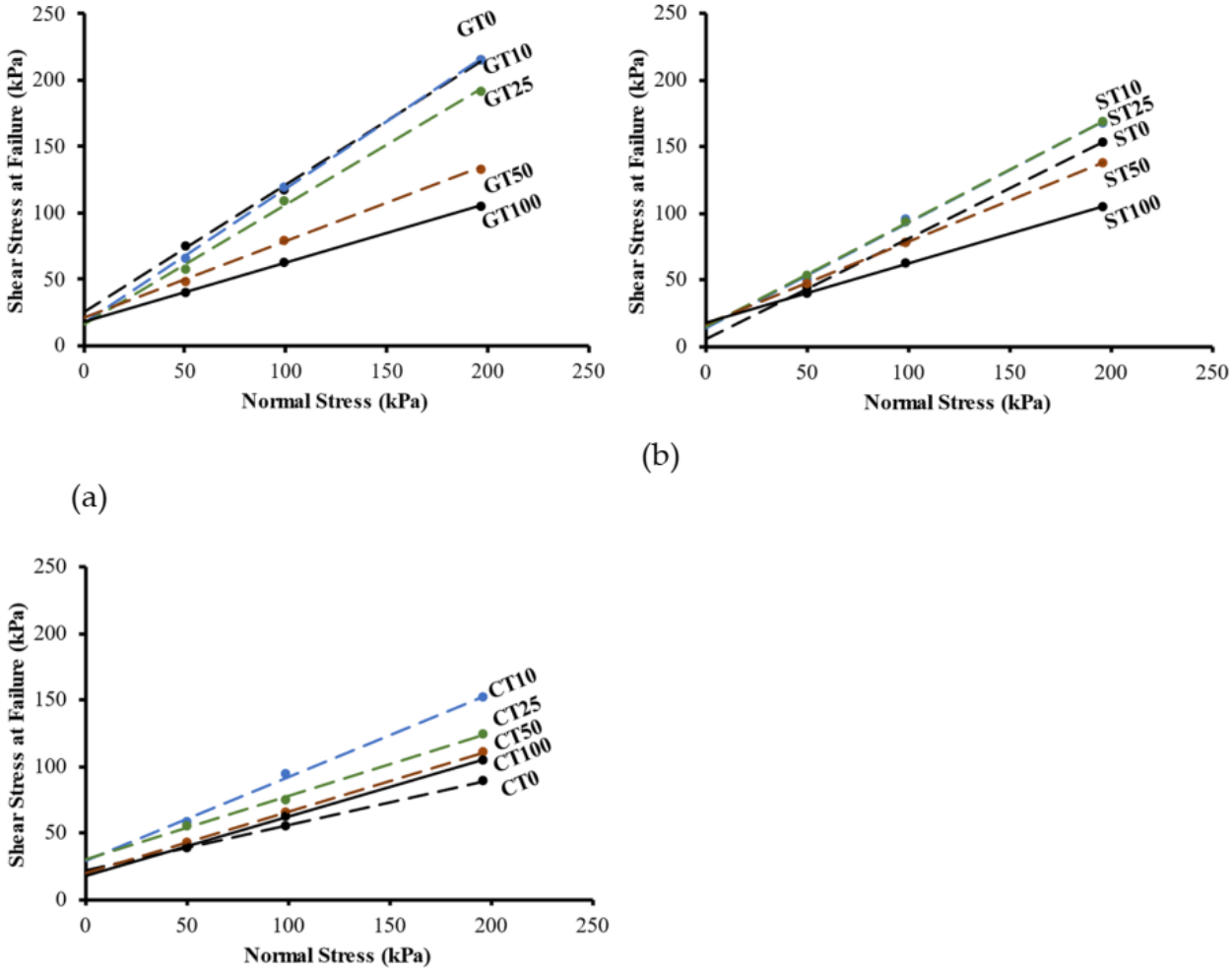

Figure 3.11: Mohr–Coulomb failure envelopes for the (a) gravel-TDA, (b) sand-TDA, and (c) clay-TDA mixtures

of the shear strength parameters (φ′ and c') of the gravel-TDA, sand-TDA, and clay-TDA mixtures is presented in the following section.

Shear Strength Parameters of the Soil-TDA Mixtures

Figure 3.12 shows the angle of internal friction plotted against the TDA content for the gravel-TDA, sand-TDA, and clay-TDA mixtures. As shown in Figure 3.12, adding up to 10% TDA by weight to the gravel increased the angle of internal friction slightly, from 44º to 45.4º. The further addition of TDA up to 25% by weight then reduced the angle of internal friction from 45.4◦ to 42.2◦. In general, the addition of up to 25% TDA by weight to the gravel did not change the angle of internal friction significantly. It may be argued that for these mixtures, gravel was the dominant particle in the shear plane and thus controlled the shear strength behavior of the mixtures. Adding more than 25% TDA by weight to the gravel then sharply reduced the angle of internal friction.

Figure 3.12 also shows that adding up to 10% TDA by weight to the sand increased the angle of internal friction slightly, from 37.1º to 38.4º (an increase of approximately 4%). In general, the addition of up to 25% TDA by weight to the sand did not change the angle of internal friction significantly. It may be argued that for mixtures containing up to 25% TDA by weight, sand was the dominant particle in the shear plane and thus controlled the shear strength behavior of the mixtures. Increasing the TDA content from 25% to 50% then sharply reduced the angle of internal friction from 38.3° to 31.8° (a reduction of about 20%). The angle of internal friction then continued to decrease as the TDA content increased, up to 100% TDA. The addition of up to 10% TDA by weight to the clay increased the angle of internal friction considerably, from 18.8◦ to 32.3◦ (an increase of approximately 72%). It may be argued that the adhesion between clay particles resulted in a bond with the TDA particles and contributed to the reinforcement of the soil upon shearing at all the confining pressures considered. Thus, the angle of internal friction increased up

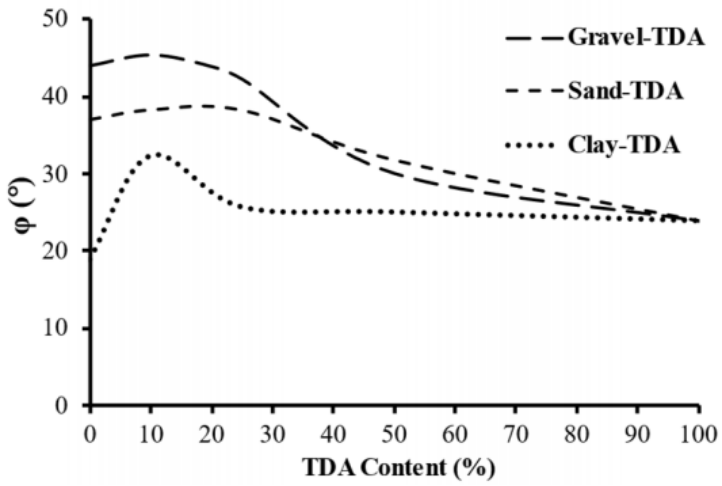

Figure 3.12: The angle of internal friction versus TDA content for the gravel-TDA, sand-TDA, and clay-TDA mixtures

to a TDA content of 10%. However, further increasing the TDA content to more than 10% then significantly reduced the angle of internal friction. It may be argued that for clay-TDA mixtures containing more than 10% TDA by weight, the clay particles were not able to create a bond with the TDA particles, and therefore the angle of internal friction decreased. In general, adding up to 10% TDA by weight to the clay significantly enhanced the angle of internal friction. However, adding up to 10% TDA by weight to the gravel or sand only slightly increased the angle of internal friction. Furthermore, adding more than 10% TDA to the clay then sharply reduced the angle of internal friction; however, adding up to 25% TDA to the gravel or sand changed the angle of internal friction only slightly. It should be noted that the further addition of TDA to the gravel or sand, beyond 25% TDA by weight, then reduced the angle of internal friction significantly. However, adding more than 25% TDA to the clay did not significantly change the angle of internal friction.

Figure 3.13 shows the cohesion intercept plotted against the TDA content for the gravel-TDA, sand TDA, and clay-TDA mixtures. The cohesion intercept obtained for the gravelly and sandy soils mixed with TDA is referred to as apparent cohesion. It may be argued that the application of

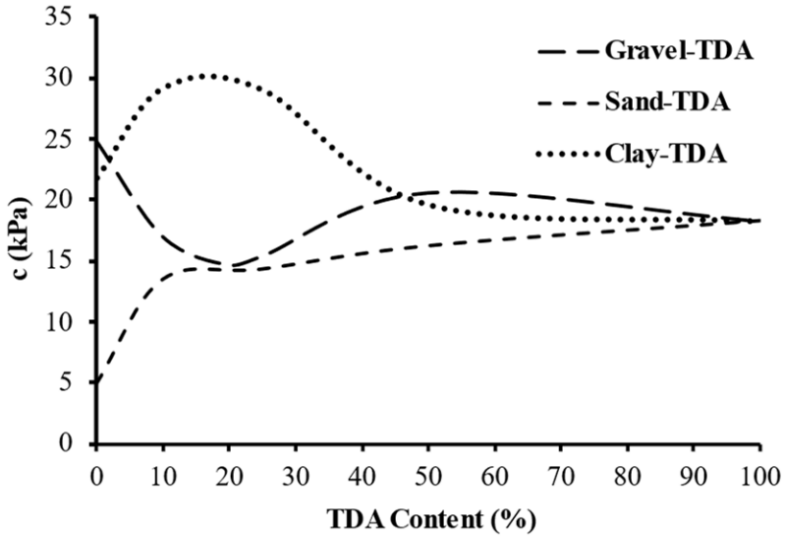

Figure 3.13: The angle of internal friction versus TDA content for the gravel-TDA, sand-TDA, and clay-TDA mixtures

high confining pressures ranging from 50.1 to 196.4 kPa to the specimens upon shearing resulted in apparent cohesion in these mixtures. At lower confining pressures, the shear stress cannot mobilize completely through the shear plane, which can result in some slip and pull-out effects during shearing. In other words, confining pressures lower than 50 kPa can influence the shear strength properties of the mixtures and contribute to an apparent friction angle (Gray and Ohashi [49]). Therefore, to avoid an apparent friction angle, the confining pressures of 50.1, 98.8, and 196.4 kPa were considered in this study.

As seen in Figure 3.13, the addition of up to 25% TDA by weight to the gravel decreased the cohesion intercept from 24.8 to 15.4 kPa. An explanation may be that due to the high flexibility of the TDA particles, adding up to 25% TDA by weight to the gravel increased the mobilization of shear stress in the shear plane, and thus decreased the apparent cohesion. Increasing the TDA content from 25% to 50% then increased the apparent cohesion from 15.4 to 20.6 kPa. It may be argued that the gravel-TDA mixtures containing more than 25% TDA by weight had a strain-hardening behavior, and their shear strength parameters were thus obtained at 10% relative

horizontal displacement. Therefore, a larger displacement at failure increased the apparent cohesion. As shown in Figure 3.13, the addition of TDA to the sand increased the apparent cohesion. An explanation may be that because the TDA particles were coarser than the sand grains, the TDA decreased the mobilization of shear stress in the shear plane upon shearing at all the confining pressures considered, thus increasing the apparent cohesion.

Furthermore, the sand-TDA mixtures containing more than 25% TDA by weight had a strain-hardening behavior, and their shear strength parameters were thus obtained at 10% relative horizontal displacement. Therefore, a larger displacement at failure increased the apparent cohesion. It should be noted that the cohesion results obtained for the clay were not solely attributable to the confining pressures. There is also adhesion between clay particles in a natural condition, which contributed to the cohesion. It was observed that the addition of up to 25% TDA by weight increased the cohesion from 21.8 to 29 kPa. It may be argued that the addition of up to 25% TDA by weight to the clay decreased the mobilization of shear stress upon shearing at the confining pressures considered, thus increasing the cohesion intercept. For clay-TDA mixtures containing more than 25% TDA by weight, the cohesion intercept then decreased. This may be attributable to the lower percentage of clay in the mixtures, causing the adhesion between clay particles to become less significant. Hence, the observed cohesion for these mixtures would be due mainly to the confining pressure, causing the cohesion intercept to decrease.

In general, adding up to 25% TDA by weight to the gravel caused a sharp decrease in the cohesion intercept. However, the addition of up to 25% TDA by weight to the sand or clay resulted in increased cohesion. It should be noted that for the sand, the cohesion intercept continued to increase as the TDA content increased. When the TDA content increased from 25% to 50%, the cohesion of the gravel-TDA mixtures increased, and the cohesion of the clay-TDA mixtures

decreased. The further addition of TDA, beyond 50% by weight, did not significantly change the cohesion intercept of the clay or gravel mixtures.

Shear Modulus

The shear modulus is a mechanical parameter used to analyze the behavior of material during shearing. Equation (2) was used to calculate the shear modulus (Das [51]):

$$G = {}^{\tau}/_{\varepsilon} \tag{12}$$

where G is shear modulus, τ is shear stress, and ε is shear strain. The shear modulus can be determined by using this equation and referring to the shear stress versus shear strain behavior of the soil-TDA mixtures. To compare the shear modulus of the mixtures used in this study, the secant shear modulus (G50) was defined as 50% of the shear strength divided by the corresponding shear strain. Figure 3.14 shows the secant shear modulus plotted against the TDA content for the soil-TDA mixtures at confining pressures of 50.1, 98.8, and 196.4 kPa. It can be seen that the addition of TDA to the gravel decreased the secant shear modulus at all the confining pressures considered. However, it should be noted that at a confining pressure of 196.4 kPa, the decrease in the shear modulus was not significant for a TDA content of up to 10% by weight. It can also be noticed from Figure 3.14 that adding up to 10% TDA by weight to the sand did not affect the secant shear modulus significantly. However, the further addition of TDA to the sand, beyond 10% by weight, then sharply decreased the secant shear modulus at all the confining pressures considered.

It can be concluded that for both gravel-TDA and sand-TDA mixtures, the stiffness behavior of the mixtures is governed by the parent solid particles at low TDA contents. As the TDA content increases, the behavior of the TDA particles starts controlling the stiffness behavior of the mixture and results in the sharp stiffness decline. On the other hand, for the clay mixtures, as shown in

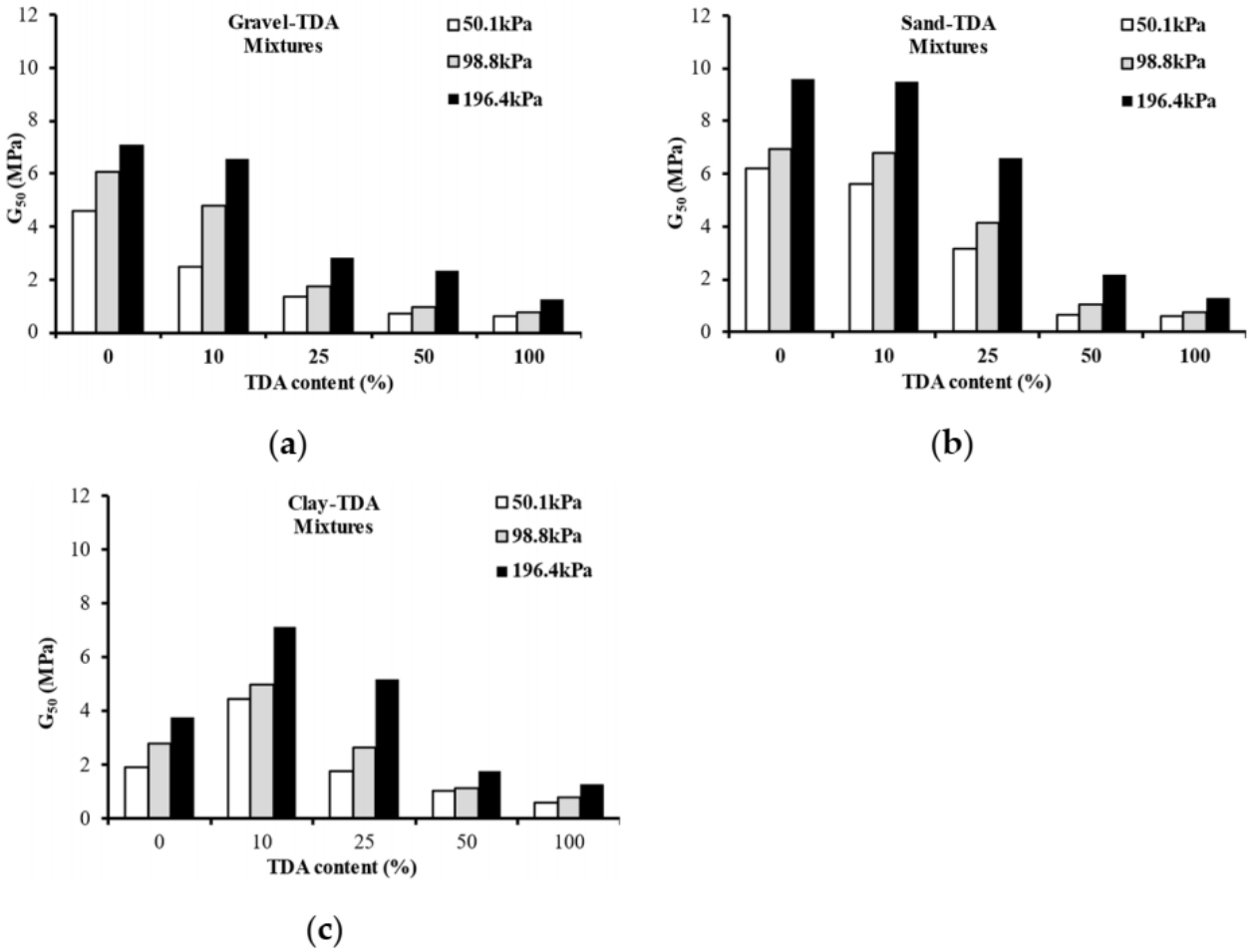

Figure 3.14: Secant shear modulus versus TDA content for the (a) gravel-TDA, (b) sand-TDA, and (c) clay-TDA mixtures.

Figure 3.14, adding up to 10% TDA by weight to the clay significantly increased the secant shear modulus at all the confining pressures considered. However, the further addition of TDA, beyond 10% by weight, then sharply reduced the secant shear modulus at all the confining pressures. This behavior is different than that observed in the other two mixture groups. The initial increase in the stiffness of the clay-TDA mixture with low TDA content is different than the behavior observed in the gravel-TDA and sand-TDA mixtures. A possible cause of this behavior change may be related to the fact that the pure solid gravel and sand particles in the mixture matrix had a higher stiffness than that of the rubber TDA particles. Moreover, there were fewer available voids in the gravel and sand in their pure state, and therefore introducing the TDA to them increased the voids

and reduced the collective stiffness of the mixture. On the other hand, the used clay sample was softer and had more voids than the used gravel and sand samples. Accordingly, the stiffness of the pure clay was almost 50% of that of the gravel and the sand. However, the mixing effort introduced during mixing the clay with the TDA particles (at low TDA contents) compacted the voids and enhanced the stiffness of the mixture. When the TDA content increased to 50% and more, however, segregation started to occur in the mixture and consequently, the stiffness decreased.

Finally, it is evident from Figure 3.14 that for mixtures containing the same amount of TDA, increasing the confining pressure from 50.1 to 196.4 kPa considerably enhanced the secant shear modulus.

Normalized Lateral Earth Pressure at Rest

The normalized lateral earth pressure at rest is an important factor used in the design of a geotechnical application such as a retaining wall. The angle of internal friction and the dry unit weight of the soil are two variables that affect the normalized lateral earth pressure. Equation (13) was used to determine the normalized lateral earth pressure at rest (Braja 2014):

$$\frac{p_o}{z} = (1 - sin\varphi')\gamma_d \quad (13)$$

where $\frac{p_o}{z}$ is the normalized lateral earth pressure at rest, z is the depth. Figure 3.15 shows the normalized lateral earth pressure at rest plotted against the TDA content for the gravel-TDA, sand-TDA, and clay-TDA mixtures.

It can be seen that adding up to 10% TDA by weight to the soils decreased the normalized lateral earth pressure at rest. For the clay-TDA mixture, adding up to 10% TDA by weight significantly reduced the normalized lateral earth pressure at rest; however, increasing the TDA content from

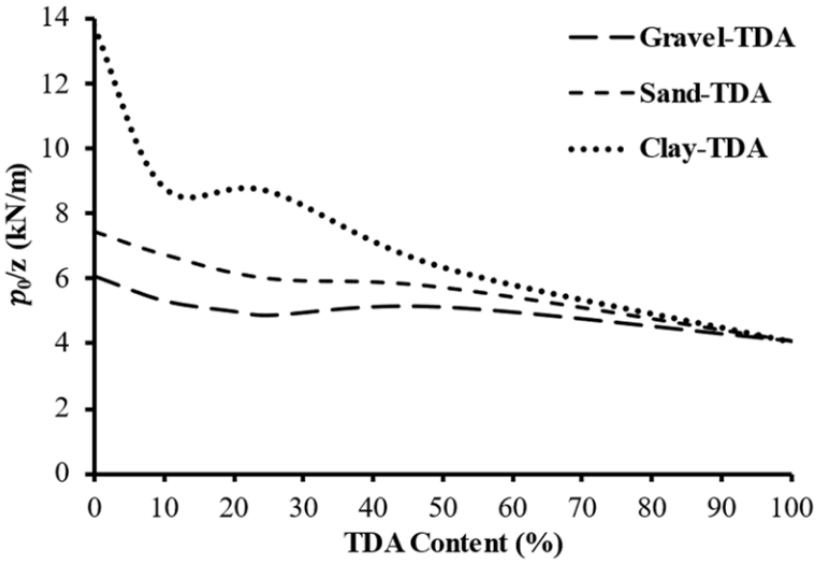

Figure 3.15: Normalized lateral earth pressure at rest versus TDA content for the gravel-TDA, sand-TDA, and clay-TDA mixtures.

10% to 25% then stabilized the normalized lateral earth pressure at rest. In contrast, for the gravel-TDA and sand-TDA mixtures, the normalized lateral earth pressure at rest continued to decrease as the TDA content increased from 10% to 25%. With the further addition of TDA, beyond 25% by weight, the normalized lateral earth pressure at rest continued to decrease for the clay-TDA mixtures but did not change significantly for the gravel-TDA and sand-TDA mixtures. Hence, it can be concluded that the addition of 25% TDA by weight to gravel results in a 20% reduction in the lateral earth pressure. Likewise, the addition of 25% TDA by weight to sand results in a 19.5% reduction in the lateral earth pressure. However, adding only 10% TDA by weight to clay can reduce the lateral earth pressure by 36%, which can result in huge savings.

Conclusions

The main objective of this study was to investigate the shear strength behavior of coarse-grained to fine-grained soils containing 0% to 100% TDA by weight, with TDA particles less than 75 mm in length. In addition, the compressibility behavior upon the shearing of TDA and soil-TDA mixtures with various TDA contents was evaluated at different confining pressures. The shear

strength parameters of mixtures with various TDA contents were determined and compared according to the Mohr–Coulomb failure criterion. The effect of the TDA content on the normalized lateral earth pressure was then investigated. The following conclusions can be drawn from this study:

- The dry unit weight of the gravel-TDA, sand-TDA, and clay-TDA mixtures decreased almost linearly as the TDA content increased;
- The addition of TDA to the gravel decreased the shear resistance upon shearing at all the confining pressures considered. However, the addition of TDA to the sand or clay initially increased and then decreased the shear resistance upon shearing at all the confining pressures. It was also found that increasing the confining pressure enhanced the shear resistance of the mixtures;
- The gravel-TDA and sand-TDA mixtures containing up to 25% TDA by weight were initially compressed, and then dilated upon shearing at all the confining pressures considered. The addition of TDA to the gravel or sand increased the compressibility behavior of the mixtures upon shearing at all the confining pressures. A similar observation was made for the clay-TDA mixtures at a confining pressure of 50.1 kPa. However, at confining pressures of 98.8 and 196.4 kPa, the compressibility behavior of the clay-TDA mixture initially decreased with the addition of up to 10% TDA by weight, and then increased with further addition of TDA;
- Adding up to 10% TDA by weight to the gravel or sand increased the angle of internal friction slightly by about 3%. In general, adding up to 25% TDA by weight to the gravel or sand did not significantly change the angle of internal friction. However, the addition of further TDA, beyond 25%, to the gravel-TDA and sand-TDA mixtures then sharply

decreased the angle of internal friction. In contrast, the addition of up to 10% TDA by weight to the clay sharply increased the angle of internal friction, which then decreased with further addition of TDA;

- The addition of up to 25% TDA by weight to the gravel decreased the apparent cohesion. In contrast, the addition of up to 25% TDA by weight to the sand or clay caused the cohesion intercept to increase. The cohesion intercept for the sand-TDA mixtures then continued to increase as the TDA content increased. However, increasing the TDA content from 25% to 50% by weight enhanced the cohesion of the gravel-TDA mixtures and reduced the cohesion of the clay-TDA mixtures;
- The addition of TDA to the gravel or sand decreased the secant shear modulus at all the confining pressures considered. However, for the clay, the secant shear modulus increased at all the confining pressures with the addition of up to 10% TDA by weight, and then declined as the TDA content increased further. For mixtures with the same TDA content, increasing the confining pressure from 50.1 to 196.4 kPa significantly enhanced the secant shear modulus;
- Adding up to 10% TDA by weight to the gravel, sand, or clay reduced the normalized lateral earth pressure at rest. The reduction was the sharpest for the clay-TDA mixture. For the gravel and sand, the normalized lateral earth pressure at rest decreased as the TDA content increased from 10% to 25% by weight, and then did not change significantly as the TDA content increased further. However, for the clay, the normalized lateral earth pressure at rest stabilized as the TDA content increased from 10% to 25% and then decreased sharply with further addition of TDA.

4. Dynamic Properties of Granulated Rubber Using Different Laboratory Tests

4.1. Introduction

Several researchers have conducted dynamic and cyclic laboratory soil tests to investigated the dynamic characteristics of granulated rubber using different tests. For example, Feng and Sutter (2000) obtained the shear modulus and damping ratio for a granulated rubber material that has a particle size range of 2.00 to 4.76 mm using a resonant column test. Moreover, Hazarika et al. (2010) performed cyclic triaxial tests to investigate the granulated rubber behavior under cyclic loading. It was found that its behavior under cyclic loading was viscoelastic. In addition, mixing parent soil with tire chips could prevent liquefaction if a proper percentage of tire chips were used. Similarly, Madhusudhan et al. (2017) performed cyclic triaxial tests under a wide range of shear strains to calculate the shear modulus and damping ratio of pure granulated rubber and sand-rubber mixtures. It was found that a sand-rubber mixture containing 10% rubber could be used effectively for seismic base isolation of low-rise buildings. In addition, Sarajpoor et al. (2020) used dynamic hollow cylinder tests to investigate the various parameters that could affect granulated rubber and sand-rubber mixtures behavior under dynamic loads.

Based on the studies mentioned above, the obtained dynamic properties of granulated from different tests could vary. Thus, it is important to highlight and understand the extent of the effect of using a different laboratory test to obtain shear modulus and damping ratio values. To the best of the authors knowledge, this issue has not been addressed yet for the granulated rubber material. Therefore, the following paragraph briefly shows the effect of using different laboratory tests on the obtained dynamic properties of conventional soil.

Cavallaro et al. (2003) conducted various laboratory tests on undisturbed clay samples to find their dynamic properties (i.e., soil stiffness and damping). The dynamic investigations were carried out in the laboratory using Resonant Column Test (RCT), Cyclic Torsional Shear Test (CTST) and Double Specimen Cyclic Simple Shear Test (DSCSS). The results showed that at low and intermediate shear strain, there was a significant difference between stiffness obtained from the RCT and DSCSS. While, the shear modulus obtained from CTST was in-between the RCT and DSCSS. Similarly, damping ratios obtained from RCT were consistently higher than those obtained from CTST and DSCSS. Another investigation by Cavallaro et al. (2003) was carried out to obtain the dynamic parameters for undisturbed clay samples using RCT, CTST and Cyclic Triaxial Test (CTT). It was concluded that the normalized shear modulus curves obtained from RCT and CTST were in a good agreement with each other. Whereas, the normalized shear modulus curve obtained from CTT showed a significant shear modulus degradation rate than those obtained from RCT and CTST. Furthermore, the damping ratios obtained from RCT were significantly greater than those obtained from CTST, while, the difference between RCT and CTT results was negligible.

Furthermore, Subramanian and Banerjee (2016) conducted RCTS and CTSTs on cement-treated marine clay to investigate the variation of the obtained shear modulus and damping ratios. Similar to the findings of Cavallaro et al. (2003), the shear modulus obtained from RCTs were higher than those from CTSTs. Moreover, the damping ratios calculated from RCTs and CTSTs did not vary significantly. On the other hand, when the cement content increased to 10%, there was a significant variation between both tests. Furthermore, Bedr et al. (2019) investigated the shear modulus and damping ratio of Algiers Marls. A variety of laboratory testing apparatuses were used to conduct

this investigation (i.e., CTT, DSCSS, CTST and RCT). The calculated normalized shear modulus curves from RCTs showed a rapid shear modulus degradation compared to the CTST and DSCSS. Furthermore, there was no significant variation observed in the damping ratios calculated from all the test apparatuses.

All the above-mentioned research studies indicate that using different testing techniques could lead to a significant variation in dynamic parameters. Hence, this paper aims to investigate the effect of using cyclic triaxial test (CTT) and cyclic simple shear test (CSST) in determining shear modulus and damping ratio. The output of this work is further compared with other published work regarding the dynamic properties of granulated rubber.

4.2. Tested Material and Test Apparatuses

The granulated rubber used herein was supplied by Atlantic Rubber Paving Inc. Figure 4.1 shows the gradation curve for the used material. The size of the granulated rubber ranges from 2.83 to 4.76 mm. Furthermore, its uniformity (C_u) and curvature (C_c) coefficients are 1.43 and 0.97, respectively. According to ASTM D6270 classification of tire shreds, the material used falls in the category of granulated rubber, which has a particle size range of 0.425 to 12 mm.

Figure 4.2 shows components of the triaxial testing equipment used in this study. The triaxial cell can accommodate a sample size of 70 mm in diameter and 150 mm in height. The resulting height to diameter ratio of 2 is consistent with the ASTM D3999 recommendation. Furthermore, two pressure-volume controllers were used to measure and control the cell pressure and pore-water pressure. Additionally, the axial deviatoric load was applied using an Instron 8501 hydraulic loading frame. An external load cell and a linear variable displacement transducer (LVDT) were attached to the load frame to measure the deviatoric load and axial displacement of the specimen.

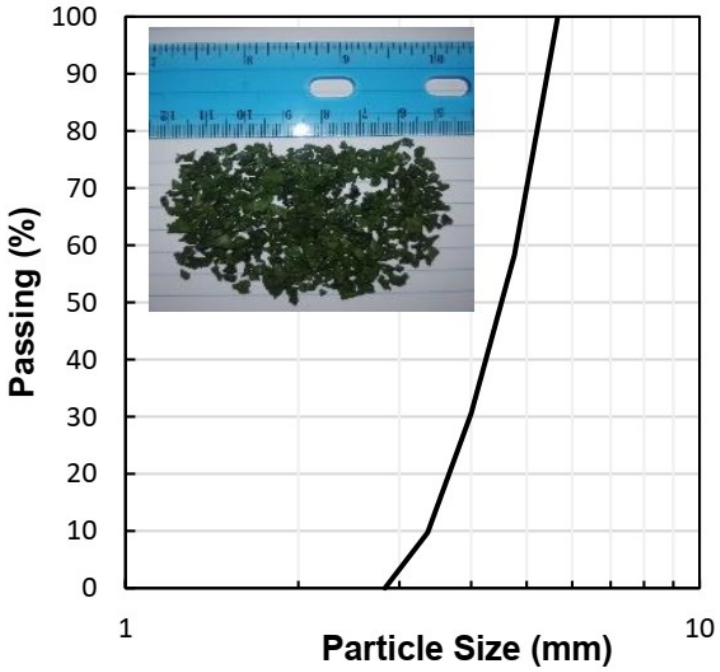

Figure 4.1: Gradation curve for granulated rubber.

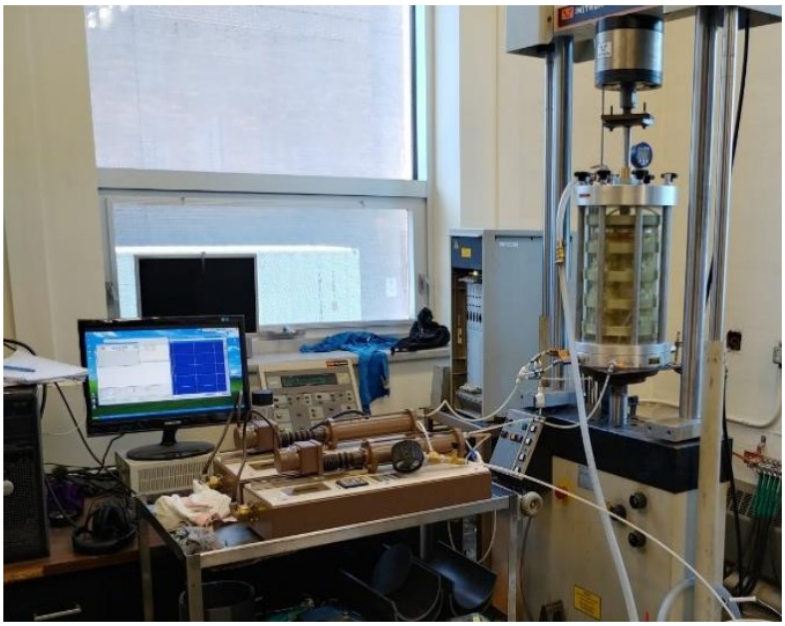
Figure 4.2: Cyclic triaxial test set up, adapted from Moussa and El Naggar [9]

A cyclic direct simple shear (DSS) device manufactured by GDS Instruments was used to conduct the cyclic simple shear tests. This apparatus can accommodate a specimen size of 70 mm in diameter and up to 28.1 mm high inside 26 Teflon coated steel rings. Each steel ring has a thickness

of 1.1 mm. However, before placing the granulated rubber, a latex membrane was used to cover the inside circumference of the specimen mold. Figure 4.3 shows the cyclic DSS device used and a mounted specimen inside the steel rings. Two porous stainless-steel discs with sharp concentric teeth were placed at the top and bottom of the specimen to transfer the shear load to the specimen. A 2 kN load cell and 2 LVDTs (with a range of ±10 mm) are used to measure shear and normal forces and displacements of the specimen.

4.3. Testing Program and Sample Preparation

Multi-stage loading undrained cyclic triaxial tests were carried out in this study under strain-controlled conditions. The confining pressures (σ_c) used herein were 25, 50 and 100 kPa, and the shear strain (γ) amplitude varied from 0.1 to 10%. Each stage corresponds to a certain shear strain amplitude; however, the confining pressure was kept constant throughout all the stages for each test. As stated by the ASTM D3999 standard for determining modulus and damping properties of soils, no generation of excess pore water pressure is allowed between each stage; therefore, 20

Figure 4.3: A DSS specimen mounted for testing

cycles with extremely small axial stains were applied between the stages to dissipate any excess pore water pressure generated between each stage. Multi-stage loading cyclic simple shear tests (CSST) were also conducted similar to the CTT. However, since the DSS device was able to capture smaller shear strain amplitudes, the shear strain amplitudes for the CSST varied from 0.01 to 10%. Furthermore, the vertical stresses (σ_v) used were 25, 50, 100 and 200 kPa corresponding to vertical stress levels on buried pipelines, culverts, or shallow foundations. Table 4.1 summarizes the testing scheme used in this study. Both C.T.T. and CSST tests were performed at a cyclic loading frequency of 0.5 Hz.

Because of the large specimen size, CTT specimens were prepared by tamping granulated rubber in five layers in the specimen mold. Each layer was compacted by 20 blows of the tamping rod. All specimens were prepared in a dry condition as the dry density of the TDA is not significantly influenced by introducing water (Kowalska 2016). In addition, all specimens were saturated until Skempton's pore pressure coefficient (B-value) became greater than 0.97. The CSST specimens was also compacted using a tamping rod; however, since the height of the specimen was only 28.1 mm, the granulated rubber material was placed in three layers instead of five, and each layer was compacted by 25 blows of the tamper. Furthermore, all specimens were flushed with water until there was almost no air trapped inside the specimens.

Table 4.1: Summary of the testing program.

Table	γ (%)	σ'_c or σ'_{vc} (kPa)	No. of Cycles Per Stage
CTT	0.1, 1, 2, 5, 7.5, 10	25, 50, 100	Stage one: 100 Other Stages: 50
CSST	0.01, 0.05, 0.1, 1, 2, 5, 7.5, 10	25, 50, 100, 200	All Stages: 10

4.4. Results and Discussion

Due to the enormous amount of data obtained from both CTT and CSST, a MATLAB code was developed to process and calculate the dynamic properties of the granulated rubber material. The obtained data from CCT are a series of hysteretic stress-strain curves, an example of which is shown in Figure 4.4a. The procedure presented by ASTM D3999 [28] was adapted to calculate the shear modulus (G) and damping ratio (ξ) from the hysteretic stress-strain curves. On the other hand, the output of CSST is a series of hysteretic shear stress-shear strain curves, and an example is shown in Figure 4.4b.

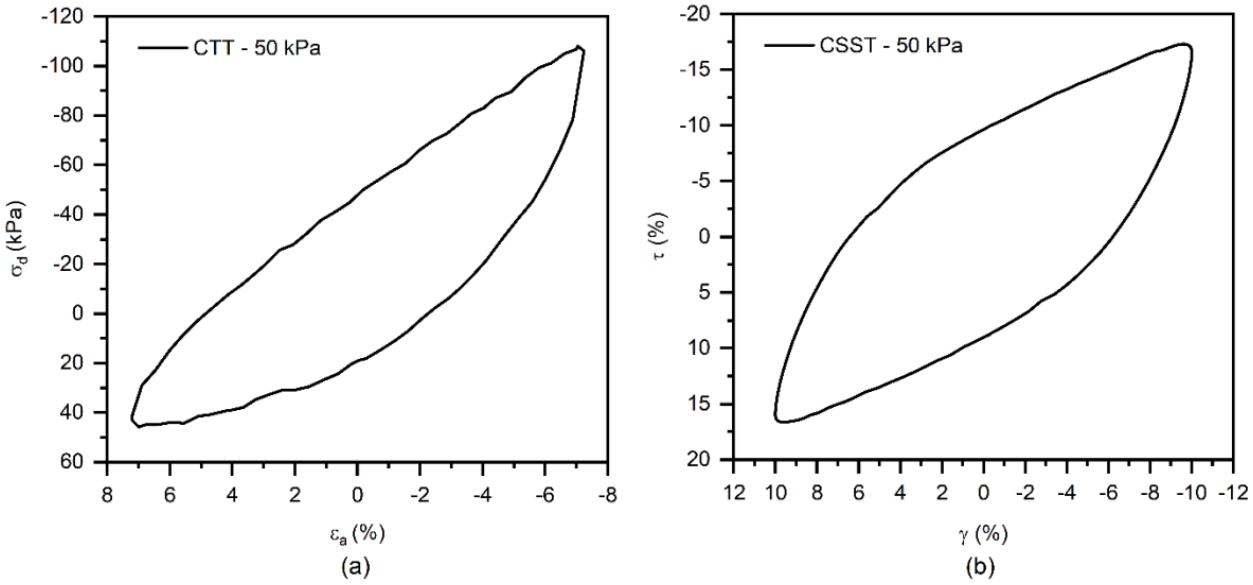

Figure 4.4: Hysteretic loops at γ = 10% from (a) CTT and (b) CSST.

Backbone Curves

The backbone curves for both tests were obtained by plotting the maximum and minimum shear stress versus the maximum and minimum shear strain from a specific hysteretic loop at each strain level. In the present study, the 10th hysteretic loop was used to plot the backbone curves (Figure 4.5). Figure 4.6 shows the backbone curves for the CTT and CSST at consolidation stresses of 25,

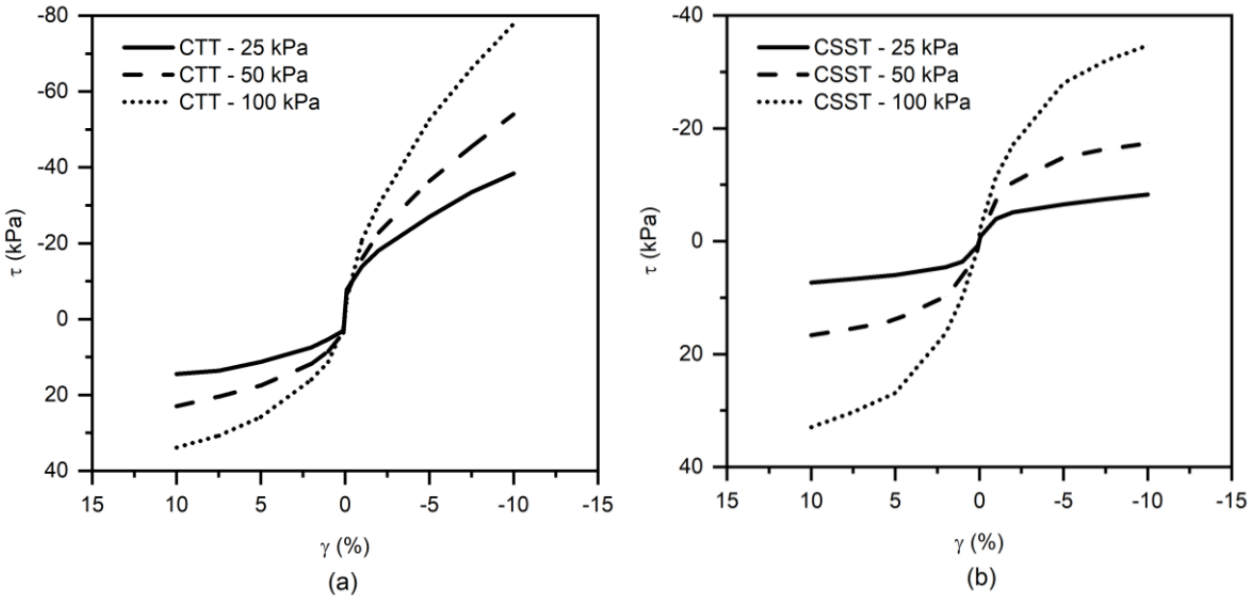

Figure 4.5: Backbone curves at different consolidation stresses from (a) CTTs and (b) CSSTs tests.

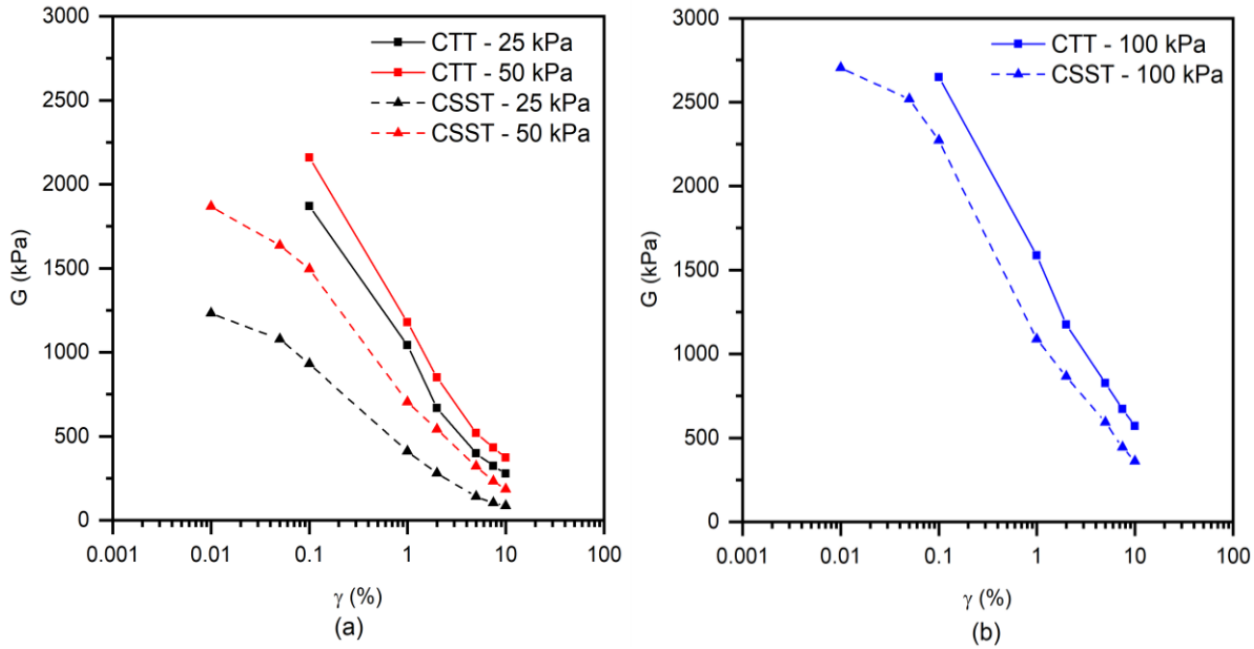

Figure 4.6: Comparisons of shear modulus with shear strain amplitude under consolidation stresses of (a) 25 and 50, and (b) 100 kPa

50 and 100 kPa. The following equations were used to convert the deviatoric stress and axial strain from the CTT to shear stress (τ) and shear strain (γ):

$$\tau = 0.5\sigma_d \tag{14}$$

$$\gamma = \frac{3}{2}\varepsilon_a \quad (15)$$

where σ_d = effective deviatoric stress, and ε_a = axial strain. As shown in Figure 4.5 the backbone curves obtained from CTT tests show that the granulated rubber behaves almost like a bilinear material with a slight nonlinearity under all confining pressures. Moreover, none of the CTT backbone curves are symmetric with respect to the origin, which is expected since the hysteretic loop was not symmetric as well, as shown in Figure 4.5a. This is because of the anisotropic stiffness of granulated rubber, being higher in compression than in extension. In contrast, the backbone curves obtained from CSST tests show more significant nonlinearity under all vertical stresses in comparison to those plotted from CTTs. Additionally, all curves are symmetric about the origin. However, none of the backbone curves obtained from either CTT or CSST tests show a peak shear stress even at a high strain level (i.e., 10%).

Shear Modulus

Shear modulus was calculated for both tests from the 10th cycle at each shear strain level for all consolidation stresses. Figure 4.7 shows the variations of shear modulus with shear strain amplitude for consolidation stresses of 25, 50 and 100 kPa. In general, it could be observed that as shear strain increases, the shear modulus decreases nonlinearly. Despite the similar ranges of shear moduli from both tests, shear moduli at a given consolidation stress are significantly different between both tests.

As indicated in Figure 4.6, the difference in shear moduli from CTT and CSST is the highest at a small shear strain amplitude of 0.1%. This is likely because of the different shear plane orientations with respect to the orientation of the rubber particles in these two tests. Shearing occurs mostly along the rubber particles in the CSST tests, while the shearing direction crosses through the rubber

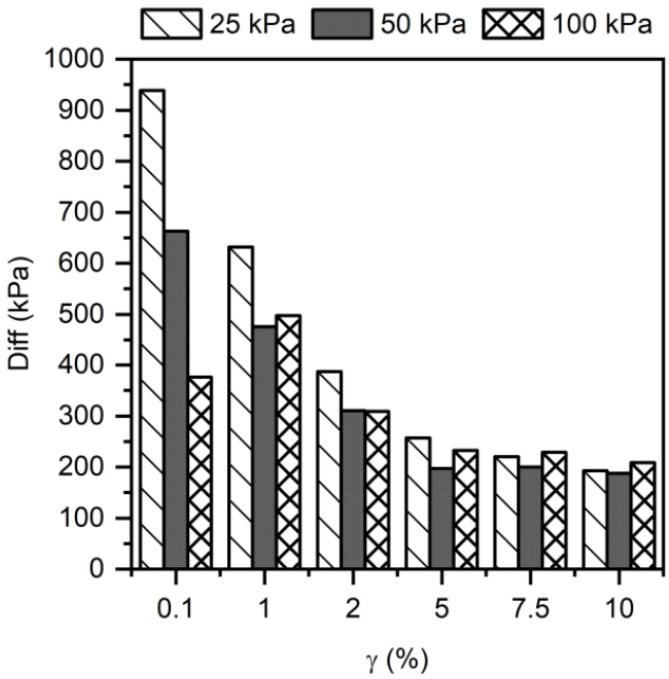

Figure 4.7: Variation between the shear modulus values obtained from CTT and CSST

particles in the CTT tests and thus mobilizes their pull-out resistance resulting in higher shear moduli. However, as the shear strain amplitude increases, this difference decreases. This could be due to stiffness degradation at higher shear strains. So as the material is subjected to higher shear strains, it loses most of its stiffness, and thus the difference between the calculated shear moduli from both tests is reduced. Furthermore, this difference in shear moduli is larger at the low consolidation stress of 25 kPa.

Damping Ratio

Damping ratios obtained from CTT and CSST tests are compared in Figure 4.8. According to this figure, the damping ratios calculated from CTT at shear strains of less than or equal to 1% under all confining stresses are dramatically larger than those determined from CSST tests. However, at higher shear strains, the difference between damping ratios from both tests reduces. In addition,

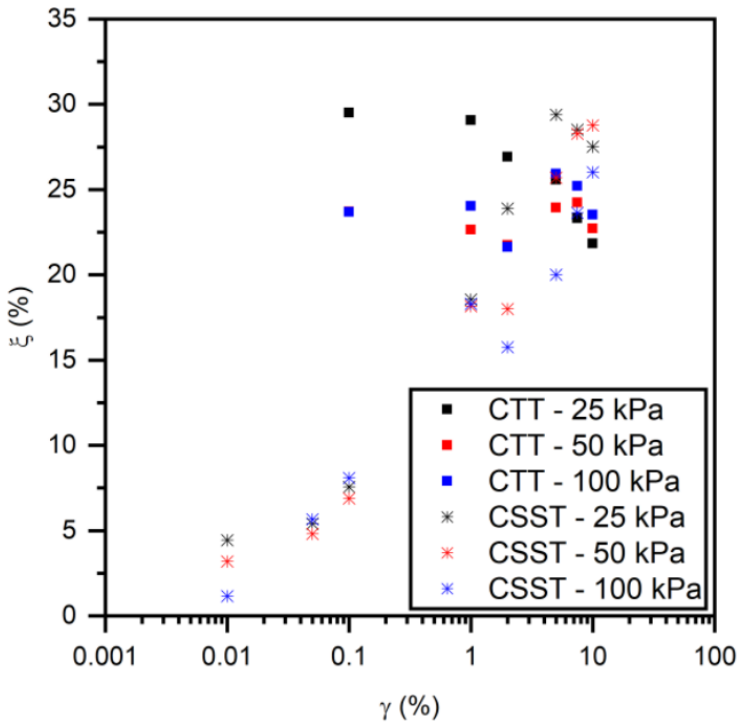

Figure 4.8: Comparison of damping ratios with shear strain amplitude from CTT and CSST

both tests indicate that the granulated rubber's damping ratio is independent of the consolidation stress.

Comparison of Dynamic Properties with Those from Literature

Feng and Sutter [21] conducted resonant column tests on granulated rubber material with a particle size range of 2 to 4.76 mm. The consolidation pressure and shear strain ranged from 69 to 483 kPa and 0.0035 to 0.09%, respectively. The results of these resonant column tests at σ'_v = 207 kPa are compared with a CSST test of this study at σ'_v = 200 kPa in Figure 4.9. It is clear that there is a significant discrepancy between the shear moduli obtained from both tests. Such difference between shear moduli from resonant column and CSST tests has also been observed in the testing of natural sediments (Bedr et al. 2019). This could be due to the difference in the strain rate and the number of cycles used in RCT and CSST tests. On the other hand, damping ratios calculated

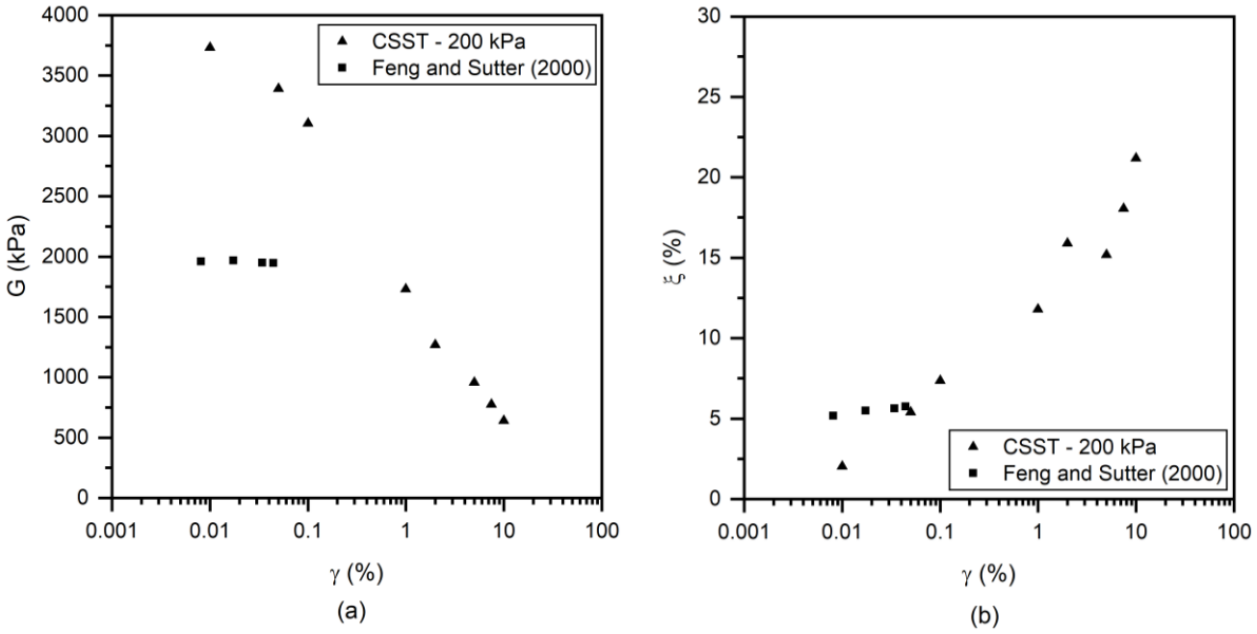

Figure 4.9: Comparisons between the (a) shear moduli (b) damping ratios of CSSTs and Feng and Sutter (2000).

from both tests are in a good agreement with each other, especially at shear strain levels of 0.034% and 0.044%.

The CTT and CSST results of the present study are further compared in Figure 4.10 with those obtained by Madhusudhan et al. (2017) and Sarajpoor et al. (2020) at a consolidation stress of 100 kPa. Madhusudhan et al. (2017) conducted CTT tests on a granulated rubber material with particle sizes of less than or equal to 2 mm. In addition, Sarajpoor et al. (2020) conducted dynamic hollow cylinder tests on sand-rubber mixtures as well as a pure granulated rubber. The granulated rubber particle sizes were between 3.9 and 6.0 mm.

As shown in Figure 4.10, shear moduli obtained from these tests are in a very good agreement with those of this study. Similarly, at low shear strain amplitudes (i.e., <1%), damping ratios obtained from the CSST tests are close to those reported by Madhusudhan et al. (2017) and Sarajpoor et al. (2020). Nevertheless, there are significant variations and differences in damping ratios at shear

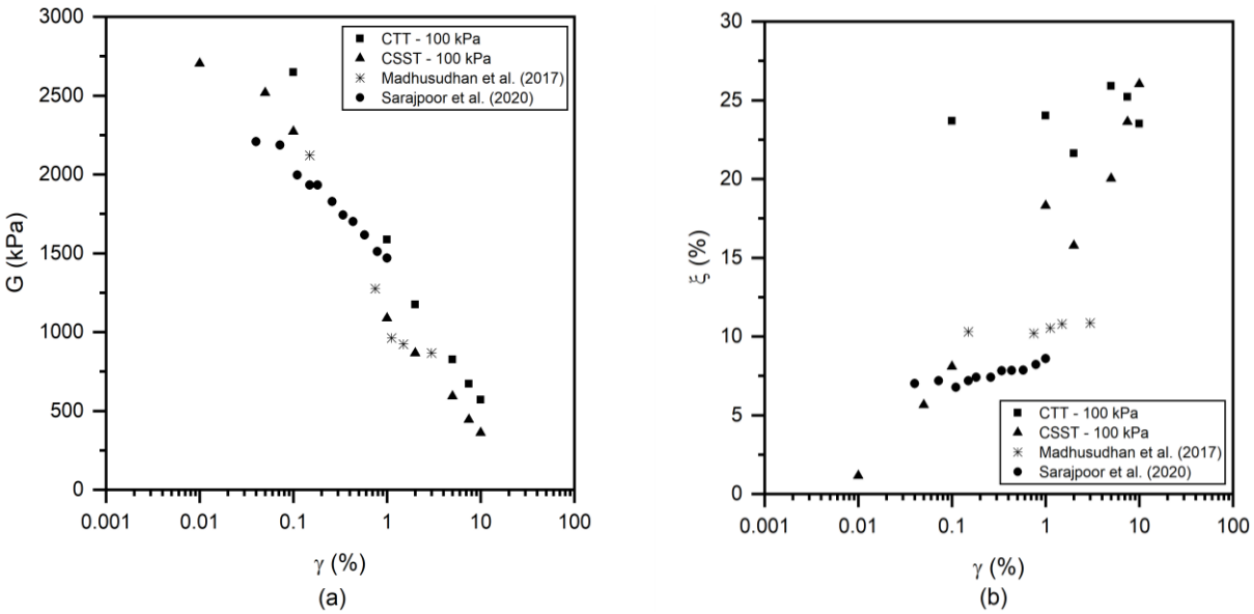

Figure 4.10: Comparisons of the (a) shear moduli and (b) damping ratios obtained from the CTTs and CSSTs in this study, with those from Madhusudhan et al. [30] and Sarajpoor et al. [23].

strain amplitudes larger than 1%. Some factors which could cause fluctuation in the damping ratios are the specimen preparation technique, sample size, aggregates size and the loading pattern.

Furthermore, the behavior of pure granulated rubber is compared to the behavior of natural soil and sand-rubber mixtures. Anastasiadis et al. (2012) and Senetakis et al. [32] conducted several RCT on pure granulated rubber and sand-rubber mixtures. The obtained results from Anastasiadis et al. [31] and Senetakis et al. [32] are compared with the obtained results herein as shown in Figure 4.11 where R3, Parent Sand (C2D03), and R3-65/35 refer to pure rubber (D50 = 2.9 mm), pure sand and a mixture of sand and rubber with a rubber content of 35% by weight, respectively. Note that the maximum shear moduli were obtained at shear strain levels of 0.01% and 0.1% in the CSST and CTT experiments of this study, while those reported by Anastasiadis et al. (2012) and Senetakis et al. (2012) correspond to shear strains of 1.15 × 10−4% to 4.6 × 10−3%. According to Figure 4.11a, the shear modulus of granulated rubber is significantly lower than that of pure soil and sand-rubber mixture, indicating the reduction of stiffness due to the inclusion of granulated

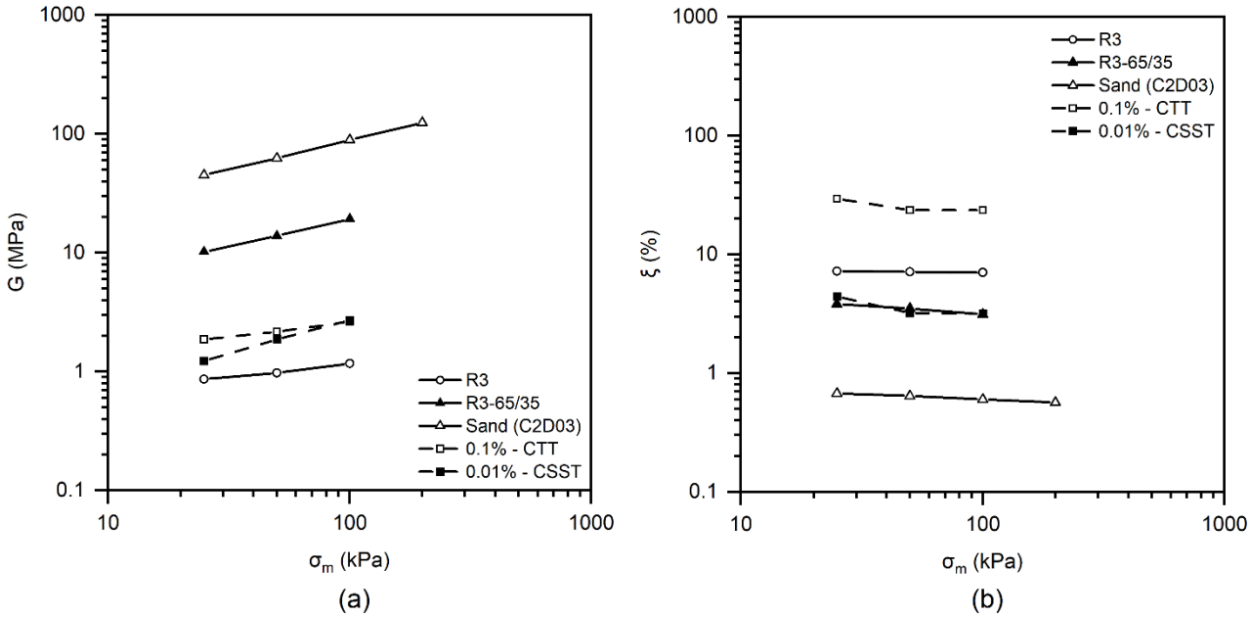

Figure 4.11: Relation between vertical consolidation stresses and (a) shear moduli and (b) damping ratios.

rubber. In addition, similar to the findings by Feng and Sutter (2000), Gmax from RCT are lower than those from CSST and CTT tests. Figure 4.11b further demonstrates that adding 35% of granulated rubber by weight to sand results in damping ratios almost identical to those obtained from the CSST of this study. Nevertheless, the highest damping ratios are obtained from the CTT tests.

4.5. Conclusions

Cyclic triaxial and cyclic simple shear tests were carried out in this study to investigate the effect of different laboratory testing methods on the shear modulus and damping ratio of a granulated rubber material. The confining pressures and shear strain amplitudes range for the CTT were 25 to 100 kPa, and 0.1 to 10%, respectively. Whereas, vertical stresses and shear strain amplitudes considered for CSST were respectively 25 to 200 kPa, and 0.01 to 10%. Based on the obtained results and comparisons with the literature, the following conclusions are made:

- The backbone curves plotted from the CTT indicate that the behavior of granulated rubber under cyclic loading could be simulated by a bilinear material model. However, the backbone curves plotted from CSST show that the behavior of the material is nonlinear under cyclic loading.
- Shear moduli obtained from the CTT and CSST ranged from 278 to 2647 kPa and from 85 to 2270 kPa, respectively.
- As shear strain increased, the difference between the obtained shear moduli from both tests decreased.
- At low shear strain amplitudes (i.e., 0.1%), damping ratios calculated from CTT are significantly larger than those from CSST.
- Damping ratios of granulate rubber material obtained from both tests were independent of consolidation stress.
- Comparison with the literature showed that the damping ratios of granulated rubber could be significantly different from one testing technique to another. Thus, investigating the damping ratio of rubber material using different techniques is recommended.
- The shear modulus values obtained from the dynamic hollow cylinder test, CSST and CTT are in good agreement with each other. Conversely, the results obtained by RCT were significantly different than the results of CSST, which could be attributed to the strain rate and the number of cycles used.
- Dynamic properties of granulated rubber could vary significantly from one test to another.

5. Conclusions

This report explored the feasibility of using TDA and mixtures of TDA and sand or gravel as an alternative backfilling material. Over the course of the research, direct shear tests, simple shear tests, consolidated drained triaxial tests, and cyclic triaxial tests were performed on different samples of TDA and TDA mixtures to explore their static and dynamic characteristics. The results of these tests were discussed, and a number of empirical equations were derived. Below is a brief summary of the conducted research followed by a section summarizing the major drawn conclusions.

5.1. Summary of the conducted research

Available TDA triaxial data obtained with large-scale machines is limited and is not comprehensive. In this research, a series of consolidated drained triaxial tests have been performed on TDA in accordance with ASTM D7181-11. The TDA tested is roughly the same size as that used in many civil engineering projects (i.e., tire chips TDA). The tests were performed by using a large-scale triaxial machine. Furthermore, in order to replicate a variety of real-world conditions, the tests were performed for a wide range of confining pressures to simulate TDA layers at different embedment depths. The results of deviatoric stress versus strain, corrected for volume change as per ASTM D7181-11, are presented and discussed, and empirical equations for a number of strength and stiffness parameters are proposed. The empirical equations are then used to develop a hyperbolic material model for TDA. This provides practicing engineers with the information they need to incorporate the TDA in their design. Also, the effect of sample size on the TDA shear strength and stiffness parameters were investigated.

Mixing soil with TDA content has great potential as a lightweight backfilling material which reduces the TDA's self-ignition problem and provides lower compressibility. Previous researchers

have primarily focused on the shear strength behaviour of TDA content with sizes smaller than 20 mm in length mixed with a single type of soil, mainly sandy soil. In contrast, limited studies have been conducted on clayey and gravelly soils mixed with TDA content with sizes larger than 20 mm. Therefore, one of the objectives of this study was to investigate the shear strength behaviour of large size TDA content with lengths up to 75 mm mixed with various soil types. Also, the effect of TDA content on the compressibility behaviour of the mixtures was determined. Another objective was to find the effect of various confining pressures on the shear strength and compressibility behaviour of the TDA-soil mixtures. Also, the effect of TDA content on the shear strength parameters of the mixtures, including the angle of internal friction and cohesion, was determined.

Several researchers have conducted dynamic and cyclic laboratory soil tests to investigate the dynamic characteristics of granulated rubber using different tests. It was found that its behaviour under cyclic loading was viscoelastic. In addition, mixing parent soil with tire chips could prevent liquefaction if a proper percentage of tire chips were used. It was also found that a sand-rubber mixture containing 10% rubber could be used effectively for seismic base isolation of low-rise buildings. None of the previous researchers characterized the dynamic properties of large-size TDA. Hence, another objective of this research project was to conduct full dynamic characterization of large size TDA roughly the same size as that used in many civil engineering projects.

5.2. Main Findings of this Research

Based on the results of the present study and comparisons with the literature, the following conclusions are made:

- The stress-strain response of the tire derived aggregates is found to be nonlinear at the start and then behaves almost linearly afterwards. The particle rearrangement during axial loading could be the reason for the observed initial nonlinear stress-strain behaviour.

- Parameters such as particle size and shape, the presence or absence of steel, and the type of test conducted (i.e., direct shear or triaxial tests) can influence the obtained shear strength parameters of tire derived aggregates.

- The angle of internal friction of TDA increases as the size of the used shear box decreases, while the cohesion does not show a definite trend.

- The increase in the obtained TDA angle of internal friction observed for the typical small shear box (60 x 60 mm) could affect the design; thus, such results must be used with caution. Therefore, for evaluations of TDA shear strength, the use of a direct shear box with an aspect ratio of shear box width to maximum particle size (W/D_{max}) of 4 or larger is recommended.

- ASTM D3080-11 recommends a W/D_{max} ratio greater than 10. This ratio should not be imposed for TDA since the results of the TDA tests showed that the same shear strength was obtained when using shear boxes with a W/D_{max} ratio as low as 4.

- It was also found that the stiffness and the effective angle of internal friction of TDA increase by increasing the maximum particle size.

- The addition of TDA content to the gravel, sand, and clay decreased the dry unit weight of the mixtures almost linearly.

- The addition of TDA content to the gravel decreased the shear resistance of the mixtures upon shearing at all the considered confining pressures. However, adding TDA content to the sand and

clay initially increased the shear resistance and then decreased upon shearing at all the confining pressures. Also, increasing the confining pressures enhanced the shear resistance of the mixtures.

- Adding up to 10% TDA content by weight to the gravel and sand increased the angle of internal friction slightly (by about 3%). In general, adding up to 25% TDA content by weight to the gravel and sand did not significantly change the angle of internal friction. Then, adding more than 25% TDA content to the soils decreased the angle of internal friction sharply. However, adding up to 10% TDA content to the clay sharply increased the angle of internal friction, and then reduced at a higher TDA content.

- The addition of TDA content up to 20% by weight to the gravel decreased the apparent cohesion. However, the addition of TDA content up to 20% by weight to the sand and clay increased the cohesion intercept. The increase in the cohesion intercept was continued for the sand at a higher TDA content. However, increasing TDA content from 20 to 40 % enhanced the cohesion for the gravel-TDA mixtures and reduced for the clay-TDA mixtures.

- Adding TDA content up to 10% by weight to the gravel, sand, and clay decreased the normalized lateral earth pressure at rest. This reduction was shaper for the clay-TDA mixture up to 10% TDA content. Increasing the TDA content from 10 to 25% in the gravel and sand decreased the normalized lateral earth pressure at rest and then did not change significantly at a higher TDA content. However, adding TDA content from 10 to 25% to the clay stabilized the normalized lateral earth pressure at rest.

- The conducted dynamic testing revealed that the backbone curves plotted from the cyclic triaxial testing indicate that a bilinear material model could simulate the behaviour of granulated rubber

under cyclic loading. However, the backbone curves plotted from the cyclic simple shear tests show that the material's behaviour is nonlinear under cyclic loading.

- In general, it could be observed that as the shear strain increases, the shear modulus of TDA decreases nonlinearly.

- Also, the damping of TDA increases nonlinearly as the shear strain increases.

5.3. Next Research Phase

Since TDA is a rubber-based material and carries its characteristics, it has an excellent damping ability recommending it to be used as a vibrations barrier when vibrations control is required. This concept is supported by the results of the extensive material characterization program presented in this report. Furthermore, preliminary numerical modelling analyses conducted by our team indicated substantial merit for TDA to be used as a damping material, substituting other expensive options like geofoam. Hence, after completing this first phase of the research reported herein, a second phase involving an experimental demonstration of the proposed system is underway. The primary focus of the second phase of the project will be the development and concept demonstration of the proposed use of TDA to control ground-borne vibrations. The experimental proof-of-concept is a critical step in the innovation process and is widely used by companies to provide experimental evidence on the applicability of a newly proposed system. This effort is expected to eventually result in a practical introduction of the proposed TDA system to practicing engineers and designers, alleviating any technical concerns or hurdles that may hinder its adoption in actual projects. The new proposed TDA system will offer an added value to the economy in Nova Scotia in the field of environmental technologies and manufacturing. These two fields are

among the top strategic sectors that both the provincial government of Nova Scotia and the federal government of Canada are striving to support in order to achieve economic sustainability.

References

"2015 U.S. Scrap Tire Management Summary." (2017). Accessed May 2018. <https://www.ustires.org/sites/default/files/MAR_028_USTMA. pdf>

"Annual Report 2016." (2016). Accessed May 2018. https://www.catraonline.ca/,<https://www.catraonline.ca/storage/files/shares/publicationsen/catra-annualreport-final 03apr2017-pdf.pdf>

963–979.

Ahmed, I., and C. Lovell. Rubber Soils as Lightweight Geomaterial. Transportation Research Record: Journal of the Transportation Research Board, 1993. 1422: 61–70.

Ahn, I.S.; Cheng, L.; Fox, P.; Wright, J. Material properties of large-size tire derived aggregate for civil engineering applications. J. Mater. Civ. Eng. 2015, 27, 04014258. [CrossRef]

Aliabdo, A. A., A. E. M. A. Elmoaty, and M. M. Abdelbaset. 2015. "Utilization of Waste Rubber in Non-structural Applications." Construction and Building Materials 91: 195–207. doi:10.1016/j.

Anastasiadis, A.; Senetakis, K.; Pitilakis, K. Small-strain shear modulus and damping ratio of sand-rubber and gravel-rubber mixtures. Geotech. Geol. Eng. 2012, 30, 363–382.

Anastasiadis, A.; Senetakis, K.; Pitilakis, K. Small-strain shear modulus and damping ratio of sand-rubber and gravel-rubber mixtures. Geotech. Geol. Eng. 2012, 30, 363–382.

Anim, K., and A. Fakhimi. Effect of Deformation Rate on Shear Strength of Questa Rock Pile Materials. American Rock Mechanics Association, 2012.

ASTM C136/C136M-14. Standard Test Method for Sieve Analysis of Fine and Coarse Aggregates; ASTM International: West Conshohocken, PA, USA, 2014.

ASTM D3080/D3080M-11. Standard Test Method for Direct Shear Test of Soils under Consolidated Drained Conditions. ASTM International, West Conshohocken, PA, 2011.

ASTM D6270-08. Standard Test Methods for Laboratory Compaction Characteristics of Soil using Modified Effort (56,000 ft-lbf/ft3 (2,700 kN-m/m3)). ASTM International, West Conshohocken, PA, 2012.

ASTM D6913-04. Standard Test Methods for Particle-Size Distribution (Gradation) of Soils using Sieve Analysis. ASTM International, West Conshohocken, PA, 2004.

ASTM D7181-11. Method for Consolidated Drained Triaxial Compression Test for Soils; ASTM International: West Conshohocken, PA, USA, 2011.

ASTM. (2017). “Standard practice for use of scrap tires in civil engineering applications.” D6270 08, West Conshohocken, PA.

ASTM. 2011. Method for Consolidated Drained Triaxial Compression Test for Soils. West Conshohocken,PA. D7181-11

ASTM. 2014. Standard Test Method for Sieve Analysis of Fine and Coarse Aggregates, C136/C136M-14. West Conshohocken, PA.

Atkinson, J.; Sallfors, G. Experimental determination of stress-strain-time characteristics in laboratory and in situ tests. In Proceedings of the 10th European Conference on Soil Mechanics and Foundation Engineering, Florence, Italy, 26–30 May 1991;

Baldi, G.; Hueckel, T.; Pellegrini, R. Thermal volume changes of the mineral–water system in low-porosity clay soils. Can. Geotech. J. 1988, 25, 807–825.

Bedr, S.; Bedr, S.; Mezouar, N.; Mezouar, N.; Verrucci, L.; Verrucci, L.; Lanzo, G.; Lanzo, G. Investigation on shear modulus and damping ratio of Algiers marls under cyclic and dynamic loading conditions. Bull. Eng. Geol. Environ. 2019, 78, 2473–2493.

Benda, C. C. Engineering Properties of Scrap Tires Used in Geotechnical Applications. Materials and Research Division, Vermont Agency of Transportation., Montpelier, 1995.

Bernal, A., R. Salgado, R. Swan, and C. Lovell. Interaction between Tire Shreds, Rubber-Sand and Geosynthetics. Geosynthetics International, Vol. 4, No. 6, 1997, pp. 623–643.

Bosscher, P. J., T. B. Edil, and S. Kuraoka. Design of Highway Embankments using Tire Chips. Journal of Geotechnical and Geoenvironmental Engineering, Vol. 123, No.4, 1997, pp. 295–304.

BSI. (1990). “Methods of Test for Soils for Civil Engineering Purposes. Shear Strength Tests (Effective Stress).” BS 1377–1378:1990, London, UK.

Carroll, M. D., and T. F. Zimmie. Sample Size Effects using the NGI Direct Simple Shear Apparatus. Defense Technical Information Center, VA, 1979.

Cavallaro, A.; Lanzo, G.; Pagliaroli, A.; Maugeri, M.; Lo Presti, D. A comparative study on shear modulus and damping ratio of cohesive soil from laboratory tests. In Proceedings of the 3rd Int Symp on Deformation Characteristics of Geomaterials, Lisse, The Netherlands, 1 January 2003; pp. 257–265.

Cecich, V., L. Gonzales, A. Hoisaeter, J. Williams, and K. Reddy. Use of Shredded Tires as Lightweight Backfill Material for Retaining Structures. Waste Management & Research, Vol. 14, No. 5, 1996, pp. 433–451.

Cerato, A., and A. Lutenegger. Specimen Size and Scale Effects of Direct Shear Box Tests of Sands. Geotechnical Testing Journal, Vol. 29, No. 6, 2006, pp. 507–516.

Cetin, H., M. Fener, and O. Gunaydin. 2006. "Geotechnical Properties of Tire-cohesive Clayey Soil Mixtures as a Fill Material." Engineering Geology 88 (1–2): 110–120. doi:10.1016/j.enggeo.2006.09.002.

Chaney, R.; Demars, K.; Masad, E.; Taha, R.; Ho, C.; Papagiannakis, T. Engineering Properties of Tire/Soil Mixtures as a Lightweight Fill Material. Geotech. Test. J. 1996, 19, 297–304. Computers and Geotechnics, Elsevier 126 October, 2020c: 103761. 10.1016/j.compgeo.2020.103761.conbuildmat.2015.05.080.

Dadkhah, R., M. Ghafoori, R. Ajalloeian, and G. Lashkaripo. The Effect of Scale Direct Shear Test on the Strength Parameters of Clayey Sand in Isfahan City, Iran. Journal of Applied Sciences, Vol. 10, No. 18, 2010, pp. 2027–2033.

Duncan, J. M., and C.-Y. Chang. 1970. "Nonlinear Analysis of Stress and Strain in Soils." Journal of Soil Mechanics & Foundations Division 96 (5): 1629–1653. doi:10.1061/JSFEAQ.0001458.

Eaton, R. A., R. J. Roberts, and D. N. Humphrey. 1994. Gravel Road Test Sections Insulated with Scrap Tire Chips: Construction and the First Year's Results. Gravel Road Test Sections Insulated with Scrap Tire Chips: Construction and the First Year's Results, Tech.. U.S. Army Cold Regions Research and Engineering Laboratory. Hanover, NH.

Edinçliler, A., G. Baykal, and A. Saygılı. 2010. "Influence of Different Processing Techniques on the Mechanical Properties of Used Tires in Embankment Construction." Waste Management 30 (6): 1073–1080. doi:10.1016/j.wasman.2009.09.031.

El Naggar, H., K. Zahran, and A. Moussa. 2021. Effect of the Particle Size on the TDA Shear Strength and Stiffness Parameters in Large-Scale Direct Shear Tests . Vol. 1 (1), 1–17. Basel, Switzerland: Geotechnics, MDPI.

El Naggar, H., P. Soleimani, and A. Fakhroo. 2016. "Strength and Stiffness Properties of Green Lightweight Fill Mixtures." Geotechnical and Geological Engineering 34 (3): 867–876. doi:10.1007/s10706-016- 0010-1.

El Naggar, H.; Ashari, M.; Mahgoub, A. Development of an Empirical Hyperbolic Material Model for TDA Using Large Scale Triaxial Testing. Int. J. Geotech. Eng. 2021.

El Naggar, H.; Zahran, K.; Moussa, A. Effect of the Particle Size on the TDA Shear Strength and Stiffness Parameters in Large-Scale Direct Shear Tests. Geotechnics 2021, 1, 1. [CrossRef]

Engstrom, G. M., and R. Lamb. Using Shredded Waste Tires as a Lightweight Fill Material for Road Subgrades. Minnesota Department of Transportation, 1994. 3. Liu, H. S., J. L. Mead,

and R. G. Stacer. Environmental Effects of Recycled Rubber in Light-Fill Applications. Rubber Chemistry and Technology, 2000 Vol. 73, No. 3, pp. 551–564.

Feng, Z.Y.; Sutter, K.G. Dynamic Properties of Granulated Rubber/Sand Mixtures. Geotech. Test. J. 2000, 23, 338–344.

Foose, G. J., C. H. Benson, and P. J. Bosscher. Sand Reinforced with Shredded Waste Tires. Journal of Geotechnical Engineering, Vol. 122, No. 9, 1996, pp. 760–767.

Fox, P. J., S. S. Thielmann, M. J. Sanders, C. Latham, I. Ghaaowd, and J. S. Mccartney. 2018. "Large-Scale Combination Direct Shear/Simple Shear Device for Tire-Derived Aggregate." Geotechnical Testing Journal 41 (2): 20160245. doi:10.1520/GTJ20160245.

Gabry´s, K.; Sas, W.; Soból, E.; Głuchowski, A. Application of bender elements technique in testing of anthropogenic soil—Recycled concrete aggregate and its mixture with rubber chips. Appl. Sci. 2017, 7, 741.

Garga, V.K.; Zhang, H. Volume changes in undrained triaxial tests on sands. Can. Geotech. J. 1997, 34, 762–772.

Geosyntec Consultants. Guidance Manual for Engineering Uses of Scrap Tires. Maryland Department of the Environment, 2008.

Geotechnical and Geological Engineering. Springer, Germany Madhusudhan, B. R., A. Boominathan, and S. Banerjee. 2020. Cyclic Simple Shear Response of Sand-rubber Tire Chip Mixtures.

Ghaaowd, I., J. S. Mccartney, S. S. Thielmann, M. J. Sanders, and P. J. Fox. 2017. "Shearing Behavior of Tire-Derived Aggregate with Large Particle Size. I: Internal and Concrete Interface Direct Shear." Journal of Geotechnical and Geoenvironmental Engineering 143 (10): 04017078. doi:10.1061/(ASCE)GT.1943-5606.0001775.

Hazarika, H., and K. Yasuhara (Edited by). (2007). Scrap Tire Derived Geomaterials-Opportunities and Challenges: Proceedings of the International Workshop IW-TDGM 2007 (Yokosuka, Japan, 23-24 March 2007). Cleveland, Ohio, United States: CRC Press.

Hazarika, H.; Hyodo, M.; Yasuhara, K. Investigation of tire chips-sand mixtures as preventive measure against liquefaction. In Ground Improvement and Geosynthetics; ASCE: Reston, VA, USA, 2010; pp. 338–345.

Holtz, R.; Kovacs, W. An Introduction to Geotechnical Engineering; Prentice-Hall, Inc.: Upper Saddle River, NJ, USA, 1981; ISBN 0-13-484394-0.

Humphrey, D. N., and R. A. Eaton (1993). "Tire Chips as Subgrade Insulation: Field Trial." Symposium on Recovery and Effective Reuse of Discarded Materials and By-Products for Construction of Highway Facilities, Denver, CO.

Humphrey, D. N., and W. L. Nickles. 1994. “Tire Chips as Subgrade Insulation and Lightweight Fill.” In Proceedings of the 18th Annual Meeting of the Asphalt Recycling and Reclaiming Association 1: 83–105.

Humphrey, D. N., and W. P. Manion. 1992. “Properties of Tire Chips for Lightweight Fill.” In Grouting, Soil Improvement and Geosynthetics, 1344–1355. New York, NY: ASCE.

Humphrey, D.N., and Eaton, R.A. (1995), “Field Performance of Tire Chips as Subgrade Insulation for Rural Roads,” Proceedings of the Sixth International Conference on Low-Volume Roads, Transportation Research Board, Washington, D.C., Vol. 2, pp. 77–86

Humphrey, D.N., Sandford, T.C., Cribbs, M.M., and Manion, W.P. (1993), “Shear Strength and Compressibility of Tire Chips for Use as Retaining Wall Backfill,” Transportation Research Record No. 1422, Transportation Research Board, Washington, D.C., pp. 29–35

Humphrey, D.N., Sandford, T.C., Cribbs, M.M., Gharegrat, H.G., and Manion, W.P. (1992), “Tire Chips as Lightweight Backfill for Retaining Walls – Phase I,” A Study for the New England Transportation Consortium, Department of Civil Engineering, University of Maine, Orono, Maine, 137 pp

Humphrey, D.N.; Manion, W.P. Properties of tire chips for lightweight fill. In Grouting, Soil Improvement and Geosynthetics; ASCE: Reston, VA, USA, 1992; pp. 1344–1355.

International Conference on Soil Mechanics and Foundation Engineering, Montreal, QC, Canada, 8–15 September 1965; Volume I,pp. 273–277. International Journal of Geomechanics. New York, NY: American Society of Civil Engineers.

Islam, M.N.; Siddika, A.; Hossain, M.B.; Rahman, A.; Asad, M.A. Effect of particle size on the shear strength behaviour of sands.Aust. Geomech. J. 2011, 46, 85–95.

Kim, D.; Ha, S. Effects of Particle Size on the Shear Behavior of Coarse Grained Soils Reinforced with Geogrid. Materials 2014, 7,

Kirkpatric, W.M. Effects of Grain Size and Grading on the Shearing Behaviour of Granular Materials. In Proceedings of the 6th

Kowalska, M. 2016. “Compactness of Scrap Tyre Rubber Aggregates in Standard Proctor Test.” Procedia Engineering 161: 975–979. doi:10.1016/j.proeng.2016.08.836.

Kowalska, M. Compactness of scrap tyre rubber aggregates in standard proctor test. Procedia Eng. 2016, 161, 975–979.

La Rochelle, P.; Leroueil, S.; Trak, B.; Blais-Leroux, L.; Tavenas, F. Observational approach to membrane and area corrections in triaxial tests. Adv. Triaxial Test. Soil Rock STP 1988, 977, 715–731.

Lade, P.V. Triaxial Testing of Soils; Wiley, Blackwell: New York, NY, USA, 2016.

Lee, H. J., and H. S. Roh. 2007. "The Use of Recycled Tire Chips to Minimize Dynamic Earth Pressure during Compaction of Backfill." Construction and Building Materials 21 (5): 1016–1026. doi:10.1016/j. conbuildmat.2006.02.003.

Lee, J. H., R. Salgado, A. Bernal, and C. W. Lovell. 1999. "Shredded Tires and Rubber-Sand as Lightweight Backfill." Journal of Geotechnical and Geoenvironmental Engineering 125 (2): 132–141. doi:10.1061/(ASCE) 1090-0241(1999)125:2(132).

Madhusudhan, B. R., A. Boominathan, and S. Banerjee. 2017. "Static and large-strain dynamic properties of sand-rubber tire shred mixtures." J. Mater. Civ. Eng. 29 (10): 04017165. https://doi.org/10.1061/(ASCE)MT.1943-5533.0002016.

Madhusudhan, B. R., A. Boominathan, and S. Banerjee. 2019a. Engineering Properties of Sand-rubber Tire Shred Mixtures. International Journal of Geotechnical Engineering.

Madhusudhan, B. R., A. Boominathan, and S. Banerjee. 2019b. Factors Affecting Strength and Stiffness of Dry Sand-rubber Tire Shred Mixtures.

Mahgoub, A., and H. El Naggar. 2019a. "Using TDA as an Engineered Stress-Reduction Fill over Pre-existing Buried Pipes." ASCE, Journal of Pipeline Systems Engineering and Practice 1: 10. doi:10.1061/28ASCE29PS.1949-1204.0000362.

Mahgoub, A., and H. El Naggar. 2019b. "Using TDA Underneath Shallow Foundations: Simplified Design Procedure." International Journal of Geotechnical Engineering 1–15. doi:10.1080/19386362.2019.1690415.

Mahgoub, A., and H. El Naggar. 2020a. "Using TDA Underneath Shallow Foundations: Field Tests and Numerical Modelling." Journal of

Mahgoub, A., and H. El Naggar. 2020b. "Innovative Application of Tire derived Aggregate around Corrugated Steel Plate Culverts." Journal of Pipeline Systems Engineering and Practice 11 (3): 04020025. doi:10.1061/(ASCE)PS.1949-1204.0000466.

Mahgoub, A., and H. El Naggar. 2020c. "Coupled TDA–Geocell Stress Bridging System for Buried Corrugated Metal Pipes." Journal of Geotechnical and Geoenvironmental Engineering 146 (7): 04020052. doi:10.1061/(ASCE)GT.1943-5606.0002279.

Mahgoub, A., and H. El Naggar. Using TDA as an Engineered Stress-Reduction Fill over Pre-Existing Buried Pipes. Journal of Pipeline Systems Engineering and Practice, Vol. 10, No. 1, 2019. https://doi.org/10.1061/ (ASCE)PS.1949-1204.0000362.

Mahgoub, A.; El Naggar, H. Coupled TDA-Geocell Stress-Bridging System for Buried Corrugated Metal Pipes. J. Geotech. Geoenvironmental Eng. 2020, 146, 04020052.

Manion, W.P., and Humphrey, D.N. (1992), "Use of Tire Chips as Lightweight and Conventional Embankment Fill, Phase I – Laboratory," Technical Paper 91–1, Technical Services Division, Maine Department of Transportation, Augusta, Maine, 151 pp

Mccartney, J. S., I. Ghaaowd, P. J. Fox, M. J. Sanders, S. S. Thielmann, and A. C. Sander. 2017. "Shearing Behavior of Tire-Derived Aggregate with Large Particle Size. II: Cyclic Simple Shear." Journal of Geotechnical and Geoenvironmental Engineering 143 (10): 04017079. doi:10.1061/ (ASCE)GT.1943-5606.0001781.

Meles, D., A. Bayat, and D. Chan. 2013. "One-dimensional Compression Model for Tire-derived Aggregate Using Large-scale Testing Apparatus." International Journal of Geotechnical Engineering 8 (2): 197–204. doi:10.1179/1939787913Y.0000000019.

Mirzaeifar, H., A. Abouzar, and R. Abdi. Effects of Direct Shear Box Dimensions on Shear Strength Parameters of Geogrid-Reinforced Sand. Proc., 66th Canadian Geotechnical Conference and the 11th Joint CGS/IAH-CNC Groundwater Conference, At Montreal, Quebec, Canada, 2013.

Moayed, R. Z., M. Alibolandi, and A. Alizadeh. Specimen Size Effects on Direct Shear Test of Silty Sands. International Journal of Geotechnical Engineering, 2016, pp. 198–205. https://doi.org/10.1080/19386362.2016.1205166.

Moo-Young, H., K. Sellasie, D. Zeroka, and G. Sabnis. 2003. "Physical and Chemical Properties of Recycled Tire Shreds for Use in Construction." Journal of Environmental Engineering 129 (10): 921–929. doi:10.1061/ (ASCE)0733-9372(2003)129:10(921).

Moussa, A., and H. El Naggar. 2020. "Numerical Evaluation of Buried Wave Barriers Performance. International Journal of Geosynthetics and Ground Engineering, Springer." 6 (4): 56. 10.1007/s40891-020-00240-z.

Moussa, A., and H. El Naggar. 2021. "Dynamic Characterization of Tire Derived Aggregates." Journal of Materials in Civil Engineering, ASCE 33: 2. doi:10.1061/(ASCE)MT.1943-5533.0003583.

Palmeira, E., and G. Milligan. Scale Effects in Direct Shear Tests on Sand. International Journal of Rock Mechanics and Mining Sciences, Vol. 28, No. 6, 1991, p. A340.

Parsons, J. D. Progress Report on an Investigation of the Shearing Resistance of Cohesionless Soils. Proc., International Conference on Soil Mechanics and Foundation Engineering, Harvard University, Vol. 2, 1936, pp. 133–138.

Pehlken, A., and E. Essadiqi. Scrap Tire Recycling in Canada. MTL 2005-08(CF). CANMET Materials Technology Laboratory, 2005.

Sarajpoor, S.; Kavand, A.; Zogh, P.; Ghalandarzadeh, A. Dynamic behavior of sand-rubber mixtures based on hollow cylinder tests. Constr. Build. Mater. 2020, 251, 118948.

Sas, W.; Głuchowski, A.; Szyma´nski, A. The geotechnical properties of recycled concrete aggregate with addition of rubber chips during cyclic loading. Int. J. GEOMATE 2017, 12, 25–32.

Senetakis, K.; Anastasiadis, A.; Pitilakis, K. Dynamic properties of dry sand/rubber (SRM) and gravel/rubber (GRM) mixtures in a wide range of shearing strain amplitudes. Soil Dyn. Earthq. Eng. 2012, 33, 38–53.

Shahrokhi-Shahraki, R.; Kwon, P.S.; Park, J.; O'Kelly, B.C.; Rezania, S. BTEX and heavy metals removal using pulverized waste tires in engineered fill materials. Chemosphere 2020, 242, 125281.

Shakri, S. M., J. M. Noor, T. A. Nazaruddin, and A. M. Hafez. Effects of shear Box Size on Shear Strength between Modified Sand-Column (PFA-Sand Mixture) and Soft Soil. International Journal of Structural and Civil Engineering Research, Vol. 6, No. 1, 2017, pp. 13–18.

Shalaby, A., and R. A. Khan. 2005. "Design of Unsurfaced Roads Constructed with Large-size Shredded Rubber Tires: A Case Study." Resources, Conservation and Recycling 44 (4): 318–332. doi:10.1016/j.resconrec.2004.12.004.

Soltani, A.; Taheri, A.; Deng, A.; O'Kelly, B.C. Improved Geotechnical Behavior of an Expansive Soil Amended with Tire-Derived Aggregates Having Different Gradations. Minerals 2020, 10, 923.

Sparkes, J., H. El Naggar, and A. Valsangkar. 2019. "Compressibility and Shear Strength Properties of Tire-Derived Aggregate Mixed with Lightweight Aggregate." ASCE, Journal of Pipeline Systems Engineering and Practice 1: 10. doi:10.1061/28ASCE29PS.1949-1204.0000354.

Standard Test Methods for the Determination of the Modulus and Damping Properties of Soils Using the Cyclic Triaxial Apparatus; ASTM, D3999; ASTM: Conshohocken, PA, USA, 2003.

Strenk, P. M., J. Wartman, D. G. Grubb, D. N. Humphrey, and M. F. Natale. Variability and Scale Dependency of Tire-Derived Aggregate. Journal of Materials in Civil Engineering, Vol. 19, No. 3, 2007, pp. 233–241.

Tika, T. E., P. R. Vaughan, and L. Lemos. Fast Shearing of Pre-Existing Shear Zones in Soil. Ge´otechnique, Vol. 46, No. 2, 1996, pp. 197–233.

Vangla, P.; Latha, G.M. Influence of Particle Size on the Friction and Interfacial Shear Strength of Sands of Similar Morphology.Int. J. Geosynth. Ground Eng. 2015, 1, 1–12. Volume 3, pp. 915–956.

Wang, J.-J.; Zhang, H.-P.; Tang, S.-C.; Liang, Y. Effects of Particle Size Distribution on Shear Strength of Accumulation Soil. J. Geotech. Geoenvironmental Eng. 2013, 139, 1994–1997.

Warith, M., and S. M. Rao. 2006. "Predicting the Compressibility Behaviour of Tire Shred Samples for Landfill Applications." Waste Management 26 (3): 268–276. doi:10.1016/j.wasman.2005.04.011.

Wartman, J., M. F. Natale, and P. M. Strenk. 2007. "Immediate and TimeDependent Compression of Tire Derived Aggregate." Journal of Geotechnical and Geoenvironmental Engineering 133 (3): 245–256. doi:10.1061/(ASCE)1090-0241(2007)133:3(245).

Wu, W. Y., C. C. Benda, and R. F. Cauley. 1997. "Triaxial Determination of Shear Strength of Tire Chips." Journal of Geotechnical and Geoenvironmental Engineering 123 (5): 479–482. doi:10.1061/(ASCE)1090-0241(1997)123:5(479).

Xiao, M., M. Ledezma, and C. Hartman. 2015. "Shear Resistance of Tire Derived Aggregate Using Large-Scale Direct Shear Tests." Journal of Materials in Civil Engineering 27 (1): 04014110. doi:10.1061/(ASCE)MT.1943-5533.0001007.

Xiao, M., M. Ledezma, and C. Hartman. Shear Resistance of Tire-Derived Aggregate using Large-Scale Direct Shear Tests. Journal of Materials in Civil Engineering, Vol. 27, No. 1, 2013. https://doi.org/10.1061/(ASCE)MT.1943-5533.0001007.

Yamamuro, J., and P. Lade. Effects of Strain Rate on Instability of Granular Soils. Geotechnical Testing Journal, Vol. 16, No. 3, 1993, pp. 304–313.

Yi, Y., D. Meles, S. Nassiri, and A. Bayat. 2015. "On the Compressibility of Tire-derived Aggregate: Comparison of Results from Laboratory and Field Tests." Canadian Geotechnical Journal 52 (4): 442–458. doi:10.1139/cgj-2014-0110.

Youwai, S., and D. T. Bergado. 2003. "Strength and Deformation Characteristics of Shredded Rubber Tire – Sand Mixtures." Canadian Geotechnical Journal 40 (2): 254–264. doi:10.1139/t02-104.

Zahran, K., and H. El Naggar. 2020. "Effect of Sample Size on TDA Shear Strength Parameters in Direct Shear Tests." Transportation Research Record 2674 (9): 1110–1119. doi:10.1177/0361198120934482.

Zhang, T., Cai, G., Liu, S. & Duan, W. 2016. Laboratory observation of engineering properties and deformation mechanisms of cemented rubber-sand mixtures. Construction and Building Materials, 120, 514-523.

Zornberg, J. G., A. R. Cabral, and C. Viratjandr. 2004. “Behaviour of Tire Shred/sand Mixtures.” Canadian Geotechnical Journal 41 (2): 227–241.